University of São Paulo
"Luiz de Queiroz" College of Agriculture

Effects of pH and cations on phosphate-molecules adsorption into hematite and on P forms in an Oxisol amended with lime and phosphogypsum

Ruan Francisco Firmano

Thesis presented to obtain the degree of Doctor in Science. Area: Soils and Plant Nutrition

Piracicaba
2020

Ruan Francisco Firmano
Agronomist

Effects of pH and cations on phosphate-molecules adsorption into hematite and on P forms in an Oxisol amended with lime and phosphogypsum

versão revisada de acordo com a resolução CoPGr 6018 de 2011

Advisor:
Prof. Dr. **LUÍS REYNALDO FERRACCIÚ ALLEONI**

Thesis presented to obtain the degree of Doctor in Science. Area: Soils and Plant Nutrition

Piracicaba
2020

Dados Internacionais de Catalogação na Publicação
DIVISÃO DE BIBLIOTECA – DIBD/ESALQ/USP

Firmano, Ruan Francisco

Effects of pH and cations on phosphate-molecules adsorption into hematite and on P forms in an Oxisol amended with lime and phosphogypsum / Ruan Francisco Firmano. - - versão revisada de acordo com a resolução CoPGr 6018 de 2011 - - Piracicaba, 2020.

161 p.

Tese (Doutorado) - - USP / Escola Superior de Agricultura "Luiz de Queiroz".

1. Acidez do solo 2. Óxidos de ferro 3. Adsorção 4. Especiação química 5. Espectroscopia 6. Luz síncrotron 7. Infravermelho 8. Carbono orgânico I. Título

To the land workers with calluses in their hands and a serene gaze, who till the earth, love their children, and believe in their homeland.

All my effort and this thesis is **dedicated** to you.

ACKNOWLEDGEMENTS

I thank the São Paulo Research Foundation (FAPESP) for the financial support, including the doctorate scholarship (grant 2018/08586-8) and research intern abroad (BEPE – Doctorate, grant 2019/01213-4). This study was also financed in part (prior FAPESP) by the Coordenação de Aperfeiçoamento de Pessoal de Nível Superior - Brasil (CAPES) - Finance Code 001.

The doctoral period in the Luiz de Queiroz College of Agriculture (University of São Paulo) and training abroad in the College of Agriculture and Bioresources (University of Saskatchewan) were years of valued learning. I owe a great debt to my advisor, Dr. Luís R.F. Alleoni, by every incentive, the wise guidance and the opportunity of pursuing my Doctorate. I would also like to express my gratitude to Dr. J. Derek Peak, my supervisor in Canada, for the enriching discussions and outstanding scientific support. It is fair to remember that this thesis would not have been idealized without the dedication of Dr. Carlos A.C. Crusciol (UNESP). Therefore, I am grateful to him and his research group for having made available the experimental area and assistance throughout this process, especially those of colleague M.Sc. João Bossolani.

I am also grateful for the scientific discussions I had with Dr. Adilson de Oliveira Jr., Dr. Celia R. Montes, Dr. Cesar de Castro, Dr. Marcelo Alves, Dr. Hudson W. P. Carvalho and Dr. Michael P. Schmidt. I was very fortunate to have worked with so friendly and helpful people in field and laboratories. Special thanks to Dr. Marina Colzato, Dr. Débora Ishida, Leandro L. Goia and Ednéia C. S. Mondoni. My acknowledgements to Embrapa Instrumentation, especially to Dr. Ladislau Martin Neto and Dr. Luiz A. Colnago.

To my friends Dr. Renan R. Barzan, Dr. Luiz T. Jordão, Dr. Valter Casarin and M.Sc. Fabio Lima, who believed in my competence. I would also like to express my gratitude to the friends from ESALQ and USASK, Dr. Adijailton J. de Souza (Dija), Dr. Alexys G.F. Boim, Dr. Cintia M. Lopes, M.Sc. Douglas G. Viana (Dougrinha), Dr. Dener M. de Oliveira (Denzel), Dr. Eloá M. Araújo, Dr. Flávio A. Pinto, Dr. J.M. Damian (Galo cinza

missioneiro), Felipe Hipólito dos Santos (Cão), M.Sc. Matheus Bortolanza S., M.Sc. Nicole C. Cheng, Dr. Rafaela A. Migliavacca, M.Sc., Mayara Rodrigues (Roy), Dr. Willfrand Pervajanu, Dr. Letícia Pierri, Dr. Luciana A. Garcia, M.Sc. Caio T. Fongaro (Caião), M.Sc. Rodolfo F. Costa, M.Sc. Rafael Silva Santos (Chico), M.Sc. Rodrigo N. de Sousa (Crok), M.Sc. Thais M. Soares, Dr. Tatiana F. Rittl (Xuxa, Sorvetão), Dr. Elessandro Bornhofen (Gauchim), M.Sc. Katie Hyde, M.Sc. Han Fu (China), M.Sc. Tony Tian, among others. I am grateful to all the residents of the USPEÃO Student Residence for the receptivity in my first days in Piracicaba and all the moments of joy that we spent together.

I also leave here my sincere recognition of the friendship of four brothers, Dr. Acácio de Mira (Chapa), Dr. João A. Antonangelo (Jão), Dr. Frederico P. Gomes (Tigre) and Dr. Matheus S. C. Barreto (Baiano), your presence made me smile when I needed it most. I could not forget to mention my parents, José A. Firmano and Vania M. Fabiano Firmano, as well as my brother, R. Samuel Firmano, his wife Tatiana Fiori, and their daughter Valentina F. Firmano, for the faith in my journey. There are no words that express my thankfulness for this love. I am also grateful to my grandfather, Benedito Fabiano, a man remarkable in simplicity and intelligence. I could not forget the friendship and support of Alessandro G. Machado, Amanda L. Mantovani, Andressa Crescêncio, Carlos H. Milhate, Cayo A. C. Buffalo, M.Sc. Celso Heinzen Jr., Felipe Andrade S., Fernando V. de Melo, Luiz G. Manoel, Raul D. de Nóbrega, among many others.

It has been six years full of learnings and challenges since the beginning of my graduate studies at ESALQ. All the experiences in this unique college have shaped a good part of my personal and professional character. The completion of this particular doctoral project will always remind me of how important it is to have creative and passionate people around me.

My deep **gratitude**.

"Todo caminho da gente é resvaloso.
Mas também, cair não prejudica demais,
a gente levanta, a gente sobe, a gente volta!
O correr da vida embrulha tudo, a vida é assim:
esquenta e esfria, aperta e daí afrouxa,
sossega e depois desinquieta.
O que ela quer da gente é coragem..."

João Guimarães Rosa, Grande Sertão: Veredas (1956)

"Be yourself. Especially, do not feign affection. Neither be cynical about love; for in the face of all aridity and disenchantment it is as perennial as the grass.
Nurture strength of spirit to shield you in sudden misfortune. But do not distress yourself with dark imaginings. Many fears are born of fatigue and loneliness.
Beyond a wholesome discipline, be gentle with yourself. You are a child of the universe, no less than the trees and the stars; you have a right to be here..."

Max Ehrmann, The Desiderata of Hapiness (1927)

"It is not our part to master all the tides of the world, but to do what is in us for the succour of those years wherein we are set, uprooting the evil in the fields that we know, so that those who live after may have clean earth to till..."

Dr. John R. R. Tolkien, The Return of the King (1955)

CONTENTS

ABSTRACT

Effects of pH and cations on phosphate-molecules adsorption into hematite and on P forms in an Oxisol amended with lime and phosphogypsum

Phosphorus (P) has intrigued scientists worldwide since its discovery in 1669. The remarkable adsorption of P in soils from intertropical regions, which mostly cover underdeveloped countries, has been continuously studied and makes management with this oxyanion challenging in cultivated areas. The overall objective was to investigate relationships among pH, calcium (Ca) and magnesium (Mg) in a molecular-scale, as well as among P, iron (Fe) and carbon (C) chemistry in soils at field-scale. The thesis begins in **chapter two** with a molecular-level study between the surface of minerals and phosphate molecules in the face of pH and cations (Ca and Mg) variations, mimicking what commonly occurs in acidic soils after the lime addition. The presence of Mg influenced the adsorption of *myo*-inositol hexa*kis*phosphate (IHP_6), which, like phosphate, exhibited two adsorption mechanisms. Kinetic parameters of IHP_6 and inorganic phosphate adsorption were more influenced by pH than by the presence of cations in the colloidal systems. In the following three chapters, the indirect effects of prolonged management with aluminum (Al) suppressors, such as lime or phosphogypsum, are addressed in an Oxisol under no-till system. **Chapter three** explores the mineralogical and physicochemical properties of Fe forms, especially Fe-(hydr)oxides and phases associated with C. Lime broadcast apparently did not increase the association of Fe-oxides with organic C, but affected the potential adsorption of P in the soil. Crystalline Fe phases were affected by the prolonged use of lime and phosphogypsum, but the phases of lesser structural arrangement were found just in a native forest soil. In **chapter four**, an associative approach was made between spectroscopy and chemical fractionation techniques in order to clarify how inorganic forms of P (P_i) respond to the prolonged addition of these amendments. Most P species were associated with Fe-(hydr)oxides as hematite and goethite of varied structural orders. Sequential extractions were performed and high proportions of P associated with kaolinite were identified and correlated with residual P concentrations, which indicates storage of non-labile P forms in the phyllosilicate. Finally, in **chapter five**, the emphasis was on organic forms of P (P_o) and their relationships with the activity of enzymes that mineralize P and C in the soil profile, as well as the yield performance of soybeans (*Glycine max* L.). There was a stratification of certain chemical attributes and enzymes in the soil, but the joint use of Al-suppressors increased the general availability of nutrients and soybean yields. The use of lime and/or phosphogypsum, however, did not promote an increase in P_o identified by ^{31}P nuclear magnetic resonance, composed mainly of IHP_6.

Keywords: 1. Oxisol 2. Lime 3. Gypsum 4. Long-term management 5. Spectroscopy

RESUMO

Efeitos do pH e cátions na adsorção de moléculas fosfatadas em hematita e nas formas de P em um Latossolo manejado com calcário e fosfogesso

O comportamento do fósforo (P) intriga cientistas em todo o mundo desde sua descoberta em 1669. A notável adsorção de P em solos de regiões intertropicais, que abrangem a maioria dos países menos desenvolvidos, tem sido continuamente estudada e torna desafiador o manejo com esse oxiânion em áreas cultivadas. O objetivo geral foi investigar relações entre pH, cálcio (Ca) e magnésio (Mg) a nível molecular, bem como do P, ferro (Fe) e carbono (C) nos solos a nível de campo. A tese tem início no **capítulo dois** com um estudo a nível molecular entre a superfície de minerais e moléculas fosfatadas em resposta a variações em pH e cátions (Ca e Mg), o que mimetiza o que comumente ocorre em solos ácidos após a adição de calcário. A presença de Mg influenciou a adsorção de *myo*-inositol hexa*kis*phosphate (IHP_6), que assim como a de fosfato manifestou dois mecanismos de adsorção. Parâmetros cinéticos da adsorção de IHP_6 e fosfato inorgânico foram mais influenciados pelo pH do que pela presença de cátions no sistema coloidal. Nos três capítulos seguintes são abordados os efeitos indiretos do manejo prolongado com supressores de alumínio (Al), como calcário ou fosfogesso, em um Latossolo sob sistema de semeadura direta. O **capítulo três** explora as propriedades mineralógicas e físico-químicas de formas de Fe, em especial óxidos e hidróxidos de Fe e fases associadas ao C. A adição de calcário aparentemente não aumentou a associação de Fe-oxides com C orgânico, mas afetou o potencial de adsorção de P no solo. Formas mais ou menos cristalinas de Fe foram afetadas pelo uso prolongado de calcário e fosfogesso, porém as fases de menor arranjo estrutural foram encontradas em solo de mata nativa. Já no **capítulo quatro** foi feita uma abordagem associativa entre técnicas de espectroscopia e fracionamento químico a fim de esclarecer como formas inorgânicas de P respondem à adição prolongada desses supressores de Al. A maioria das espécies de P estavam associadas a (hidr)óxidos de Fe como hematita e goethita de variadas ordens estruturais. Também foram identificadas altas proporções de P associado à caulinita, que se correlacionou com teores de P residuais após extrações sequenciais, o que indicou armazenamento de formas pouco lábeis no oxiânion no filossilicato. Por fim, **no capítulo cinco** a ênfase foram formas orgânicas de P e sua relação a atividade de enzimas que mineralizam P e C no perfil do solo, bem como o desempenho produtivo da soja (*Glycine max* L.). Houve estratificação de certos atributos químicos e enzimas no solo mas a adição conjunta de supressores de Al aumentou a disponibilidade de boa parte dos nutrientes avaliados e as produtividades da soja. Contudo, o uso calcário e, ou gesso não promoveu aumento de formas orgânicas de P identificadas por ressonância nuclear magnética do ^{31}P, compostas majoritariamente por IHP_6.

Palavras-chave: 1. Latossolo 2. Calcário 3. Gesso 4. Manejo prolongado 4. Espectroscopia

List of abbreviations and acronyms

A	ampere
Å	angstrom
AEC	anion exchange capacity
Acid-P	acid phosphomonoesterase
$Al^{3+}/_{ex}Al$	exchangeable aluminum
Alk-P	alkaline phosphomonoesterase
(aq)	aqueous
ATR-FTIR	Attenuated Total Reflectance Fourier Transform Infrared
C	degree celsius (centigrade)
CEC	cation exchange capacity
CEC*t*	total cation exchange capacity
CEC*e*	efective cation exchange capacity
CLS	Canadian Light Source
CV	coefficient of variation
D_2O	deuterated water
$_{DCB}Fe$	iron extracted with DCB solution
dm^3	cubic decimer
DNA	deoxyribonucleic acid
DRS	Diffuse Reflectance Spectroscopy
E_0	edge reference energy
EDTA	ethylenediaminetetraacetic acid
EXAFS	Extended X-ray Absorption Fine Structure
eV	electron volts
g	gram
(g)	gaseous
Gth/Gt	goethite
×g	gram-force
Fh	ferrihydrite
h	hour
ha	hectare
H+Al	potential acidity
Hem/Hm	hematite
Hz	hertz (cycles/s)
ICP-MS	Inductively Coupled Plasma Mass Spectrometry
ICP-OES	Inductively Coupled Plasma Optical Emission Spectrometry
IF	infrared
IHP_6	*myo*-inositol hexa*kis*phosphate
k	constant parameter
K	degree kelvin
kg	kilogram
Kln	kaolinite

l	liter
L	lime treatment
LCF	linear combination fitting
LNLS	Brazilian Synchrotron Light Laboratory
LPG	lime + phosphogypsum treatment
min	minute
mol l^{-1}	molar
n	number of statistical replications
NMR	Nuclear Magnetic Ressonance
NV	native vegetation site
OC	organic carbon
p	statistical confidence level
Pa	pascal
PG	phosphogypsum treatment
pH	hydrogen potential
P_i	inorganic phosphorus
P_o	organic phosphorus
ppm	parts per million
RNA	ribonucleic acid
s	second
SOC	soil organic carbon
SOM	soil organic matter
SGM	High Resolution Spherical Grating Monochromator
SSA	Specific Surface Area
SSD	Silicon Drift Detector
SXS	Soft X-ray Spectroscopy
UV	ultraviolet
UW	ultrapure water
v/v	volume-based
w/w	weight-based
V	volt
W	watt
XAS	X-ray Absorption Spectroscopy
XANES	X-ray Absorption Near Edge Structure
XRD	X-Ray Diffraction
XRF	X-Ray Fluorescence
XPS	X-Ray Photoelectron Spectroscopy
yr	year
ZCP	zero charge point
β-gluc	β-glucosidase
λ	wavelenght
ζ	zeta potential

1. GENERAL INTRODUCTION

The biogeochemical cycles of phosphorus (P), iron (Fe) and carbon (C) converge intensively in soils. The interactions among these plant-nutrients occur across scales, with implications from atomic to field levels. Acid soils represent ~50% of the total arable land area in the planet, being mostly found in tropical and subtropical regions (Fageria et al. 2013). As they are concentrated in areas of intense weathering, these soils generally have low pH_{H_2O} (< 4.5) and high concentrations of exchangeable aluminum (Al^{3+}), hampering the obtention of profitable yields in agricultural systems. Phosphorus deficiency in cultivated plants and low P fertilizer efficiency are other common issues in these soils (Casanova et al. 2002; Jacobs et al. 2015; Caires et al. 2017). To ameliorate these problems, lime or phosphogypsum applications are recommended and usually improve the soil chemical environment.

One of the most notable enhancements in soils continuously managed with lime is the increase in organic carbon (OC) contents over time (Briedis et al. 2012; Carmeis Filho et al. 2017; Inagaki et al. 2017). The OC buildup in lime-amended soils has been mainly attributed to the stabilizing effect of Ca in organo-mineral complexes and higher biomass production over time (Rowley et al. 2018). However, there is a lack of information regarding Mg effects on organic molecules and organo-mineral associations. The few studies that address this issue focus on theoretical models or unusual minerals in tropical soils (Stachowicz et al. 2008; Yoshimura et al. 2015; Mendez and Hiemstra 2020). Therefore, studies that mimic processes in oxidic soils after liming are important, particularly inquiring the effects of pH variations and cations in systems with hematite, the widely found Fe-oxide in sediments and soils between tropics (Schaerfer et al. 2008).

The increase in diversity and quantity of OC by liming leads to other questions like if liming could also increase the contents of organic forms of P or low crystalline forms of Fe, which are commonly associated with C. Furthermore, no changes in pH are expected with the addition of phosphogypsum alone (Zoca and Penn 2017), so

different effects from the isolated use of lime could occur. Other factors such as high phosphogypsum solubility compared to lime, absence of Mg, and abundance of sulfur (S) in its composition make it interesting to investigate the effects of these amendments.

Despite having a simple structure, hematite tends to have a high zero charge point (ZPC) and retain high amounts of phosphate (PO_4). It is estimated that in 1 m^3 soil may easily contain several millions of m^2 of reactive surface area. Each m^2 of reactive surface can bind at least 1 mol of oxyanions at a surface loading of 1 μmol m^{-2} oxide. For PO_4, this is equivalent to ~1000 kg ha^{-1} (Weng et al. 2012). The same natural oxide surfaces may also bind organic compounds, among them organic forms of P. However, a particular mineral species, such as a Fe-oxide, may have more or less ordered crystalline arrangements (Lounsbury et al. 2019). This will result in different reactivities, which are generally higher in low-crystalline oxides. Although these properties and reactions have already been studied directly (Sakharov et al. 2016), there are few studies that address the indirect effect of management practices on these topics.

Instrumental advance in the fields of chemistry and physics has had positive repercussions for soil science over the past two decades (Kruse et al. 2015). A striking example is the use of synchrotron light in samples derived from natural environments, such as soil or sediments (Catlow 2015). Other techniques based on light wave properties, such as X-Ray Diffraction (XRD), X-Ray Fluorescence (XRF), X-Ray Photoelectron Spectroscopy (XPS), Infrared (IF) spectroscopy, colorimetry, microscopy, as well as those based on light particle properties, as Nuclear Magnetic Resonance (NMR), allowed deeper evaluations of soil components and processes, yielding novel findings as those of Chen et al. 2014, De Souza Bahia et al. 2015, Cade-Menun et al. 2018, Poggenburg et al. 2018, and Yan et al. 2018.

Overall, this thesis integrates cross-scale approaches from the fundamentals of surface chemistry of minerals to field-scale investigations regarding long-term amendments management. The objectives in this study were to: (**i**) evaluate how

variations in pH and the presence of divalent cation interfere the adsorption of phosphate-molecules onto hematite; and to examine the effects of the prolonged broadcast of Al-suppressors in (**ii**) Fe fractions and (hydr)oxides with variable structural order, (**iii**) inorganic P species and operationally defined fractions, and finally (**iv**) organic forms of P and its link with enzymes, chemical attributes and yields.

REFERENCES

Briedis C, De Moraes Sá JC, Caires EF, et al (2012) Changes in organic matter pools and increases in carbon sequestration in response to surface liming in an Oxisol under long-term no-till. Soil Sci Soc Am J 76:151–160.

Cade-Menun BJ, Elkin KR, Liu CW, et al (2018) Characterizing the phosphorus forms extracted from soil by the Mehlich III soil test. Geochem Trans 19:1–17.

Caires EF, Sharr DA, Joris HAW, et al (2017) Phosphate fertilization strategies for soybean production after conversion of a degraded pastureland to a no-till cropping system. Geoderma 308:120–129.

Carmeis Filho ACA, Penn CJ, Crusciol CAC, Calonego JC (2017) Lime and phosphogypsum impacts on soil organic matter pools in a tropical Oxisol under long-term no-till conditions. Agric Ecosyst Environ 241:11–23.

Casanova E, Salas AM, Toro M (2002) Evaluating the effectiveness of phosphate fertilizers in some Venezuelan soils. Nutr Cycl Agroecosystems 63:13–20.

Catlow, CRA (2015) Synchrotron radiation techniques in materials and environmental science. Phil Trans Royal Soc A 373:20130162.

Chen C, Dynes JJ, Wang J, Sparks DL (2014) Properties of Fe-organic matter associations via coprecipitation versus adsorption. Environ Sci Technol 48:13751–

De Souza Bahia ASR, Marques J, Siqueira DS (2015) Procedures using diffuse reflectance spectroscopy for estimating hematite and goethite in Oxisols of São Paulo, Brazil. Geoderma Reg 5:150–156.

Fageria NK, Moreira A, Castro C, Moraes MF (2013) Optimal acidity indices for soybean production in Brazilian Oxisols. Commun Soil Sci Plant Anal 44:2941–2951.

Inagaki TM, de Moraes Sá JC, Caires EF, Gonçalves DRP (2017) Why does carbon increase in highly weathered soil under no-till upon lime and gypsum use? Sci Total Environ 599–600:523–532.

Jacobs B, Shen J, Chan NI, et al (2015) Integrating legacy soil phosphorus into sustainable nutrient management strategies for future food, bioenergy and water security. Nutr Cycl Agroecosystems 104:393–412.

Kruse J, Abraham M, Amelung W, et al (2015) Innovative methods in soil phosphorus research: A review. 43–88.

Lounsbury AW, Wang R, Plata DL, et al (2019) Preferential adsorption of selenium oxyanions onto {1 1 0} and {0 1 2} nano-hematite facets. J Colloid Interface Sci 537:465–474.

Mendez JC, Hiemstra T (2020) Ternary complex formation of phosphate with Ca and Mg ions binding to ferrihydrite: experiments and mechanisms. ACS Earth Sp Chem 4:545–557.

Poggenburg C, Mikutta R, Schippers A, et al (2018) Impact of natural organic matter coatings on the microbial reduction of iron oxides. Geochim Cosmochim Acta 224:223–248.

Rowley MC, Grand S, Verrecchia ÉP (2018) Calcium-mediated stabilisation of soil organic carbon. Biogeochemistry 137:27–49.

Sakharov BA, Drits VA, McCarty DK, Walker GM (2016) Modeling powder X-ray diffraction patterns of the clay minerals society kaolinite standards: KGA-1, KGA-1b, and KGa-2. Clays Clay Miner 64:314–333.

Schaefer C, Fabris JD, Ker JC (2008) Minerals in the clay fraction of Brazilian Latosols (Oxisols): A review. Clay Miner 43:137–154.

Stachowicz M, Hiemstra T, van Riemsdijk WH (2008) Multi-competitive interaction of $As_{(III)}$ and $As_{(V)}$ oxyanions with Ca^{2+}, Mg^{2+}, PO_3^{-4}, and CO_2^{-3} ions on goethite. J Colloid Interface Sci 320:400–414.

Weng L, Van Riemsdijk WH, Hiemstra T (2012) Factors controlling phosphate interaction with iron oxides. J Environ Qual 41:628–635.

Yan Y, Wan B, Jaisi DP, et al (2018) Effects of *Myo*-inositol Hexa*kis*phosphate on $Zn_{(II)}$ sorption on γ-Alumina: A mechanistic study. ACS Earth Sp Chem 2:787–796.

Yoshimura T, Tamenori Y, Takahashi O, et al (2015) Mg coordination in biogenic carbonates constrained by theoretical and experimental XANES. Earth Planet Sci Lett 421:68–74.

Zoca SM, Penn C (2017) An important tool with no instruction manual: A review of gypsum use in agriculture, 1st edn. Elsevier Inc.

2. PHOSPHATE AND *myo*-INOSITOL HEXA*KIS*PHOSPHATE ADSORPTION ONTO HEMATITE AS AFFECTED BY CATIONS AND pH

ABSTRACT

Myo-inositol hexa*kis*phosphate (IHP_6) is typically the most abundant and reactive form of organic phosphorus (P_o) in soils, especially with Al- and Fe-(hydr)oxides because of the presence of six phosphates in its structure. In this study, the effects of pH and cations (Ca and Mg) were investigated in batch experiments using *in-situ* attenuated total reflectance Furrier transform infrared (ATR-FTIR) spectroscopy and Mg *K*-edge X-ray Absorption Spectroscopy (XAS). The results indicate that IHP_6 has more complex IR-spectra than inorganic phosphate, even though both share certain bands of absorbances. Both Ca and Mg influenced the adsorption of IHP_6 on hematite surfaces. This influence was not so evident for phosphate. The variation in pH promoted the shift of several bands in the adsorbed IR-spectra. As for the adsorption kinetics, IHP_6 was sensitive to a pH change from 4.5 to 6.5, with a reduction in the adsorption rate at the highest pH. Phosphate, on the other hand, presented a more intense adsorption kinetics, with equilibrium after ~80 min. Two adsorption mechanisms were identified for IHP_6 and phosphate kinetics, without influence of the studied cations. However, differences in the shape of XAS spectra at the Mg *K*-edge revealed that there was probably a change in the atomic environment of Mg caused by its association with phosphate. In other evaluated organic molecules, such as IHP_6 and citrate, this effect was not observed due to the high proportions of $MgCl_2$ in the linear combination fitting (LCF). In general, the results enhance molecular-level understanding of oxyanions adsorption onto hematite surfaces that can be applied and predict IHP_6 and phosphate behaviors in oxidic soils.

Keywords: Colloidal systems; *in-situ* IR-spectroscopy; ternary complexes; Fe-oxides

2.1. Introduction

Approximatelly 30% of the total ice-free land area in the world (4 billion ha) is affected by acidity (Sumner and Noble, 2003). The low pH_{H_2O} (typically < 4.5) and the presence of exchangeable aluminum ($_{EX}Al$) restricts crop production worldwide (Kochian et al., 2004). Lime ($CaCO_3$+$MgCO_3$·H_2O) application is required in these soils to increase pH and narrow soluble and $_{EX}Al$ concentrations to negligible levels (Fageria and Baligar, 2008).

In addition to these benefits, long-term increases in soil organic carbon (SOC) by liming have been widely reported (Briedis et al., 2012a; Briedis et al., 2012b; Carmeis

Filho et al., 2017; Inagaki et al., 2017; Auler et al., 2019). For example, Murphy (2007) reported increases in organic phosphorus (P_o) mobility due to the continuous use of lime. Therefore, clarifying liming effects on soil organic components is essential to improve management practices that can reduce food security instability and yield fluctuations by climatic plights (Fornara et al., 2011).

The increase in soil organic matter (SOM) contents in limed soils is related to the increase in biomass production and the stabilization of organic compounds by calcium (Ca) (Mikutta et al., 2007; Wuddivira and Camps-Roach, 2007; Briedis et al., 2012a; Sowers et al., 2018b). Rowley et al. (2018) classified the mechanisms for Ca-mediated soil OC stabilizaiton in: (**i**) SOC occlusion by increasing soil aggregation by Ca ions; (**ii**) increased aggregate stability and SOC inclusions by $CaCO_3$ inputs; and (**iii**) organo-mineral interactions.

Advances in the knowledge of synergism in the triad mineral-metal-organic compounds has been fairly investigated over time (Davis and Bhatnagar, 1995; Weng et al., 2005; Weng et al., 2009; Sowers et al., 2018b; Yan et al., 2018a). However, limes employed in agriculture generally contain $CaCO_3$ and $MgCO_3$ in varied proportions. The use of dolomitic lime [$CaMg(CO_3)_2$] has been increasing in humid tropical agriculture, due to magnesium (Mg) deficiency in crops (Gerendás and Führs, 2013), and this is because the amounts of Mg released from weathering of Mg-bearing minerals do not meet the plants demand to sustain crop yields in highly weathered soils. Therefore, there is a lack of information about the effects of Mg on these ternary systems, especially those involving Fe oxides and organic compounds containing phosphate.

A strong evidence for Fe-Ca-OC ternary complex formation has been reported by Sowers et al. (2018ab) who concluded that Ca incorporated into ferrihydrite-Ca-OC samples was of poorly crystalline or amorphous nature, and Adhikari et al. (2018) who highlighted that Ca affected the chemical composition of incorporated OC and the mineral phase transformation of Fe during reduction. Precisely, Ca favored the incorporation of more aromatic- and phenolic-OC into co-precipitates ferrihydrite-Ca-

OC in relation to carboxylic OC. However, there is still a lack of information about direct molecular observations of Mg effects in similar systems.

Organic forms of phosphorus (P) such as *myo*-inositol hexa*kis*phosphate (IHP_6) are molecules highly retained by the surface of Fe- and Al-(hydr) oxides in natural environments. Among all possible isomers, *myo* is the most stable form of insotiol under natural conditions (Kremer et al., 2020). The IHP_6 is typically the most abundant organic form of P (P_o) in soils, reaching over 80% of P_o in certain soils. The adsorption of IHP_6 in hematite (Hm) occurs through their phosphate groups, which react with the surface of the oxide in an identical way as the free $PO_{4(aq)}$ ions by OH groups and ligand exchange with the H_2O (Goldberg and Sposito, 1985). The specific molecular arrangement and bonding formation, however, depend on the surface features of each mineral (Celi et al., 1999; Celi et al., 2003; Martin et al., 2004), and the investigation of divalent cations effects on sorption of these type of molecules is required to improve the modeling of C and P cycles in natural environments.

The propensity of each cation to form inner sphere complexes with SOC is not as well understood as the affinity of cations for non-specific exchange sites (Essington, 2015). Due to the high surface area, minerals such as ferrihydrite (Fh) are commonly used in experiments involving adsorption of organic matter and oxyanions. However, Fh is not frequent in humid tropical soils, being restricted to continuous poor drainage conditions, whereas Hm is common, especially in Oxisols (Kämpf and Curi, 2003; Singh et al., 2014). Nevertheless, Hm is the most thermodynamically stable iron oxide and is frequent in natural systems with highly weathered soils and low OC amounts.

In aqueous systems, Ca and Mg have different hydrated ionic radius [$Ca(H_2O)_8^{2+}$ - 0.11 nm] and [$Mg(H_2O)_8^{2+}$ - 0.08 nm] and different molecular configurations. Magnesium has octahedral configuration while Ca square antiprism. Based on this, we hypothesize that Mg is not as efficient as Ca in the formation of ternary Hm-Mg-IHP_6. To probe this hypothesis, we employed in-situ attenuated total reflectance Furrier transform infrared (ATR-FTIR) spectroscopy experiments, a non-invasive technique that allows the quantification of organic or inorganic molecules

adsorbed on the Hm surface under continuous flow in a closed system. The vibrational character of the measurement also provides information on the type of bonding between the adsorbent and the adsorbate. In addition, we employed X-ray Absorption Spectroscopy (XAS) on the Mg *K*-edge in Hm colloidal suspensions to understand in depth how the chemical environment around Mg atoms was influenced by the presence of organic molecules. Thus, the objective was to investigate the effects of Mg and pH in IHP_6 and phosphate molecular adsorption on the Hm surface.

2.2. Material and methods

2.2.1. Chemicals and hematite synthesis

All solutions were prepared with ultrapure water (Millipore, Bedford, USA), and all chemicals were of analytical reagent grade without any further purification. The solutions containing IHP_6 were made from a *myo*-inositol hexa*kis*(dihydrogen-phosphate) solution (50% w/w) in H_2O obtained from Sigma-Aldrich (#593648). The inorganic phosphate solutions were made from Na_2HPO_4 (>99% of purity) also obtained from Sigma-Aldrich (#S9763).

Hematite was synthesized according to the method of Cornell and Schwertmann (2003). Briefly, 60 ml of 1 mol l^{-1} ferric chloride (ACS reagent, 97% Sigma-Aldrich) solution were dropped from a 60-ml burette into 750 ml of boiling ultrapure water (UW) preheated to ~97ºC, mixing on a hot plate. The resulting suspension was kept at room temperature (~20°C) for 24 h to cool and dialyzed against UW (Nominal MWCO 6000-8000, Fisher Scientific) until the conductivity of the solution was below 18 µS. A portion of the suspension was frozen (-25ºC) for 24 h, freeze-dried (-40ºC) for 72 h and disaggregated with an agate mortar to be stored in a desiccator.

The crystal structure of Hm was identified by X-ray diffraction (XRD) with a Rigaku Ultima IV X-ray diffractometer (Rigaku Corp., Tokyo, Japan) equipped with a 1D D/teX Ultra detector using CuKα radiation (λ = 1.5418 Å). The diffractometer was

operated at 40 kV tube voltage and 40 mA tube current with a scanning rate of 1º min^{-1} at the step size of 0.02º2θ. The minerals were also subjected to Scanning Electron Microscopy (SEM) in a Phenom G2Pure (Phenom-World, Eindhoven, Netherlands) to verify the minerals morphology *(supplementary material)*. The external surface area of Hm was 70.2 m^2 g^{-1}, estimated by applying the Brunauer-Emmett-Teller (BET) equation to the N_2 sorption data.

The powdered Hm was dispersed (10 g l^{-1}) in 0.01 mol l^{-1} NaCl background electrolyte solutions, and the pHs were adjusted to 4.5 and 6.5 with 0.1 and 0.01 mol l^{-1} HCl and NaOH. The dispersions remained stirred for 72 h and during this period the pH was checked and readjusted, when necessary, every 8 h. During these readjustments, the dispersions were purged with $N_{2(g)}$ for 20 min. After this period, the pH values stabilized. A portion of the dispersions was collected and centrifuged (3000 ×g for 30 min) so that the supernatants had the P concentrations determined as negligible by inductively coupled plasma mass spectrometry (ICP-MS). The ready-made Hm dispersions with pH set at 4.5 or 6.5 were kept at room temperature (20±2ºC) under dark to avoid degradation.

2.2.2. ATR-FTIR experiments

All solutions used during the ATR-FTIR measurements were boiled for ~10 min and purged (20 min) with $N_{2(g)}$ while cooling at ~20°C to avoid partitioning of atmospheric CO_2 into solutions. The $N_{2(g)}$ purging process in the sealed vessel continued throughout all data collection time. The IR equipment was an Invenio-R FTIR spectrometer (Brunker Corp., Karlsruhe, Germany) equipped with a Balston-Parker purge gas generator and liquid N_2-cooled mercury-cadmium-telluride (MCT-A) detector.

The analyses were performed using a Bruker Platinum ATR with a single-bounce zinc selenite/diamond internal reflective element and 45° of incidence angle. During measurements, both the instrument and sample compartments were continuously purged with dry air. Spectra represents an average of 256 scans collected

at 4 cm^{-1} resolution. Collected FTIR spectra were truncated, baseline-corrected, and integrated using OPUS v.8.1 software. The truncation limits were selected to minimize the distortion from baseline correction and to avoid interference of H_2O bands and minor negative bands related to CO_2 that despite the presence in some spectra, did not affect the interpretation or deconvolution fits for adsorbed spectra. A simplified diagram of how the equipment works in a closed system is present in the supplementary material.

Before the beginning of the experiments, tests were carried out with 25 mmol l^{-1} of IHP_6 or phosphate at varying pHs to verify their IR-spectra shape in 0.01 mol l^{-1} NaCl solutions. The pH of these solutions was corrected using negligible amounts of 0.1 or 0.01 mol l^{-1} NaOH or HCl. During these measurements, the vessel was covered with aluminum foil to avoid possible degradation by light.

In the adsorption studies, Hm films were made from drop casting 10 µl of Hm suspensions (10 g l^{-1}) over the ATR crystal with pre-established pH of 4.5 or 6.5. The suspension was then dried under $N_{2(g)}$ flow during ~5 min, until the formation of a film, with no apparent residual water. Upon this dried Hm film, an additional 10 µl Hm suspension was drop cast to ensure the complete coverage of the crystal and the water removal by $N_{2(g)}$ flow was repeated. With Hm's film prepared, the background solution (0.01 mol l^{-1} NaCl) was passed through the film at a rate of 1.3 ml min^{-1} using a peristaltic pump (Thermo Scientific, FH100).

The collection of background spectra occurred first at pH 4.0, after stabilization the pH was adjusted to 9.0, and after a new stabilization adjusted to 4.5 or 6.5, depending on the pH studied in the experiment. These changes in the pH of the flowing background solution guaranteed the removal of unwanted ions that could be adsorbed to the surface of Hm, such as carbonate. The spectra of the background solution were obtained every 1 min, which allowed us to accurately assess the moment when stabilization occurred. In general, the background acquisition took ~3 h, and after that a final background was collected and the ions of interest were added to the vessel with syringes.

For the adsorption kinetics investigations, the final concentrations of 25 µmol l^{-1} of inorganic phosphate or IHP_6 solutions flowed over the Hm film for ~4 h, with 1 spectrum min^{-1}. The adsorption kinetics were run in duplicate for each set of solutions. For the modeling of adsorption, the following modified equations of the Langmuir-Freundlich (Eq. 1) kinetic model, also known as Sips model, was used:

$$IA_{(t)} = A_e \cdot k \cdot t^n / 1 + k \cdot t^n \qquad \text{Eq. 1.}$$

in which $IA_{(t)}$ is the phosphate or IHP_6 band integral (a.u.) at a specific adsorption time (t) in min, A_e is the phosphate or IHP_6 band integral (a.u.) at equilibrium (the last one), k is an empirical constant and n is the model exponent. The adsorption kinetics fitting was performed in the Origin 2020 software (Northampton, MA, USA). For this, the integrated areas of each spectrum were used in the range of 1200-750 cm^{-1} for phosphate and 1250-750 cm^{-1} for IHP_6 and scaled to maximum sum of weighted MCR components. Especially for kinetics, the spectra were not normalized since the differences between areas of the bands were crucial for obtaining the results.

For the pH envelope investigations, the initial 0.01 mol l^{-1} NaCl background electrolyte was pumped through the flow cell in the same way as described previously. However, in the last stage of obtaining the background, the pH was kept at 8.5. Following equilibration of the Hm deposit with the background solution, 25 µmol l^{-1} IHP_6 or phosphate was added at the vessel, and immediately thereafter 0.3 mmol l^{-1} Ca, Mg or neither was added. The adsorption of the molecules was examined every minute with a new IR spectrum.

When there was no longer a visual difference between the spectra (stabilization), a final spectrum was collected for a determined pH by the average of 4500 scans. After that, the pH of the solution was reduced to 7.5 (with 0.1 or 0.01 HCl) and the process repeated to obtain a new final spectrum at this pH after the new equilibrium, similarly to that performed by Elzinga and Sparks (2007). The pH range evaluated was 3.5-8.5 for both phosphate and IHP_6.

2.2.3. Mg *K*-edge XANES

Eight samples and 19 standards, including reagents and minerals, comprised our set for Mg speciation at the *K*-edge in the SGM (High Resolution Spherical Grating Monochromator) beamline 11ID-1, which belongs to the Canadian Light Source (CLS). The samples were produced by mixing Hm dispersions and solutions containing Mg and other ions such as citrate, phosphate or IHP_6. Citrate was used as an organic molecule reference for the formation of ternary systems. Each dispersion was balanced with the ions in two conditions of pH, 4.5 or 6.5, following what was done in the experiments with ATR-FTIR. The final concentrations of Hm were 5 g l^{-1}, Mg was 4 mmol l^{-1}, phosphate was 4 mmol l^{-1} and IHP_6 was 0.66 mmol l^{-1} (what yields 4 mmol l^{-1} total P, considering six phosphates per molecule), and citrate was 0.67 mmol l^{-1} what yields 4 mmol l^{-1} total C, all with 0.05 mol l^{-1} NaCl as electrolyte.

The standards were MgO (Mg oxide), $Mg(CH_3COO)_2$ (Mg acetate), $Mg(NO_3)_2{\cdot}6H_2O$ (Mg nitrate hydrate), $Mg_3(PO_4)_2{\cdot}nH_2O$ (Mg phosphate hydrate), $MgHPO_4{\cdot}3H_2O$ (Mg phosphate dibasic trihydrate), $Mg(OH)_2$ (Mg hydroxide), $MgSO_4$ (Mg sulfate anhydrous), biotite, dolomite, hectorite, labradorite, serpentine, sepiolite, ripidolite, phlogopite, monticellite, magnesite, drop coated 4 mmol l^{-1} $MgCl_2$ solution, and drop coated 0.66 mmol l^{-1} IHP_6 + 4 mmol l^{-1} $MgCl_2$ solution. On average, 15 scans were required for the samples, which were drop coated and air-dried on gold slides (Au). As for the standards samples, such as Mg-bearing minerals and Mg reagents, the number of scans needed ranged from 5 to 10.

Standard samples were disaggregated in agate crucibles, passed through 125-mesh screens and then analyzed in powder form. The solid samples were spread uniformly on carbon tapes and mounted on a sample holder. X-Ray absorption data were collected in partial fluorescence yield using a Silicon Drift Detector (SDD) in the 1300 up to 1350 eV emission range and. Magnesium oxide (MgO) was used to calibrate the Mg K-edge, (E0 ~1309 eV). Previously merged, unsmoothed and energy calibrated

(at the maximum of the first derivative) spectra were normalized at Athena software (Ravel and Newville, 2005).

The background pre-edge range was from E0 -9 to E0 -5 eV, and the normalization range from E0 +22 to E0 +40 eV. The linear combination fitting (LCF) was preceded by a visual inspection of the main features in samples and standards and performed over the -8 to +30 eV photon energy range in relation to E0. The sum of Mg species was not constrained to 100%, with fits only accepted when the sun of the percentages was in the range of 90-110%.

2.3. Results and discussion

2.3.1. Phosphate and IHP_6 spectra in solutions

The IR spectra of $IHP_{6(aq)}$ under a range of pH values was similar to those reported by Guan et al. (2006) and Yan et al. (2018b). There was a marked *v*3 band at 1072 cm^{-1} that did not manifest changes due to pH variation (Fig. 1a). Something similar was observed in 1077 cm^{-1} for the phosphate spectra (Fig. 1b). At low pHs (~4.0 – 5.0), IHP_6 presented intense peaks at 937 and 1083 cm^{-1} that probably correspond to *v*3 vibrations and occur due to decreased symmetry in the molecule caused by the protonation of the oxyacid ligand, as reported by Yan et al. (2014). More specifically, the 937 cm^{-1} band corresponds to P-OH vibration in the *myo*-inositol structure (Guan et al., 2006).

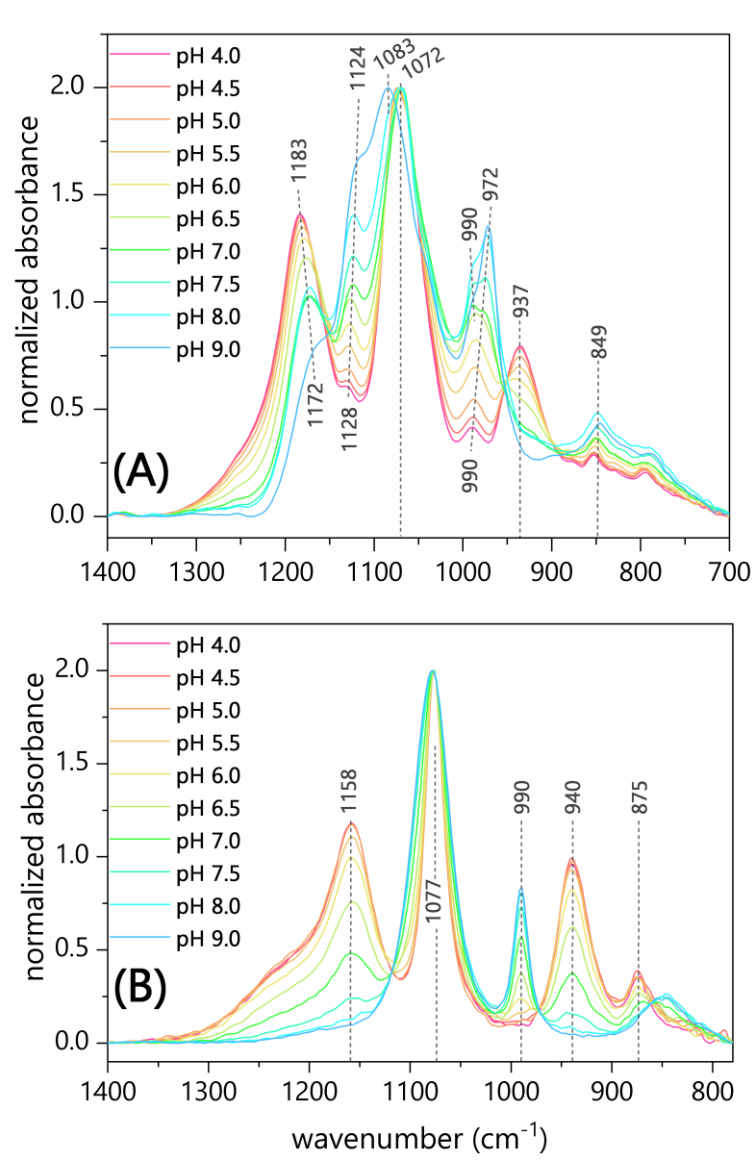

Figure 1. ATR-FTIR aqueous spectra of 25 mmol l^{-1} *myo*-inositol hexa*kis*phosphate (IHP_6) (**A**) and 25 mmol l^{-1} phosphate (**B**) at different pH values.

Interestingly, the band corresponding to the P-O asymmetric stretching vibration in the HPO_3^- terminal varied in position, ranging from 1172 to 1183 cm^{-1}, values close to those reported by Yan et al. (2018b) who observed this band in 1177 cm^{-1}. At high pH (> 8.0), low protonation caused marked changes in the spectrum, especially in the 1072 cm^{-1} band that was shifted to 1083 cm^{-1}. The *v*3 band at 990 cm^{-1}, corresponding to symmetric P-O stretching vibration, split with pH increase in two bands at 990 and 972 cm^{-1} (Fig. 1a). At high pH the peak at 849 cm^{-1} also increases its relative intensity. For Elzinga and Sparks (2007), this peak corresponds to a *v*1 band

and is more intense with the decrease in symmetry. The band at 1128-1124 cm^{-1} can be assigned to asymmetric ν(P-O-C), and intensifies to pH 12, in which IHP_6 becomes unprotonated as $C_6H_6(PO_4^{2-})_6$ ion (Guan et al, 2006).

The IR spectra of aqueous phosphate species, *i.e.* $H_3PO_4^0{}_{(aq)}$, $H_2PO_4^{1-}{}_{(aq)}$, $HPO_4^{2-}{}_{(aq)}$, $PO_4^{3-}{}_{(aq)}$, has previously been described in detail by Tejedor-Tejedor and Anderson (1990). Under low pH (4 – 5.5), the higher protonation in the phosphate ions (mostly composed of $H_2PO_4^-$) reduces the symmetry of C2*v*, dividing the ν3 vibration into three bands (940, 1077 and 1158 cm^{-1}) and the ν1 band at 875 cm^{-1} that were identified in Fig. 1b.

With the deprotonation caused by the pH increase in the solution, the vibration of these bands lost intensity. This happened due to the formation HPO_4^{2-} that was confirmed by the presence of ν3 bands at 1077 cm^{-1}, and increasing intensities of the ν3 band at 990 cm^{-1} (Fig. 1b), which occurs due to the reduction in the symmetry of phosphate ions from Td to C3*v* (Elzinga and Sparks, 2007). In general, the IR spectra of inorganic phosphate have bands that are simpler to identify because of the greater structural complexity of the IHP_6 molecule and the greater susceptibility to variations in the ligand symmetry (Guan et al., 2006).

2.3.2. IHP_6 and phosphate pH envelopes in hematite

For both phosphate and IHP_6, the stretching vibration of the P-O bond should be the focus of FTIR analysis because IHP_6 is complexed in hematite surfaces through the phosphate groups. The in-situ ATR-FTIR spectra IHP_6 and phosphate on hematite as a function of pH and cations (Ca or Mg) are illustrated in Fig. 2. In addition to the changes expected by pH variation, the presence or not of cations promoted changes in the shapes of IR spectra of both phosphate and IHP_6. The IR spectra of adsorbed IHP_6 revealed broader bands when compared to the solution $IHP_{6(aq)}$ IR spectra. More specifically, shoulder peaks at ~1113, 1006 and ~970 cm^{-1} appeared (Fig. 2). Something similar occurred for phosphate, which also presented broader peaks at ~1113, ~1040 and 1006 cm^{-1}.

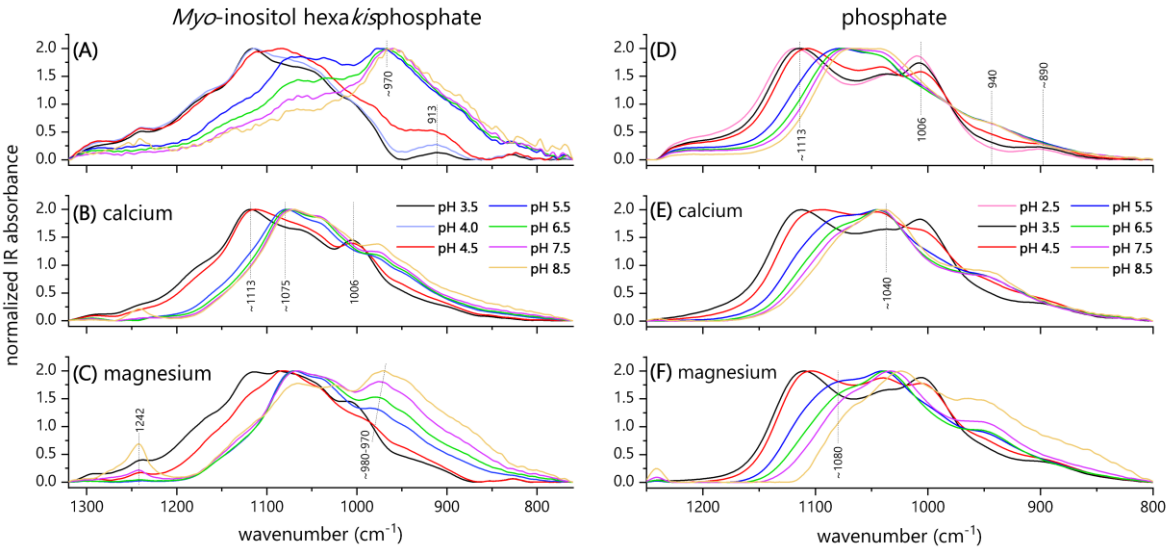

Figure 2. Baseline corrected and normalized ATR-FTIR spectra of 25 µmol l^{-1} IHP_6 (**A, B, C**) or phosphate (**D, E, F**) in the presence or not of cations (0.3 mmol l^{-1} Ca or Mg) under 0.01 mol l^{-1} NaCl ionic strength in a range of pH values.

The pH increase promoted a shift from 1113 cm^{-1} band to ~1075 cm^{-1} in IHP_6, and from 1113 cm^{-1} to ~1080 cm^{-1} due to the deprotonation. For Persson et al. (1996), bands between 1075-1065 are caused by symmetric P-O vibrations in the HPO_3^- group. In Fig. 2a the decrease in the 1075 cm^{-1} band is linked to the increase in the number of HPO_3^- groups under higher pHs (7.5-8.5). The decrease of this peak did not occur (Fig. 2b; Fig 2c) in the presence of cations, and this may be related to the retention of a cation (Ca or Mg) in two HPO_3^- groups in the IHP_6 molecule, interrupting the reduction of vibration by increasing the HPO_3^-.

Another effect of the presence of cations in the system was the lower variation of the band at 970 cm^{-1} with pH, which was more evident in the presence of Ca than in the presence of Mg (Fig. 2b; Fig 2c). The peak at ~970 cm^{-1} is usually assigned as an asymmetric P-O-C vibration, as reported by Guan et al. (2006) in IHP_6 adsorbed on Al-hydroxide. Regardless of the physical-chemical reason that led to the decrease in vibrations variation, the presence of cations made the IHP_6 adsorbed to hematite does not maintain the same structural symmetry as the pure IHP_6. This is probably due to

the binding of these cations to the phosphates of the IHP_6 and implies that the addition of amendments as lime or gypsum in oxidic soils can influence the adsorption of IHP_6.

In the highest pH values (8.5-7.5) the IR spectra of phosphate was dominated by frequencies centered at ~1080, 1040 and 940 cm^{-1}. According to Elzinga and Sparks (2007), this suggests the presence of a single phosphate species. After pH decreases, the 1085 cm^{-1} band shifts to higher wavenumbers and a new band at 1006 cm^{-1} becomes evident (Fig. 2). The presence of this new band (1006 cm^{-1}) and maintenance of shifted peaks at ~1113 cm^{-1} is an indicative that two diverse phosphate surface complexes are present in the hematite surface, probably an inner followed by an outer-sphere complex. Elzinga and Sparks (2007) attributed this phenomenon to the presence of a complex that dominates at high pHs and to another surface complex that gains importance as the pH decreases.

Our results are in line with those of Elzinga and Sparks (2007). We observed, however, the presence of the 1006 cm^{-1} band only up to pH 4.5 (Fig. 2), although Elzinga and Sparks (2007) reported the presence of this band up to pH values close to 7.0. Unlike IHP_6, the presence of cations did not promote drastic changes in the shape of the spectra for phosphate. However, the phosphate spectrum with Mg (Fig. 2f) had a wider variation in the relative intensity of the band at 940 cm^{-1}, usually assigned as $\nu 3$ vibration of $H_2PO_4^-{}_{(aq)}$. The lower vibrations variation for adsorbed phosphate compared to IHP_6, is probably due to the simpler chemical structure and less probability of formation of ionic pairs or molecular conglomerates with the studied cations.

2.3.3. IHP_6 and phosphate adsorption kinetics in hematite

The adsorption kinetic models generated from baseline-corrected IR-spectra of IHP_6 and phosphate into hematite at pH 4.5 or 6.5 in the presence or absence of cations are depicted in Fig. 3. The relative intensities of IR absorption increased with time in all conditions, indicating increased accumulation of IHP_6 or phosphate on hematite surfaces *(supplementary information)*. In general, phosphate manifested a

first rapid adsorption pattern followed by an equilibrium stage after ~80 min (Fig. 3c; Fig. 3d).

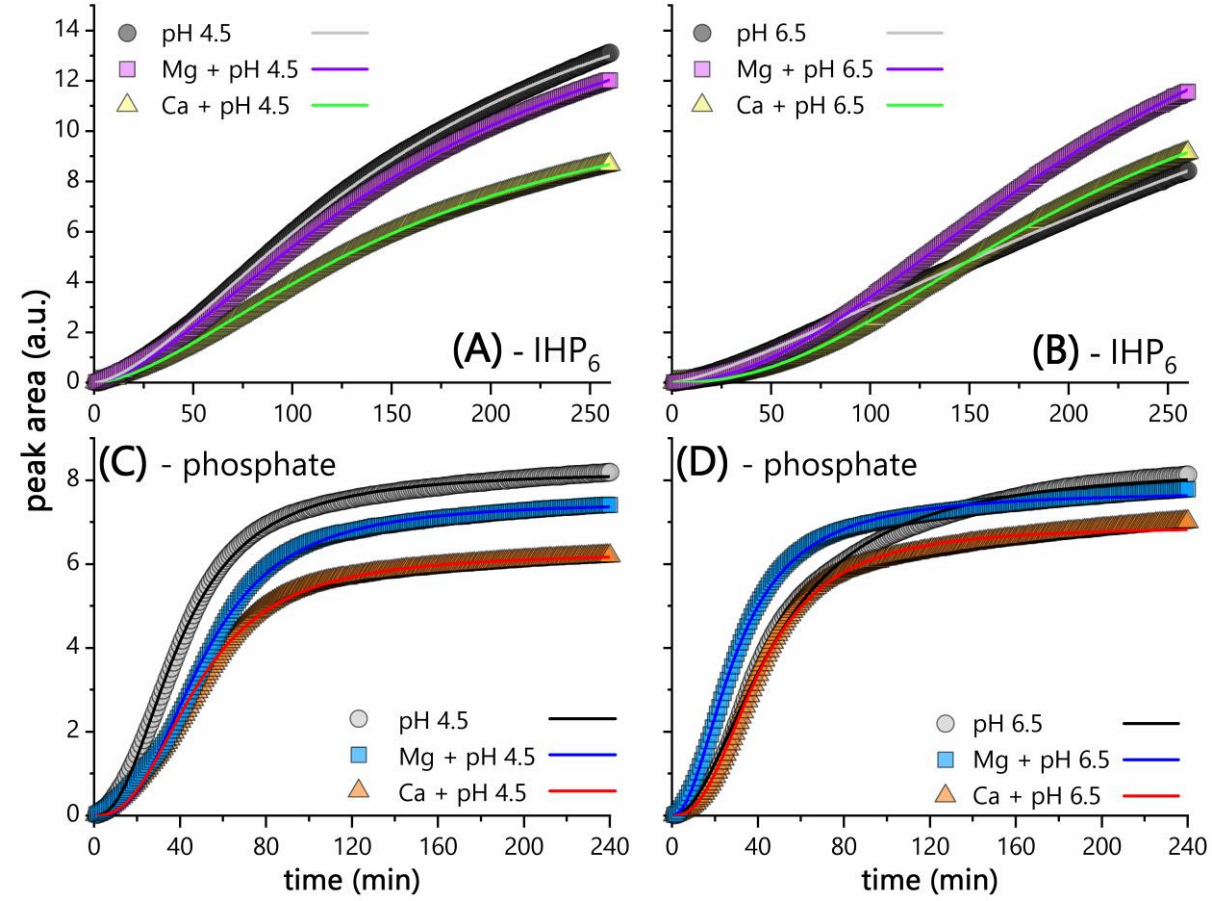

Figure 3. Adsorption kinetic curves as a function of time for the adsorption of 25 µmol l^{-1} IHP_6 (**A, B**) or phosphate (**C, D**) on hematite (0.2 mg film) in the presence of either 0.3 mmol l^{-1} Ca or Mg or absence of cations under 0.01 mol l^{-1} NaCl ionic strength. Markers in the kinetics curves represent experimental data obtained by integrating the areas of the phosphate (1200-750 cm^{-1}) or IHP6 (1250-750 cm^{-1}) bands in (a.u.), while the lines represent the fit using the Langmuir-Freundlich kinetic model.

The equilibrium adsorption of IHP_6 or phosphate is usually reached after ~60 min (Yan et al, 2014). However, in our study, the stabilization of the IHP_6 curves occurred after longer periods. This slower kinetics of IHP_6 in relation to phosphate was probably linked to the low concentrations of IHP_6 used. Another factor that may have caused this is the natural lower maximum adsorption capacity of IHP_6 (0.67 µmol m^{-2}) in relation to phosphate (1.78 µmol m^{-2}) in hematite, as reported by Yan et al. (2014). As a larger molecule than phosphate, IHP_6 has its adsorption restricted to the hematite

surface, while phosphate can easily diffuse into Fe-oxide micropores and also be adsorbed on the surfaces.

The first-order Langmuir adsorption kinetic model predicted a linear dependency of the apparent rate of IHP_6 or phosphate adsorption. This linear dependence was identified only in part of the adsorption process and was preceded by a non-linear dependence in the rate plots *(supplementary material)*. Thus, the Langmuir kinetic model could not be successfully used to compare the kinetic experiments in the present study. In this case, an adaptation to the Langmuir-Freundlich adsorption isotherm model was able to efficiently predict the results.

The model variables were adjusted using least-squares fit and revealed variations across samples in its parameters (Table 1). The curvature in the initial phase of adsorption, before equilibrium, is defined by parameter *k* of the model. The low variation of this parameter in the phosphate curves reveals that there was little influence of pH (4.5 or 6.5) and the presence of cations in the medium during adsorption. However, for IHP_6, despite no noticeable changes due to cations, the adsorption kinetic pattern was influenced by pH because increases from 4.5 to 6.5 amplified the initial curvature of the models (Fig. 3a; Fig 3b), as identified by the lower *k* values (Table 1).

Table 1. Kinetics parameters for phosphate and IHP_6 adsorption on hematite under 0.01 mol l^{-1} NaCl ionic strength in pH 4.5 or 6.5 in the presence of cations.

sample	A_e	*k*	*n*	chi-sqr	R^2
Phosphate 4.5	8.21±0.01	2.05E-	2.30±0.01	0.005	0.999
Phosphate 4.5+Mg	7.49±0.01	3.06E-	2.64±0.03	0.012	0.997
Phosphate 4.5+Ca	6.27±0.01	5.77E-	2.51±0.02	0.007	0.998
Phosphate 6.5	8.34±0.02	4.53E-	1.99±0.02	0.013	0.997
Phosphate 6.5+Mg	7.74±0.01	9.33E-	2.05±0.02	0.006	0.998
Phosphate 6.5+Ca	6.90±0.01	1.03E-	2.47±0.02	0.009	0.997
IHP_6 pH 4.5	18.81±0.08	3.24E-	1.56±0.005	0.002	0.999
IHP_6 pH 4.5+Mg	18.47±0.07	2.83E-	1.58±0.005	0.002	0.999
IHP_6 pH 4.5+Ca	12.65±0.05	2.23E-	1.65±0.006	0.001	0.999
IHP_6 pH 6.5	27.12±0.34	2.88E-	1.32±0.004	0.001	0.999
IHP_6 pH 6.5+Mg	20.57±0.13	2.23E-	1.97±0.007	0.002	0.999
IHP_6 pH 6.5+Ca	14.64±0.07	8.21E-	2.19±0.007	0.001	0.999

myo-inositol usually forms multiple bonding on Hm surfaces (Yan et al., 2014) because of the various possibilities of association between the phosphate groups and the Hm surface. In certain microregions of the mineral surface, it is possible that several phosphate groups of the IHP_6 molecule are adsorbed to electronegative sites, and this adsorption can occur by means of mono or binuclear complexes (Fig. 4). The great diversity of association makes the IHP_6 more susceptible to the influence of pH during the adsorption process. This can occur when one or two phosphate groups lose protons while the others maintain it, influencing the adsorption of the molecule as a whole. In the case of free phosphate ions, the variation in H^+ and OH^- in the system influences each ion individually.

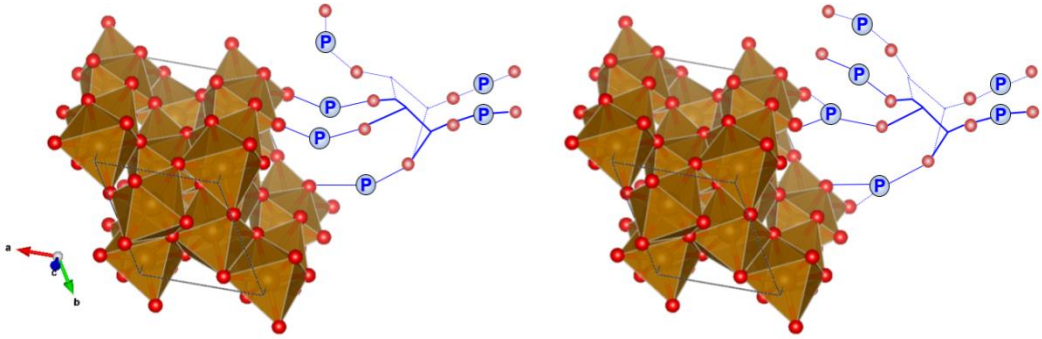

Figure 4. Some possible forms of molecular interaction between IHP_6 and hematite surface, adapted from Ognalaga et al. (1994).

2.3.4. Mg *K*-edge XANES

Most of the Mg species identified in the samples were $MgCl_2$ because this was the form of Mg added to Hm's suspension, which precipitated after the dehydration of Hm slurries drops. Attempts were made to perform the speciation with slurries on liquid cells. However, the high number of scans (> 80) and the low quality of the spectra made us analyze the samples in the drop coated way. The standard samples were analyzed in solid state (powder), which is in line with the option to measure the samples in solid state as well. The R-factor values found varied from 0.0059 to 0.0291, which represents

a reasonable data fitting (Table 2). The weighting factors did not exceed the predetermined range (90 to 110%), concentrating from 98 to 101%.

Table 2. Relative proportions of reference Mg samples based on linear combination fitting analysis of Mg K-edge XAS data.

Sample	$MgCl_2$	$MgCO_3$	$MgNO_3$	$MgHPO_4$	IHP_6 sol.	Pi sol.	R-factor [a]
	% Mg species (uncertainty) [b]						
IHP_6 (pH 4.5)	91 (1.5)	--	--	--	9 (1.1)	--	0.02869
IHP_6 (pH 6.5)	83 (2.8)	--	17 (0.5)	--	--	--	0.02905
Pi (pH 4.5)	29 (2.5)	--	--	31 (0.6)	--	40 (2.6)	0.01454
Pi (pH 6.5)	26 (2.7)	--	--	44 (0.7)	--	29 (2.8)	0.01350
citrate (pH 4.5)	93 (1.0)	07 (0.2)	--	--	--	--	0.00595
citrate (pH 6.5)	79 (1.6)	--	21 (0.8)	--	--	--	0.00470

[a] R-factor = ∑[(data-fit)2]/∑(data2) (Kelly et al., 2008).
[b] data have been re-normalized to sum 100% with uncertainties calculated in Athena; numbers in parentheses represent the uncertainties of the values.

In general, the Mg K-edge spectra are rich in features, with the reference samples revealing contrasting spectral characteristics *(supplementary material)*. Our results are in agreement with those obtained by Sánchez Del Río et al. (2005) and by Yoshimura et al. (2013), which carried out Mg speciation in a series of geological samples. These features can be observed by several variations in terms of shapes and intensities in the pre- and post-edge regions. The variations are more concentrated in the photon energies between 1305-1325 eV. The $MgCl_2$ drop coated solution (4 mmol l^{-1}) in particular manifested spectra with a small pre-edge feature at 1307 eV, and a shoulder between 1310-1311 eV after the most intense peak that concentrated at ~1309 eV.

The spectra generated by the LCF were quite similar to the $MgCl_2$ spectra in Hm slurries with IHP_6 and citrate (that was used as an organic compound reference) due to the high proportion of this salt in the samples (Fig. 5a; Fig. 5c). As there was no visual variation between spectra containing the same molecules at pH 4.5 and 6.5, only the first ones were shown in Fig. 5. However, taking just phosphate slurries into account, the shape observed was different in relation to IHP_6 and citrate, with two wide peaks between 1309-1316 eV (Fig. 5b), and this was probably linked to the contribution

of $MgHPO_4$ to the fitting in these samples, regardless of pH. The spectra of the standard $MgHPO_4$ was very similar to that observed for Hm slurries with phosphate *(supplementary material)*. Therefore, it is possible to assume that there was an association of Mg with phosphate in two different ways, since the Mg + Pi solution also contributed to the LCF (Table 2).

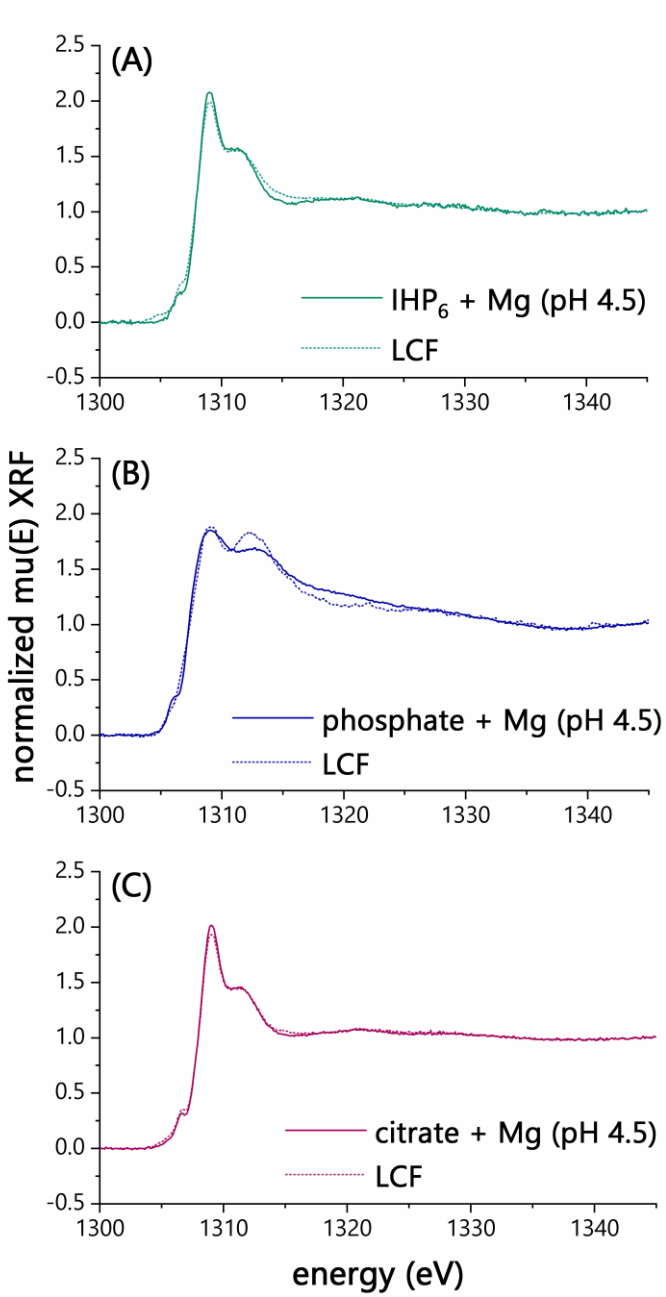

Figure 5. Linear combination fit (dot lines) of Mg *K*-edge XANES spectra (solid lines) of hematite slurries (5 g l^{-1}) with Mg (4 mmol l^{-1}) and 0.66 mmol l^{-1} IHP_6 (**A**), 4 mmol l^{-1} phosphate (**B**) and 0.67 mmol l^{-1} citrate (**C**) in pH 4.5.

The high proportions of $MgCl_2$ prevented the detailed investigation of the atomic environment surrounding the Mg atoms in the samples, and at least one other Mg-species was present in all samples. However, the fitting sometimes does not represent the presence of a specific compound in the sample. This is what probably happened for $MgNO_3$ (sample IHP_6 under pH 6.5), which represents a six-fold coordination with H_2O molecules, but that probably wasn't present in the sample. Therefore, another molecule containing Mg in a similar atomic environment could be present. The adjustment with $MgHPO_4$ (sample Pi under pH 4.5 and 6.5), in which Mg is coordinated in a closed packed structure, was expected due to the association between Mg and phosphates in $MgHPO_4$ crystals. However, IHP_6 does not seem to establish the same type of association since the species $MgHPO_4$ did not participate in the LCF of the samples, regardless of pH (Table 2).

In a desorption study of IHP_6 from goethite, Yan et al. (2015) found that the initial decrease in zeta potential (ζ), *i.e.* electrical potential at the interface that separates attached fluids from mobile fluids, is much larger for IHP_6 than for phosphate. According to these authors, this is probably related to the high influence of IHP_6 in the Fe-oxide charges within the plain of shear and also the positions of the plain of shear. Yan et al. (2015) concluded that it is possible that ternary surface complexes might be formed with free cations, IHP_6 and goethite. In our study, the formation of a ternary association among Mg-IHP_6-Hm was not conclusive. The influence of Ca and Mg on the adsorption of IHP_6 has been identified, but its mechanisms of association with the Fe-oxides surface may be more difficult to predict due to the more complex nature of the IHP_6 molecule compared to that of phosphate.

2.4. Conclusions

The presence of Mg had more marked effects on IHP_6 than on phosphate adsorption on hematite in the investigated pH range.

The pH changes brought spectral variations, such as displacement of certain bands, which are more difficult to identify for IHP_6 than for phosphate due to its more complex structure.

The adsorption of IHP_6 and phosphate followed two mechanisms, one at the beginning of the adsorption and the other already close to equilibrium, but mechanistic studies are necessary to define the specific type of complex formed in each of the adsorption phases.

Calcium and Mg did not promote significant variations in the parameters of the kinetic models, but the increase in pH to 6.5 made the adsorption of IHP_6 lengthier.

References

Adhikari D., Sowers T., Stuckey J. W., Wang X., Sparks D. L. and Yang Y. (2018) Formation and redox reactivity of ferrihydrite-organic carbon-calcium co-precipitates. Geochim. Cosmochim. Acta 244, 86–98.

Auler A. C., Caires E. F., Pires L. F., Galetto S. L., Romaniw J. and Charnobay A. C. (2019) Lime effects in a no-tillage system on Inceptisols in Southern Brazil. Geoderma Reg. 16, e00206.

Briedis C., De Moraes Sá J. C., Caires E. F., De Fátima Navarro J., Inagaki T. M., Boer A., De Oliveira Ferreira A., Neto C. Q., Canalli L. B. and Dos Santos J. B. (2012a) Changes in organic matter pools and increases in carbon sequestration in response to surface liming in an Oxisol under long-term no-till. Soil Sci. Soc. Am. J. 76, 151–160.

Briedis C., Sá J. C. de M., Caires E. F., Navarro J. de F., Inagaki T. M., Boer A., Neto C. Q., Ferreira A. de O., Canalli L. B. and Santos J. B. dos (2012b) Soil organic matter pools and carbon-protection mechanisms in aggregate classes influenced by surface liming in a no-till system. Geoderma 170, 80–88.

Carmeis Filho A. C. A., Penn C. J., Crusciol C. A. C. and Calonego J. C. (2017) Lime and phosphogypsum impacts on soil organic matter pools in a tropical Oxisol under long-term no-till conditions. Agric. Ecosyst. Environ. 241, 11–23.

Celi L., Lamacchia S., Marsan F. A. and Barberis E. (1999) Interaction of inositol hexaphosphate on clays: Adsorption and charging phenomena. Soil Sci. 164, 574–585.

Celi L., De Luca G. and Barberis E. (2003) Effects of interaction of organic and inorganic P with ferrihydrite and kaolinite-iron oxide systems on iron release. Soil Sci. 168, 479–488.

Cornell R. M. and Schwertmann U. (2003) The Iron Oxides.

Davis A. P. and Bhatnagar V. (1995) Adsorption of cadmium and humic acid onto hematite. Chemosphere 30, 243–256.

Elzinga E. J. and Sparks D. L. (2007) Phosphate adsorption onto hematite: An *in-situ* ATR-FTIR investigation of the effects of pH and loading level on the mode of phosphate surface complexation. 308, 53–70.

Essington M. E. (2015) Soil and water chemistry: an integrative approach. 2nd ed., CRC Press.

Fageria N. K. and Baligar V. C. (2008) Ameliorating soil acidity of tropical Oxisols by liming for sustainable crop production. 99, 345–399.

Fornara D. A., Steinbeiss S., Mcnamara N. P., Gleixner G., Oakley S., Poulton P. R., Macdonald A. J. and Bardgett R. D. (2011) Increases in soil organic carbon sequestration can reduce the global warming potential of long-term liming to permanent grassland. Glob. Chang. Biol. 17, 1925–1934.

Gerendás J. and Führs H. (2013) The significance of magnesium for crop quality. Plant Soil 368, 101–128.

Goldberg S. and Sposito G. (1985) On the mechanism of specific phosphate adsorption by hydroxylated mineral surfaces: A review. Commun. Soil Sci. Plant Anal. 16, 801–821.

Guan X. H., Shang C., Zhu J. and Chen G. H. (2006) ATR-FTIR investigation on the complexation of myo-inositol hexaphosphate with aluminum hydroxide. J. Colloid Interface Sci. 293, 296–302.

Inagaki T. M., de Moraes Sá J. C., Caires E. F. and Gonçalves D. R. P. (2016) Lime and gypsum application increases biological activity, carbon pools, and agronomic productivity in highly weathered soil. Agric. Ecosyst. Environ. 231, 156–165.

Inagaki T. M., de Moraes Sá J. C., Caires E. F. and Gonçalves D. R. P. (2017) Why does carbon increase in highly weathered soil under no-till upon lime and gypsum use? Sci. Total Environ. 599–600, 523–532.

Kämpf N. and Curi N. (2003) Clay minerals in brazilian soils. In Soil Science Topics (eds. Nilton Curi, J. J. Marques, L. R. G. Guilherme, J. M. Lima, and A. S. Lopes). Brazilian Soil Science Society, Viçosa. pp. 1–54.

Kochian L. V., Hoekenga O. A. and Piñeros M. A. (2004) How do crop plants tolerate acid soils? mechanisms of aluminum tolerance and phosphorous efficiency. Annu. Rev. Plant Biol. 55, 459–493.

Kremer, C., Torres, J., Bianchi, A., Savastano, M., Bazzicalupi, C. *myo*-inositol kexakisphosphate: Coordinative versatility of a natural product. Coordination Chemistry Reviews, 419, 213403.

Martin M., Celi L. and Barberis E. (2004) Desorption and plant availability of *myo*-inositol hexaphosphate adsorbed on goethite. Soil Sci. 169, 115–124.

Mikutta R., Mikutta C., Kalbitz K., Scheel T., Kaiser K. and Jahn R. (2007) Biodegradation of forest floor organic matter bound to minerals via different binding mechanisms. Geochim. Cosmochim. Acta 71, 2569–2590.

Murphy P. N. C. (2007) Lime and cow slurry application temporarily increases organic phosphorus mobility in an acid soil. Eur. J. Soil Sci. 58, 794–801.

Ognalaga M., Frossard E. and Thomas F. (1994) Glucose-1-phosphate and *myo*-inositol hexaphosphate adsorption mechanisms on goethite. Soil Sci. Soc. Am. J. 58, 332–337.

Persson P., Nilsson N. and Sjöberg S. (1996) Structure and bonding of orthophosphate ions at the iron oxide-aqueous interface. J. Colloid Interface Sci. 177, 263–275.

Ravel B. and Newville M. (2005) ATHENA, ARTEMIS, HEPHAESTUS: data analysis for X-ray absorption spectroscopy using IFEFFIT. J. Synchrotron Radiat. 12, 537–541.

Rowley M. C., Grand S. and Verrecchia É. P. (2018) Calcium-mediated stabilisation of soil organic carbon. Biogeochemistry 137, 27–49.

Singh B., Melo V. F., Novais R. F., Schaefer C. E. G. R. and Fontes M. P. F. (2014) Iron and aluminium oxides of different brazilian soils. Rev. Bras. Ciência do Solo 25, 19–32.

Sowers T. D., Adhikari D., Wang J., Yang Y. and Sparks D. L. (2018a) spatial associations and chemical composition of organic carbon sequestered in Fe, Ca, and organic carbon ternary systems. Environ. Sci. Technol. 52, 6936–6944.

Sowers T. D., Stuckey J. W. and Sparks D. L. (2018b) The synergistic effect of calcium on organic carbon sequestration to ferrihydrite. Geochem. Trans. 19, 22–26.

Sumner M. and Noble A. (2003) Soil acidification: the world story. In Handbook of Soil Acidity (ed. Z. Rengel). Marcel Dekker, New York. pp. 1–28.

Tejedor-Tejedor M. and Anderson M. (1990) Protonation of phosphate on the surface of Goethite as studied by CIR-FTIR and electrophoretic mobility. Langmuir 6, 602–611.

Weng L. P., Koopal L. K., Hiemstra T., Meeussen J. C. L. and Van Riemsdijk W. H. (2005) Interactions of calcium and fulvic acid at the goethite-water interface. Geochim. Cosmochim. Acta 69, 325–339.

Weng L., Van Riemsdijk W. H. and Hiemstra T. (2009) Effects of fulvic and humic acids on arsenate adsorption to goethite: Experiments and modeling. Environ. Sci. Technol. 43, 7198–7204.

Wuddivira M. N. and Camps-Roach G. (2007) Effects of organic matter and calcium on soil structural stability. Eur. J. Soil Sci. 58, 722–727.

Yan Y., Koopal L. K., Liu F., Huang Q. and Feng X. (2015) Desorption of *myo*-inositol hexa*kis*phosphate and phosphate from goethite by different reagents. J. Plant Nutr. Soil Sci. 178, 878–887.

Yan Y., Wan B., Jaisi D. P., Yin H., Hu Z., Wang X., Chen C., Liu F., Tan W. and Feng X. (2018a) Effects of *myo*-inositol hexa*kis*phosphate on $Zn_{(II)}$ Sorption on γ-Alumina: A Mechanistic Study. ACS Earth Sp. Chem. 2, 787–796.

Yan Y., Wan B., Liu F., Tan W., Liu M. and Feng X. (2014) Adsorption-desorption of *myo*-inositol hexa*kis*phosphate on hematite. Soil Sci. 179, 476–485.

Yan Y., Wan B., Zhang Y., Zhang L., Liu F. and Feng X. (2018b) In situ ATR-FTIR spectroscopic study of the co-adsorption of *myo*-inositol hexa*kis*phosphate and $Zn_{(II)}$ on goethite. Soil Res. 56, 526–534.

Zambrosi F. C. B., Alleoni L. R. F. and Caires E. F. (2008) Liming and ionic speciation of an oxisol under no-till system. Sci. Agric. 65, 190–203.

Supplementary information

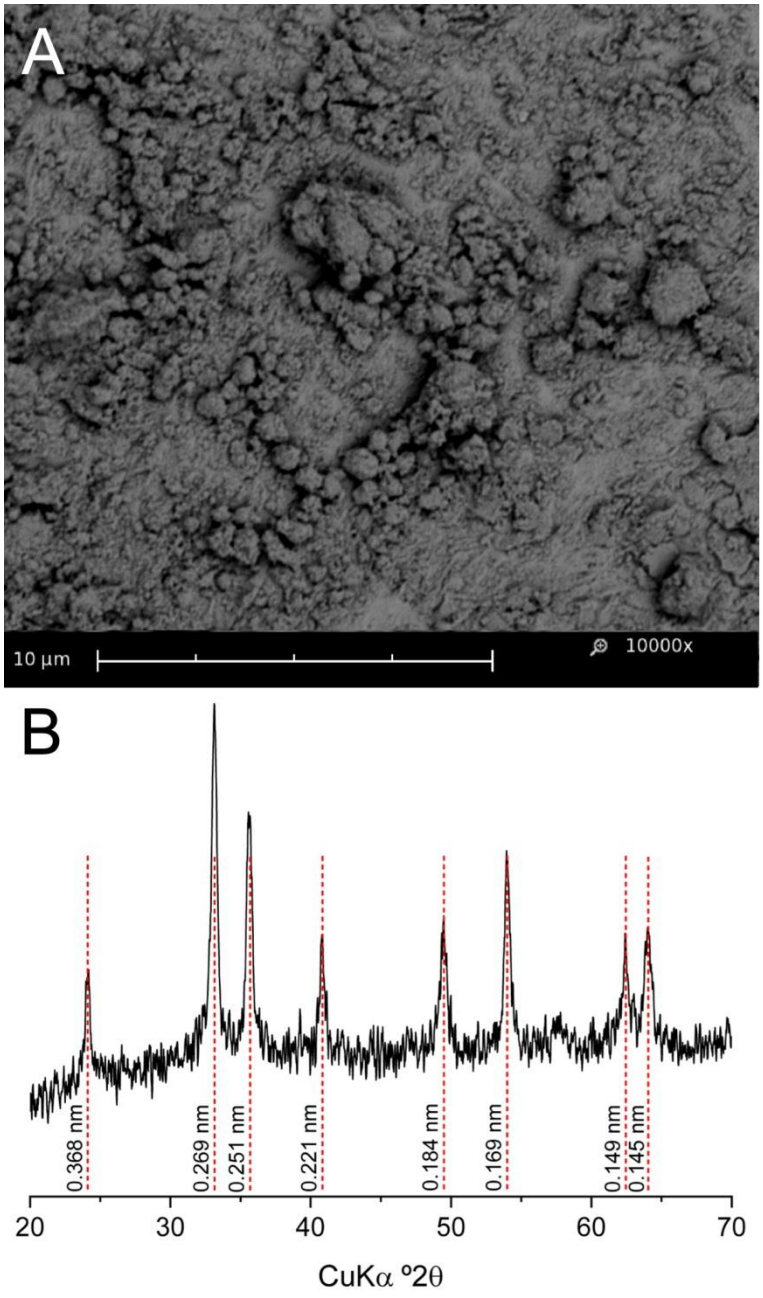

Figure S1. Scanning electron microscopy (**A**) and X-ray diffraction (**B**) of the synthetic hematite.

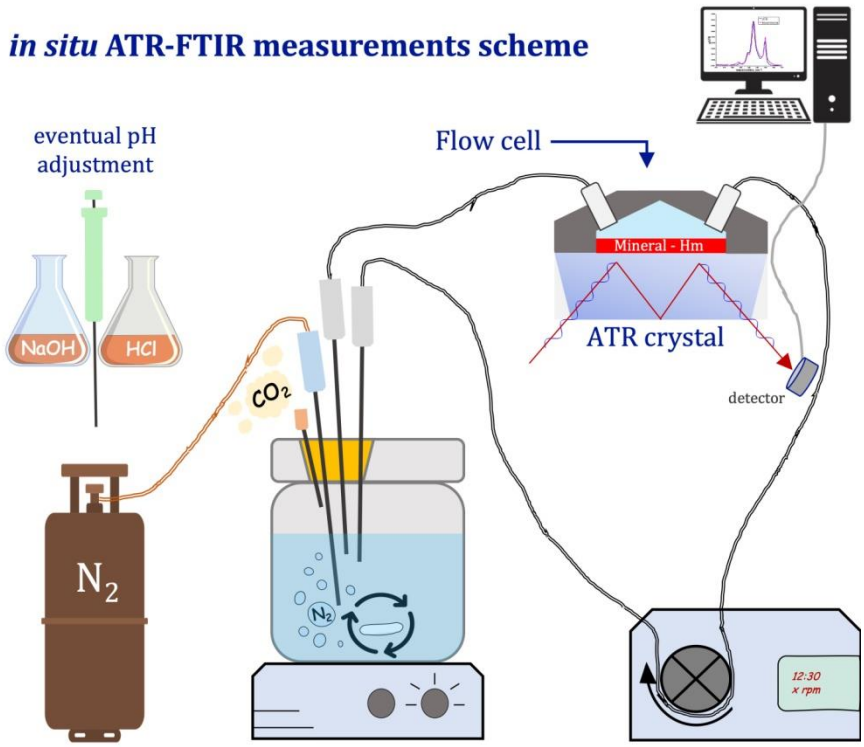

Figure S2. Illustration of the analytical scheme for *in-situ* data collection by ATR-FTIR.

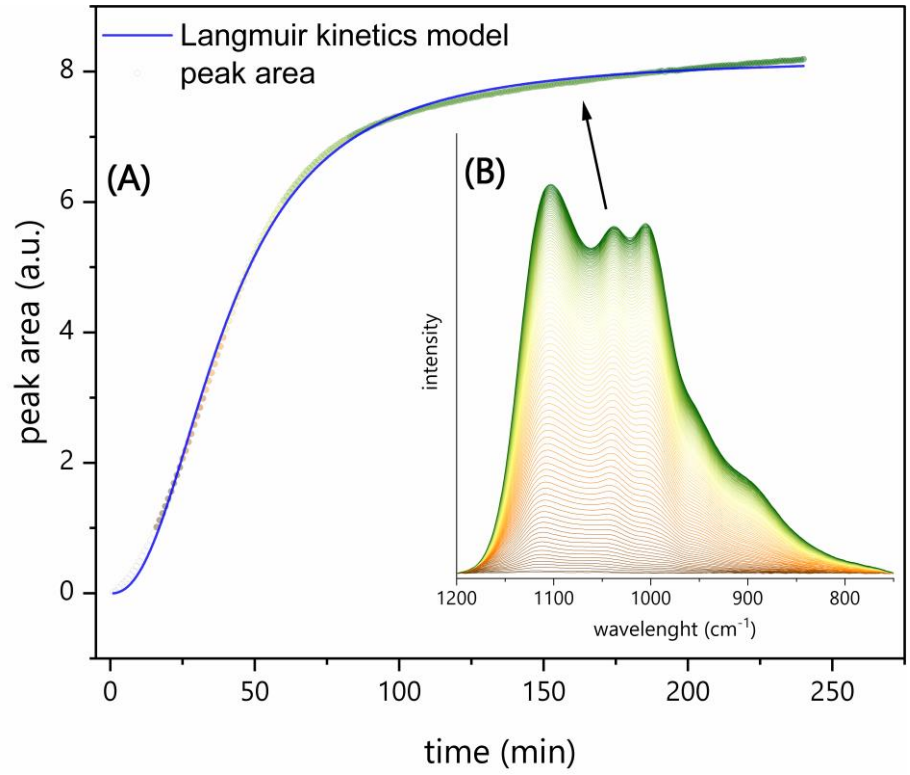

Figure S3. Scheme of how the kinetic data were obtained through the integration of bands corresponding to the studied molecule by ATR-FTIR.

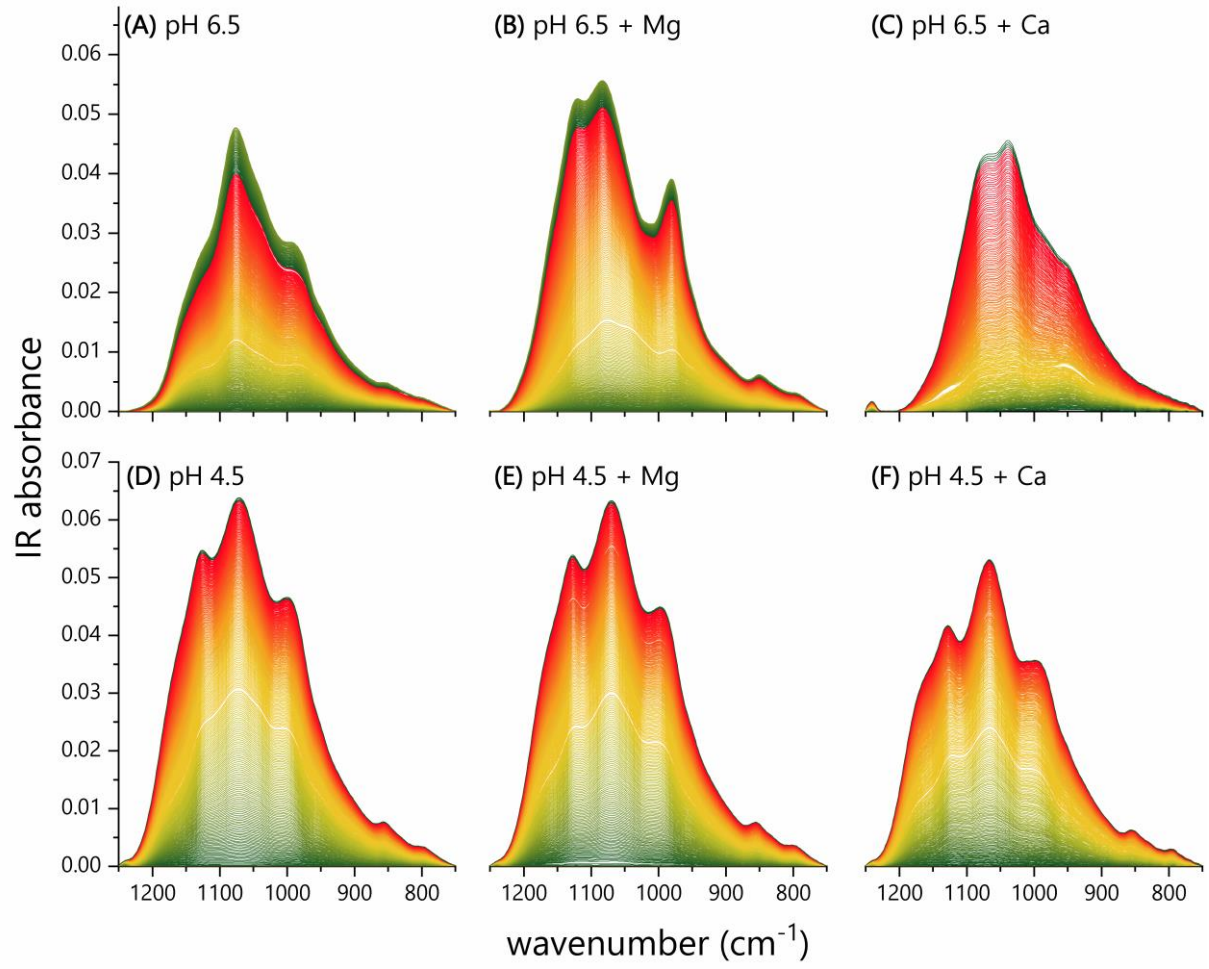

Figure S4. Infrared spectra of 25 µmol l^{-1} myo-inositol hexakisphosphate (IHP_6) under different pH values in the presence of cations. In each sub-figure there are 240 spectra, measured every minute, totaling 4 h of measurements.

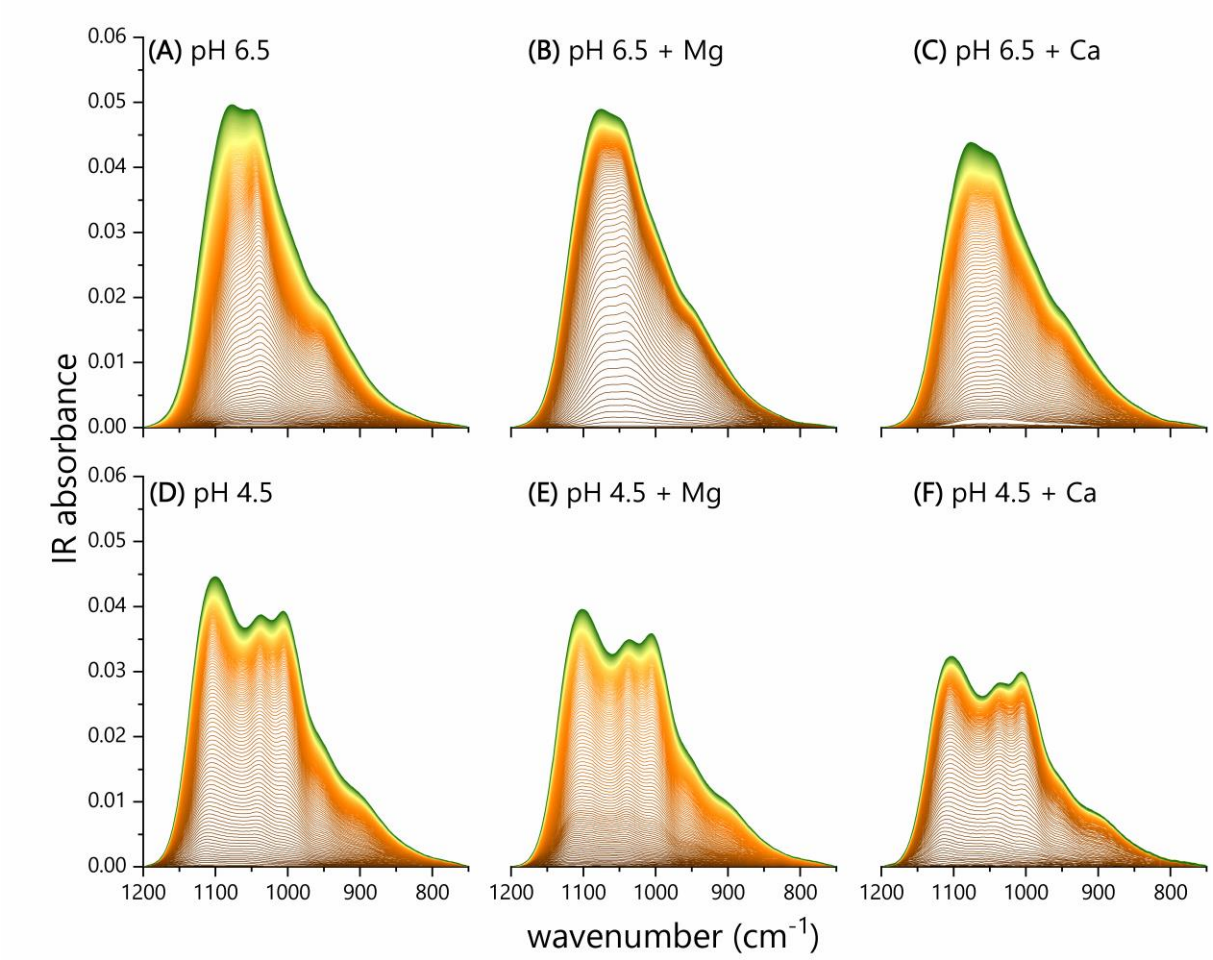

Figure S5. Infrared aqueous spectra of 25 µmol l^{-1} phosphate under different pH values in the presence of cations. In each sub-figure there are 240 spectra, measured every minute, totaling 4 h of measurements.

The logarithmic relationship between the area of the phosphate band (1200 to 750 cm^{-1}) at a given ($A_{(t)}$) time and in the final time (A_e), when the theoretical adsorption equilibrium in the system has already been reached, shows whether or not there is more than one ion adsorption mechanism. In the case of the present study, two mechanisms were observed, an initial one that fits a second order polynomial curve, followed by a linear one (Fig. S6).

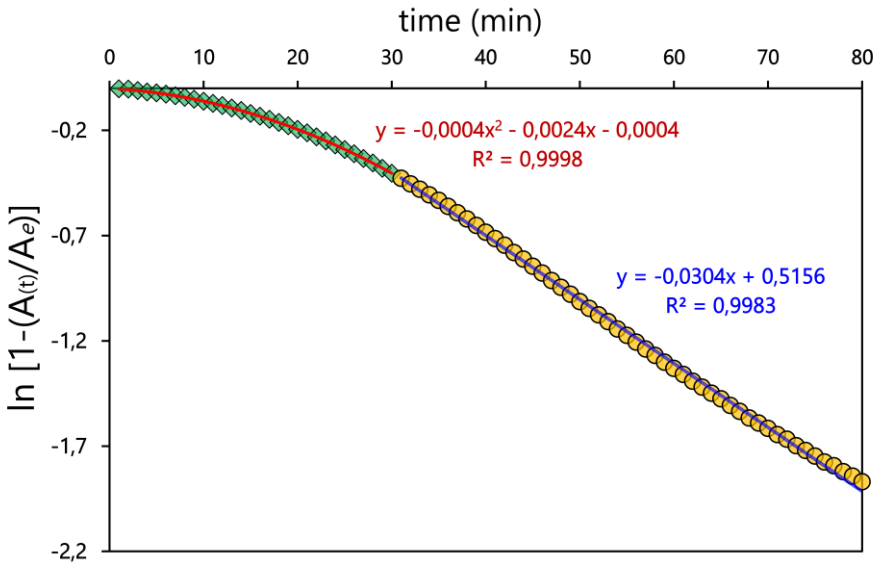

Figure S6. The empirical initial (0 to 80 min) adsorption rate of 25 µmol l^{-1} phosphate (pH 4.5 without cations) on hematite.

If linear patterns were identified, either one or two, the Langmuir kinetic equation, $A_{(t)} = b1 * (1 - e^{-r_{obs} * t})$, would be adequate to adjust the data. Tofan-Lazar and Al-Abadleh (2012) used the Langmuir equation to extract the adsorption rates of $HPO_4^{2-}{}_{(aq)}$, however they used only the initial 5 min of adsorption for this. In our case, it seemed prudent to investigate the behavior of the ln $(A_{(t)}/A_e)$ for a longer period of time (Fig. S6) compared to Tofan-Lazar and Al-Abadleh (2012). With that, we identified two distinct patterns and the Langmuir-Freundlich kinetic equation proved to be more efficient for the adjustment.

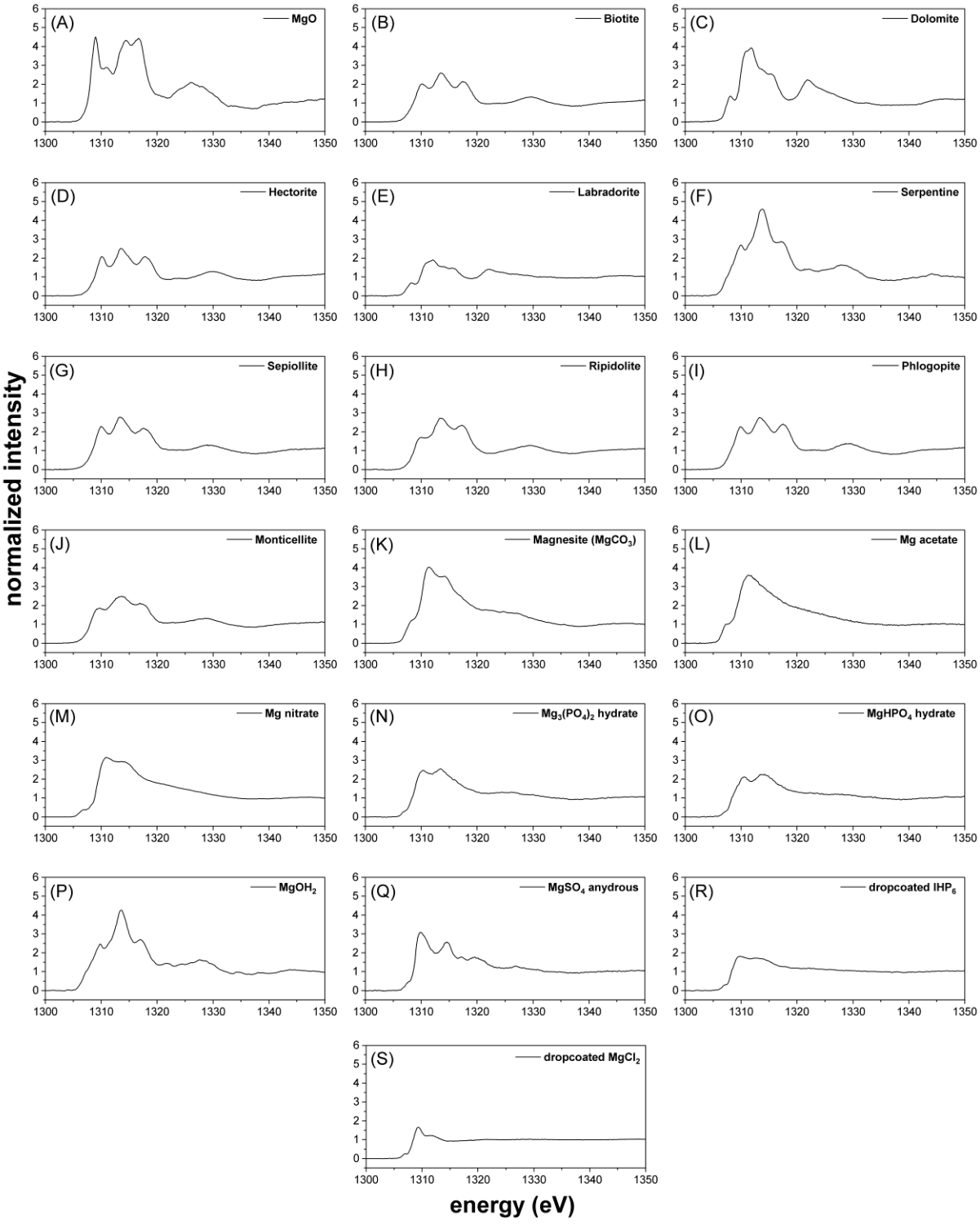

Figure S7. Magnesium K-edge XANES spectra of Mg-bearing minerals and Mg reagents that were used as reference materials. (**A**) Mg oxide; (**B**) Biotite; (**C**) Dolomite; (**D**) Hectorite; (**E**) Labradorite; (**F**) Serpentine; (**G**) Sepiollite; (**H**) Ripidolite; (**I**) Phlogopite; (**J**) Monticellite; (**K**) Magnesite; (**L**) Mg acetate; (**M**) Mg nitrate; (**N**) $Mg_3(PO_4)_2$ hydrate; (**O**) $MgHPO_4$ hydrate; (**P**) $MgOH_2$; (**Q**) $MgSO_4$ anhydrous; (**R**) drop coated IHP_6 + $MgCl_2$; (**S**) drop coated $MgCl_2$.

3. IRON-OXIDES PROPERTIES AND IRON FRACTIONATION IN AN OXISOL LONG-TERM AMENDED WITH LIME AND PHOSPHOGYPSUM

ABSTRACT

Iron (Fe) composes the structure of (hydr)oxides directly linked to carbon (C) and phosphorus (P) cycles in natural and agricultural environments. The objective was to evaluate the effects of pH and calcium (Ca) inputs in a soil in Fe fractions and Fe-(hydr)oxides structural order. Fe fractionation procedures, X-ray diffraction (XRD), diffuse reflectance spectroscopy (DRS) and X-ray absorption spectroscopy (XAS) were performed in soil samples from a long-term (18 years) experiment in which the soil was amended with lime and/or phosphogypsum. Iron species have suffered little influence of long-term lime and phosphogypsum application. However, with the exception of the Fe fraction associated with SOM, all others were influenced by treatments, including Fe fractions with higher and lower crystallinities, and it was probably related to the P retention capacity, which was also influenced by amendments.The proportions of Fe-species with low structural order were lower in soil samples from the experimental area than in samples from an adjacent native forest, indicating that the soil use for agriculture does not favor permanence of this type of Fe-species. Diffuse reflectance spectroscopy revealed low crystallinity and slightly higher structural Al concentrations in Fe-(hydr)oxides from the native forest soil.

Keywords: Soil organic carbon; Fe-(hydr)oxides crystallinity; Lime; X-ray spectroscopy; Ca bridges

3.1. Introduction

Iron (Fe) interacts with biogeochemical cycles of several elements, including carbon (C) and phosphorus (P) (Lindsay and Schwab 1982; Wilfert et al. 2015; Wang et al. 2019). The association between Fe and soil organic carbon (SOC) plays a critical role in the functionality of agricultural systems. These associations generally occur between Fe oxides and surface groups of organic molecules, yielding organomineral compounds whose stability can vary widely (Sanderman et al. 2014).

Positive effects of low-carbon farming have been extensively reported and are commonly the result of conservationist techniques (*e.g.* no-till, terraces *etc.*), fertilization with organic manures and reduction of biocides (Jenkinson and Powlson

1976; Du et al. 2014; Maillard and Angers 2014; Sanaullah et al. 2020). One of the most notable effects of no-till (NT) in humid tropical soils is the high SOC accumulation and stability over time compared to soils under conventional tillage (Briedis et al. 2012b; Castro et al. 2015; Rosolem et al. 2016). This stability, in large part, results from the associations of SOC with Fe- and Al-(hydr)oxides, that are abundant in highly weathered soils (Schaefer et al. 2008). More specifically, the association with poorly crystalline or short-range ordered (SRO) mineral phases has been reported as a notorious SOC stabilization mechanism in soils over time (Kleber et al. 2015).

Tropical and subtropical soils usually require the addition of acidity correctives due to low natural pHs (< 4.5 in H_2O) (Fageria and Baligar 2008). The application of amendments like lime or phosphogypsum decreases the bioavailability of Al^{3+} and increases the contents of cations like calcium (Ca). The increase in Ca concentrations in soils may be a determining factor for the SOC accumulation, mainly through bridges that Ca builds between organic molecules and oxides (Rowley et al. 2018).

Amendments are broadcasted, without incorporation, in soils under no-till. The carbonate ions (CO_3^{2-}) present in lime ($Ca/MgCO_3.H_2O$) promotes pH increase by the formation of hydroxyls (OH^-) that promotes Al^{3+} hydrolysis in solution. On the other hand, phosphogypsum ($CaSO_4.H_2O$) does not change the pH change, but Al becomes unavailable to plants due to the association with sulfate (SO_4^{2-}), yielding $Al_2(SO_4)_3$ that is not absorbed by plants (Oates and Caldwell 1985; Carvalho and Van Raij 1997).

The increase in the quantities and diversity of organic C species has been reported frequently in highly weathered soils that receive lime for several years (Briedis et al. 2012a, b; Inagaki et al. 2017). Conversely, the exclusive use of phosphogypsum has not promoted such effects on SOC (Carmeis Filho et al. 2017). Despite the phosphogypsum benefits, the improvement in chemical soil attributes is not as noticeable as with lime, and the production of biomass and, consequently, SOM does not reach these levels either.

The crystal structure of Fe-(hydr)oxides makes them smaller in size but highly reactive due to the higher specific surface area (SSA) in relation to phyllosilicates. The

degree of structural arrangement influences the ability to render these Fe-(hydr)oxides molecules and the ability to adsorb more or less soil organic matter (SOM) and P. According to Feng et al. (2014), Fe-(hydr)oxides with low structural order may adsorb up to six times more SOM than more crystalline ones. In these short-ordered Fe-oxides, the occlusion of some anions, such as P, may be enhanced, as reported by Simonsson et al. (2018), in long-term field experiments.

Lime-induced chlorosis and reduction in Fe bioavailability are frequently reported (Gile and Carrero 1920; Mehlich 1957; Bertic et al. 1988; Colombo et al. 2014). In general, the solubility of Fe oxides decreases ~1000 times with the increase of one pH unit (Lindsay 2001). Therefore, the contents of soluble Fe^{2+} usually decrease after liming, and the exchange complex may act as a proton sink inhibiting the occlusion of P in SRO Fe phases. Conversely, increments in Ca^{2+} and OH^- by lime may increase the stability of Fe-organic complexes, which creates a bilateral situation.

The indirect effects of long-term addition of Al-suppressors on Fe-(hydr)oxides structural order and its association with organic compounds remains limitedly studied. In this, study, we selected soil samples from a long-term field experiment with treatments involving lime and phosphogypsum, in which there was a significant increase in pH and SOC levels by the prolonged input of lime. Thus, the overall objective was to assess the effects of long-term amendments broadcast on soil Fe fractions and Fe-oxides structural order, as well as P retention, beyond some chemical attributes related to the chemistry of Fe and P. The following hypothesis were taken into account: (**i**) the increase in SOM and Ca promoted by liming increases the association of Fe-oxides with SOM; and (**ii**) the P retention potential and Fe-species with low structural order will increase, and (**iii**) such effects will not be evidenced when only phosphogypsum is added due to its low influence on soil pH and SOM accumulation.

3.2. Materials and methods

3.2.1. Site and treatments

A long-term experimental site was established in 2002 in Botucatu, state of São Paulo, Brazil (48º 23' W, 22º 51' S, 765 a.s.l.). The site has a humid tropical climate with 1500-1800 mm annually of pluvial precipitation and possible droughts in winter. The average annual temperature is 25.5ºC in the hottest month and 16.4ºC in the coldest. The soil is a clayey-loamy Typic Haplorthox (Soil Survey Staff 2014) (35% clay, 11% silt and 54% sand in the inorganic matrix). Before the beginning of the experiment, in 2001, certain chemical attributes were determined following the methodologies of Gee and Bauder (1986), Cantarella et al. (1998) and van Raij et al. (2001), as follows: 4.2 of pH in 0.01 mol l^{-1} $CaCl_2$ solution; 12 g dm^{-3} of SOC; 9 mg dm^{-3} of plant-available P (anion exchange resin); 14 mmolc dm^{-3} of exchangeable Ca; 37 mmolc dm^{-3} of potential acidity (H+Al), and 58 mmolc dm^{-3} of cation exchange capacity (CEC)

Four experimental treatments under long-term management and a reference site were investigated: **i**) control - without lime and phosphogypsum broadcast; **ii**) L - only lime broadcasted); **iii**) PG - only phosphogypsum broadcasted; **iv**) LPG - both lime and phosphogypsum broadcasted; and **v**) NV – native vegetation adjacent to the experiment (~100 m away). Each experimental plot had 46.8 m^2 (9.0 m per 5.2 m) in a randomized complete block design with four replications under NT since the experiment began. Table 1 contains the rates and the years in which the amendments were applied in the experimental area.

Table 1. Rates of amendments broadcasted in the experimental site over time.

year	2002	2004	2010	2016
Lime (kg ha^{-1})	2700	2000	2000	6300
Phosphogypsum (kg ha^{-1})	2100	2100	2100	10000

Lime rates were defined to raise the soil bases saturation (BS) to 70% (Cantarella et al. 1998) according to the chemical analysis of the 0-20 cm topsoil layer.

These analyses were performed every year to verify the need for reapplication if BS reached 50%. Phosphogypsum rates were calculated as 6x clay content at the 20-40 cm layer, according to van Raij et al. (1996), and broadcasted at the same time as lime. Bases saturation in 2004 and 2010 were not as low as in 2001, so lime rates were lower in these years (Table 1).

In 2016 lime was reapplied. The recommendation methods in this year, however, were renewed based on updates in amendments recommendation in Brazil described in Caires et al. (2015), Joris et al. (2016) and Caires and Guimarães (2018). The guarantees of the lime used were 16.6% Ca and 10.5% Mg, for the phosphogypsum were 20% Ca, 15% sulfur (S), <0.1% P and fluorine (F). P-fertilizations were carried out in the sowing line with triple superphosphate (20% P, 10% Ca) or simple superphosphate (8% P, 16% Ca, 9% S). There was no variation in P-fertilization among the treatments throughout the experiment, following the specific requirement in each crop, but keeping the same rates in each crop, application modes and fertilizers in all treatments. More details can be found at Costa and Crusciol (2016) and Carmeis Filho et al. (2017, 2018).

3.2.2. Soil sampling and preparation

Soil samples were collected in January 2018 in the topsoil layer (0-0.1 m) with an 80-mm diameter auger. Ten sampling points were randomly chosen considering an isolation of 0.5 m from the edges to the interior of the plots. From the ten collection points, two were in the sowing line, four at 11 cm from the sowing line and four at 22 cm from the sowing line. The union of equal volumes of the ten samples collected yielded a composite sample. The soil sampling procedure covered the entire area that received lime or phosphogypsum, as well as the area that received P fertilizer (sowing line). In the native forest, ten sampling points were randomly selected in a square area of 225 m^2 inside the forest. After removing visual impurities (stones, insects, plant fragments *etc.*) the samples were air-dried and slightly broken manually to pass through a 2-mm sieve and homogenized.

3.2.3. X-ray diffraction analysis in soil clay fraction

Soil samples from the experimental site and from the native forest site were analyzed for mineralogical composition. The SOM removal was performed with sodium hypochlorite as described by McDowell and Condron (2001). The clay fraction was separated by dispersion according to Gee and Or (2002). The clay fractions were disaggregated into agate crucibles and then sieved (100 mesh or 0.149 mm) for X-Ray Diffraction (XRD) powder analysis. The equipment was a Rigaku Miniflex II diffractometer with graphite monochromator and CuKα radiation (40 kV and 15 mA).

After the power diffraction, the samples were submitted to the concentration of oxides and hydroxides by treatment with 5 mol l^{-1} NaOH to remove phyllosilicates (Singh and Gilkes 1991) and then analyzed by XRD at 25°C. The clay samples were suspended in perforated porous ceramic slides after dispersion by a vacuum probe. The analyzes were performed with 0.01°2θ s^{-1} of goniometer velocity with a range of 3 to 60°2θ. The diffraction patterns corresponding to soil minerals were interpreted based on the position of the peaks, according to Brindley and Brown (1980) and Whitting and Allardice (1986).

3.2.4. Diffuse reflectance spectroscopy (DRS) analysis

Clay samples (0.149 mm-sieved) were placed in metallic sample holders with quartz windows and lightly compacted for surface homogenization. Measurements were performed on a Varian (UV-VIS-NIR) spectrometer (Varian Inc., Palo Alto, United States). The reflectance of the samples was determined on the basis of reference samples with high (black) and low (white) absorption in spectra obtained in the range of 370 to 800 nm. The wavelengths range was selected to focus on the spectral fingerprint region that includes all the main characteristic bands of Fe-based phases (Veneranda et al. 2018). The analysis was performed in triplicate, and the three spectra originated from each sample were mathematically merged to form only a spectrum with a lower noise level.

3.2.5. Soil chemical analysis

Total contents of Fe, Al, Ca and P in the bulk soil were determined by microwave assisted acid digestion (method 3052) (USEPA 1996). In the method, 0.5 g of soil reacted with concentrated acids (2 ml of HCl, 3 ml of HF and 9 ml of HNO_3) in Teflon tubes. Moist digestion was performed under the following conditions: 6.0 min heating, 9.5 min under 180°C, and 10 min cooling until ~25°C. The soil samples were fully digested, and the extracts were filtered on quantitative filter paper (Whatman 42) before determination by Inductively Coupled Plasma Optical Emission Spectrometry (ICP-OES).

Soil pH was measured with a glass electrode within soil:water and soil:0.01 mol l^{-1} $CaCl_2$ solution ratio of 1:2.5 (v/v). Soil organic carbon contents were quantified by chromic acid digestion (Heanes 1984). The potential acidity (H+Al) was estimated by the pH variation measured in the SMP solution following the methodology of Shoemaker et al. (1961). The exchangeable Al^{3+} was extracted by 1 mol l^{-1} KCl solution and quantified by the titrimetric method with 0.025 mol l^{-1} NaOH (Bertsch and Bloom 1996). Exchangeable Ca contents were extracted by an ionic exchange resin according to van Raij et al. (2001) and quantified by Atomic Absorption Spectrophotometry (AAS) in a Perkin Elmer 1100B.

Bioavailable P was extracted by anionic exchange resin (van Raij et al., 1996) and quantified according to Murphy and Riley (1962) in a Bel Photonics UV-M51 spectrophotometer. Another measured parameter was the remaining P (P_{rem}), that is an estimate of the P adsorption capacity of the soil, was proposed by Bache and Williams (1971) and adapted by Alvarez et al. (2000). In the method, 25 ml of a 60 mg l^{-1} P solution (as KH_2PO_4) reacts with 2.5 g of soil for 16 h (end-over-end agitation). After physical separation in a centrifuge (15 min at 2500×g) and filtration (Whatman 42) the Prem contents were determined by ICP-OES.

3.2.6. Fe fractionation

Air-dried 2 mm-sieved soil samples were used for the extraction of Fe fractions based on Wang et al. (2019). Briefly, the total free Fe (tf-Fe) fraction was extracted by sodium dithionite-citrate-bicarbonate (DCB), in 0,5 g of soil with 40 ml of 0.3 mol l^{-1} $Na_3C_6H_5O_7$ and 5 ml of 1 mol l^{-1} Na_2CO_3 plus 0.5 g of $Na_2S_2O_4$ after 30 min under 80°C (Mehra and Jackson 1960; McKeague and Day 1966); the Fe bound to organic matter (om-Fe) fraction was extracted by 0.1 mol l^{-1} Na-pyrophosphate (pH 10) during 16 h according to Bottinelli et al. (2017); and the reactive Fe (re-Fe) fraction was extracted by 0.2 mol l^{-1} oxalic acid-NH_4 oxalate (pH 3) during 4 h under darkness according to Vaezi et al. (2017). The extractions were not performed sequentially, using 1 g of soil in each one separately. All extracts were centrifuged (2500×g for 15 min) and passed through 0.45 mm membrane filters prior to Fe determination by Atomic Absorption Spectroscopy (AAS) in a Perkin Elmer 1100B (Perkin Elmer Corp., Norwalk, United States). The free non-crystalline Fe (nc-Fe) was obtained by the subtractions of re-Fe by om-Fe, and the free crystalline Fe (c-Fe) by the subtractions of tf-Fe by re-Fe.

3.2.7. Fe *K*-edge Extended X-ray Adsorption Fine Structure (EXAFS) spectroscopy

Equal masses of the four replicates of the composite soil samples were united. All samples and reference materials (hematite – Hem, goethite - Gth and ferrihydrite - Fh) synthetized according to Cornell and Schwertmann (2003) were milled on an agate mortar and passed through 10-µm polyamide screens (No PA 10/4 – SAATI Corp., Milan, Italy). After milling, 30 mg of the samples were added to 10 ml of isopropanol and dispersed by ultrasonic vibration. Once the suspension was obtained, the material was deposited on a cellulose acetate membrane induced by a vacuum pump. Thereafter, the membrane was sealed on a sample holder with Kapton tape. Iron *K*-edge X-ray absorption measurements were collected in transmission mode at ambient conditions (~22ºC) at the X-Ray Absorption and Fluorescence Spectroscopy beamline (XAFS-2) of the Brazilian Synchrotron Light Laboratory (LNLS).

An Fe foil was used as a reference for calibration, with E0 assigned as 7111.8 eV. The Fe *K*-edge XANES data were collected varying step sizes of 1.0 eV from 7000 to 7080 eV and 0.2 eV from 7080 to 7250 eV, with 1 s of acquisition time for all intervals. The Fe-EXAFS data were collected from 7250 to 8000 eV in *k* steps of 0.05 Å. A polynomial pre-edge function was subtracted from each averaged (n = 3), unsmoothed and energy calibrated spectrum, and the data were normalized into the EXAFS region using the Athena software in the computer package IFEFFIT (Ravel and Newville, 2005). A cubic spline fit was used above the absorption edge in order to remove the background and the data were k^3-weighted to enhance the *k* values. Normalized EXAFS spectra were filtered over a *k* range of ~2.8 to ~13 $Å^{-1}$ (Abdala et al., 2015).

3.2.8. Statistical analysis

Data were analyzed considering their replication. Analyses of variance (one-way ANOVA) and *Tukey* test at $p = 0.05$ level were conducted to compare soil chemical attributes and Fe fractions among the samples. Analyzes were performed on SPSS 20.0 (Chicago, United States), Origin version 2020 (Northampton, MA, USA) and GraphPad Prism 8.0 (San Diego, United States).

The merged diffuse reflectance spectra of the treatments were normalized (0 to 100 range) with data points *(Zi)* calculated as $Zi = [(x_i - \bar{x})/(sd)]$, where x_i is the data point $(x_1, x_2, x_3 \ldots x_n)$, $\bar{x}$ is the sample mean, and *sd* is the sample standard deviation. The Hem and Gth contents were estimated from the 2nd derivative of the *Kubelka-Munk* function (Kubelka and Munk 1931) before the normalization. Thus, the amplitudes of the Hem (A*Hem*) bands (530-570 nm) and Gth (A*Gth*) bands (420-450 nm) in the second derivative spectra of Fe-oxides concentrated clay samples were used, following the equations proposed by Fernandes et al. (2004).

3.3. Results and discussion

3.3.1. Clay mineralogy and Fe-oxides

After the phyllosilicates removal, the soil clay fraction between 0-10 cm revealed a predominance of hematite (Hem), goethite (Gth) and traces of anatase (Ant) and corundum (Crn) (Fig. 1). These minerals are commonly found in tropical and subtropical Oxisols and are attributed to the intense weathering caused by thermal variations and abundance of rainfall, which culminates in processes of desilication and ferralitization (Schwertmann and Murad 1983; Schaefer et al. 2008).

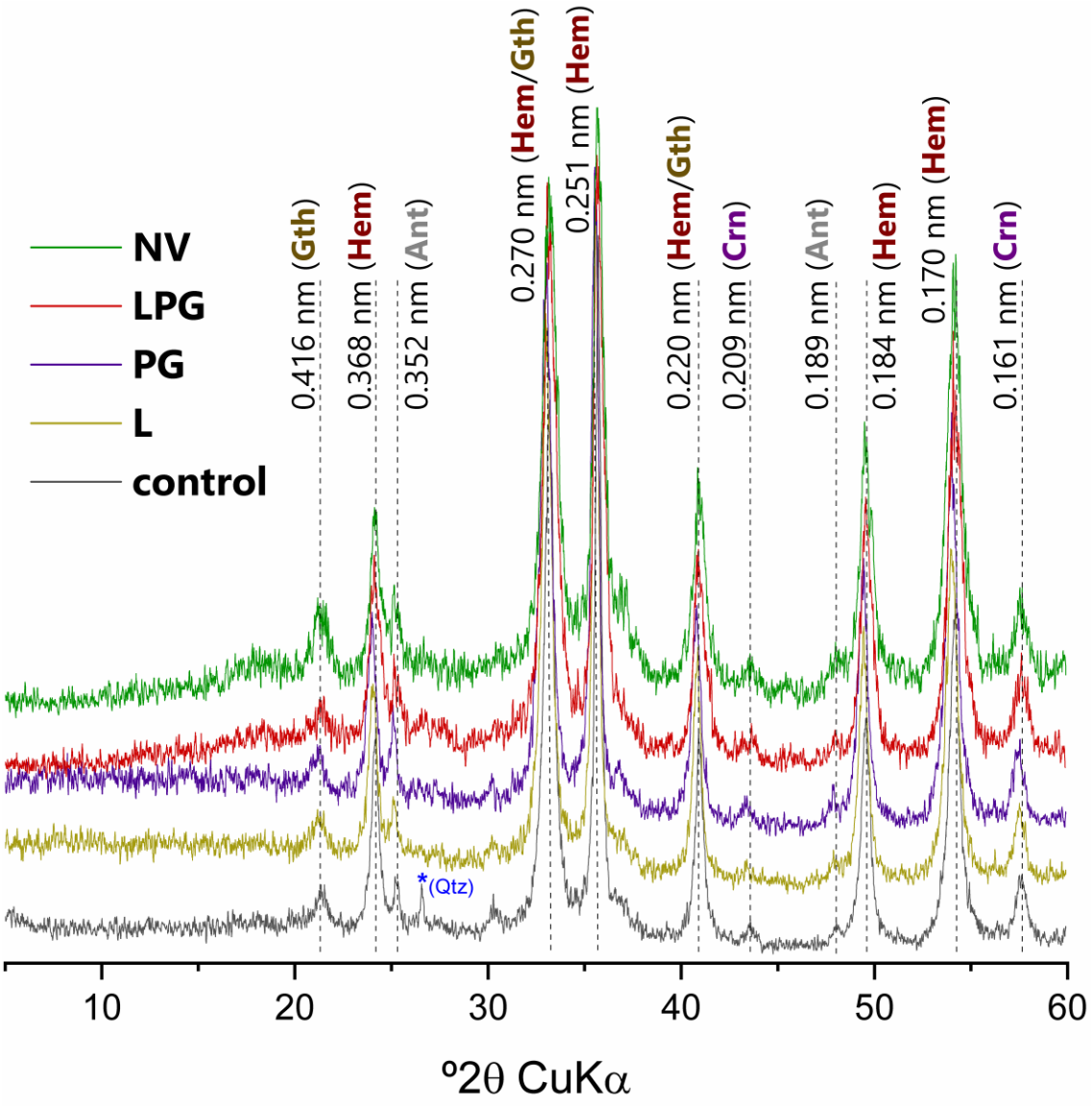

Figure 1. X-ray diffraction of clay fractions from 0-10 cm soil layer. Hem – hematite (d-spaces at 0.368; 0.270; 0.251; 0.220; 0.184; 0.170 nm), Gth – goethite (d-spaces at 0.416; 0.270; 0.220), anatase – Ant (d-spaces at 0.352; 0.189 nm), Crn – corundum (d-spaces at 0.209; 0.161 nm). *Quartz (Qtz) residues (d-space at 0.335 nm). Lime (L); phosphogypsum (PG); lime + phosphogypsum (LPG); native vegetation (NV).

No prominent variations were observed among the diffractograms, with the exception of the control treatment with a defined quartz (Qtz) peak at 0.335 nm, that can remain in the clay fraction even after extraction procedures (Sayin and Jackson 1979). The absence of differences between peak intensities for Hem and Gth indicates that the treatments did not change the crystallinity of these Fe-oxides to a degree that is detectable by conventional XRD. The absence of peaks at 0.72 nm and 0.48 nm indicates that treatment with 5 mol l^{-1} NaOH was efficient in removing Kaolinite (Kln) and Gibbsite (Gbs).

The prevalence of Hem and Gth as Fe-oxides was expected and is related to characteristics in the region such as high soil drainage, high Fe contents in the parent material, high temperatures and fast biomass decomposition, reducing Fe complexation (Schwertmann and Taylor 1989). The presence of Anatase (Ant) was also expected because of the high resistance of titanium (Ti)-oxides. These TiO_2 minerals are generally residual minerals inherited from the parent material although due to their low concentrations they do not have pronounced effects on soil chemical reactivity (Fitzpatrick et al. 1978). Corundum (α-Al_2O_3) is an Al-oxide not so common in soils, but their presence is linked with igneous or metamorphic rocks as parent materials (Schaefer et al. 2008).

There are relationships between crystallochemical and morphological features of Hem and the second-derivative spectra obtained by DRS (Torrent and Barrón, 2003). An example is the degree of substitution of Fe for Al in Hem's crystals; when this degree is high, it causes a slight displacement of the ~545 nm band to shorter wavelength values due to the presence of Al. The same applies for SSA, in which the ~545 nm band shifts to shorter wavelength (higher energy) with increasing SSA. In our study, the band mentioned by Torrent and Barrón (2003) at ~545 nm was at ~535 nm, which leads to a reasonable substitution for Al and low crystallinity in relation to the highly crystalline Hem. However, the variation in the position of this band between the samples was very

low (Fig. 2b), which does not indicate differences among treatments in the degree of Al substitution and SSA of Hem particles.

For Gth, divergences between the spectra were observed, especially regarding the band intensities at ~455 nm and the band shape at ~505 nm from the PG treatment (Fig. 2c). According to Jiang et al. (2013), the amplitude of the band at ~455 nm increases with the degree of Al isomorphic substitution by Fe in the crystalline structure of Gth. The influence of Al in the diffuse reflectance spectra is due to two factors, according to Jiang et al. (2014): **i**) the alteration in the $Fe_{(III)}$–$Fe_{(III)}$ magnetic coupling between face-sharing octahedra caused by Al incorporation in the crystals, increasing the electron pair transition band energy (Scheinost et al. 1999) and **ii**) and by the associations of smaller $Al(O,OH)_6$ octahedra with larger $Fe(O,OH)_6$ octahedra giving rise to substantial distortions that alters interatomic distances and lower the crystal symmetry, shifting the band position (Sherman and Waite 1985).

Although it is not possible to determine which of the two pathways mentioned was predominant, the differences between treatments in the 455 nm (Fig. 2c) band indicate that NV had more Al in the Gth structure, and less in LPG. This is consistent with the high levels of Al^{3+} and H+Al obtained in NV and with the low pH (Table 3). In addition, it shows that cultivation associated with Al-suppressors broadcast can have effects on the neoformation of Gth crystals, reducing the Al concentration.

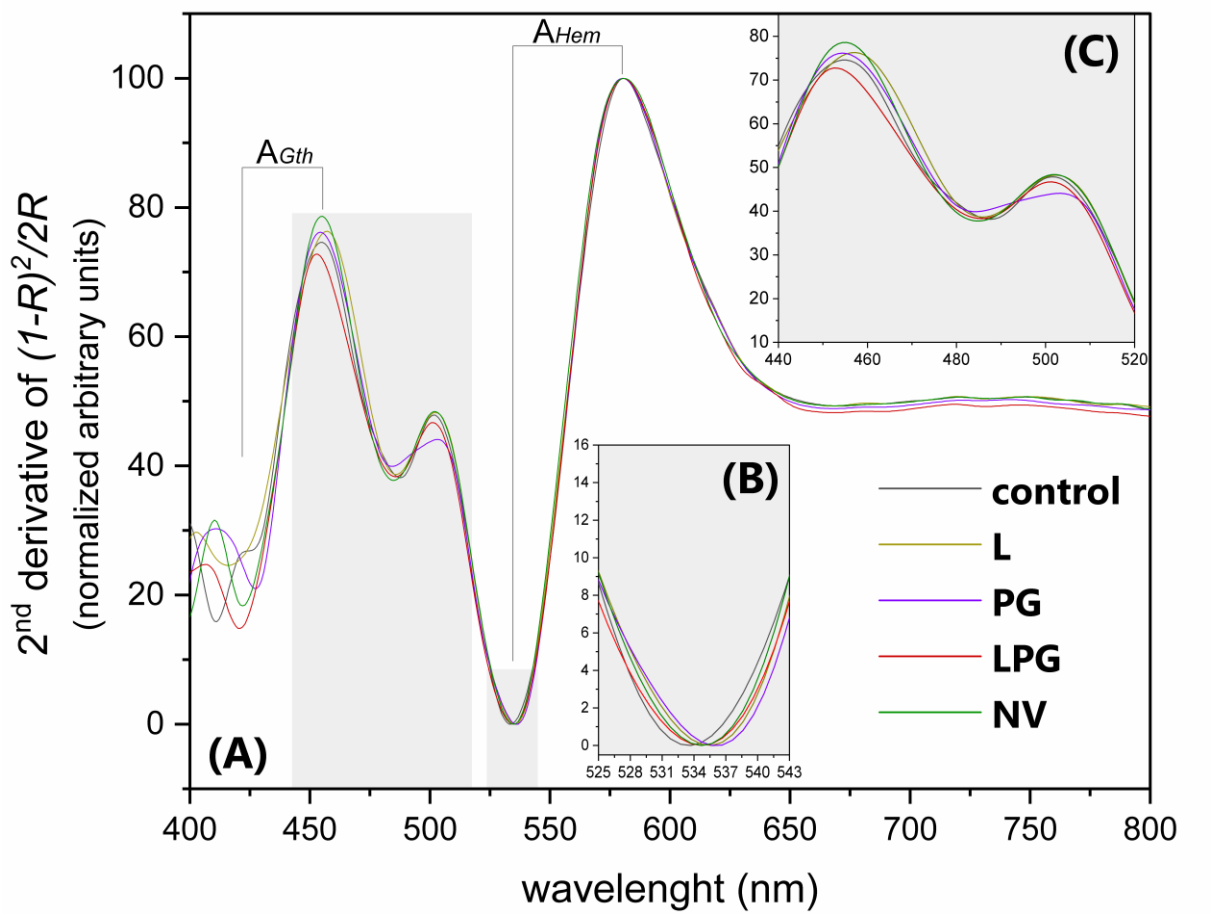

Figure 2. Normalized diffuse-reflectance spectra of Fe-oxides concentrated clay fractions of and Oxisol between 0 and 10 cm (**A**) and amplifications in the region between 525 and 543 nm (**B**) and in the region between 440 and 520 nm (**C**). Lime (L); phosphogypsum (PG); lime + phosphogypsum (LPG); native vegetation (NV).

The higher amplitude bands of Hem in Fig. 2 in relation to the Gth bands indicate higher concentrations of Hem in the soil clay fraction, which was partially confirmed by the intensity of the XRD peaks (Fig. 1) and by the strongly red color of the soil. Following the equations proposed by Fernandes et al. (2004), for samples of the clay fraction of Oxisols after the treatment for concentration of Fe-oxides (5 mol l^{-1} NaOH), it was possible to estimate the concentrations of Hem and Gth in this fraction. The procedure was performed before normalization of the second-derivative spectra and revealed an average Hem content of 60.4 g kg^{-1} and Gth of 36.2 g kg^{-1} (Table 2).

Table 2. Hematite and goethite amplitude bands, estimated contents, and Hem/(Hem+Gth) ratio in Fe-oxides concentrated clay fractions from 0-10 cm soil layer.

attribute	control	PG	L	LPG	NV
A*Hem*	0.00389	0.00382	0.00325	0.00457	0.00346
A*Gth*	0.00186	0.00211	0.00194	0.00265	0.00208
(1)Hem (g kg^{-1})	62.1	60.8	50.7	74.2	54.3
(2)Gth (g kg^{-1})	34.7	36.1	35.1	39.0	35.9
(3)Hem/(Hem+Gth) ratio	0.53	0.52	0.44	0.61	0.47

(1)Hem contents (g kg^{-1}) estimated by the equation y = -7.2+17807*A*Hem*; (2)Gth contents (g kg^{-1}) estimated by the equation y = 24.7 5389*A*Gth*; (3)Hem/(Hem+Gth) ratio estimated by the equation y = 0.02-11.52*A*Gth*+136.67*A*Hem* proposed by Fernandes et al. (2004) for Fe-oxides concentrated clay fractions. Lime (L); phosphogypsum (PG); lime + phosphogypsum (LPG); native vegetation (NV).

For Hem, the highest contents were observed in the LPG treatment and the lowest in L. As for Gth, the variations were smaller in relation to Hem, with the highest contents found in LPG and the lowest in the control. These contents of Fe-oxides (Hem + Gth) in the clay fraction are compatible with the total Fe contents found in the soil (on average 44.4 g kg^{-1}) considering that the clay fraction made up ~35% of the solid soil phase. The results are also within the reported by Bahia et al. (2015) in Oxisols from São Paulo state, in which the Fe-oxides contents ranged from 22 to 253 g kg^{-1} in the 0-20 cm soil layer. The average Hem/(Hem+Gth) ratio of ~0.52 indicated the predominance of Hem in relation to Gth in the soil (Table 2).

3.3.2. Chemical properties

The lime-amended treatments had higher pH values in relation to the other conditions (Table 3). Increases in pH were expected due to the neutralization o H+ by carbonate (CO_3^{2-}). The control treatment and the NV exhibited the lowest pH values (Table 3). These results indicate that non-amended soil samples kept the pH of natural vegetation soil. The effects of liming in reducing toxic forms of Al^{3+} were confirmed by the low contents (~1 mmolc dm^{-3}) found in L and LPG (Table 3). The potential acidity (H+Al) of the soil was also reduced to values that corresponds to ~28% of those observed in the control treatment. These changes are mainly due to the increase in pH that favored the Al hydrolysis.

Table 3. Selected soil chemical attributes in the 0-0.01 m layer of an Oxisol.

attribute	control	PG	L	LPG	NV
pH H_2O	4.6 c	4.9 b	5.8 a	6.0 a	4.5 c
pH 0.01 mol l^{-1} $CaCl_2$	4.0 c	4.3 b	5.2 a	5.4 a	3.9 c
SOC (g dm^{-3})	30 b	32 b	34 b	35 b	49 a
H+Al ($mmol_c$ dm^{-3})	67 b	55 b	29 c	25 c	113 a
Al^{3+} ($mmol_c$ dm^{-3})	11 b	8 b	2 c	1 c	19 a
Ca^{2+} ($mmol_c$ dm^{-3})	5 c	28 b	43 a	52 a	7 c
P (mg dm^{-3})	33 ab	32 ab	31 b	38 a	10 c
Total Fe (g kg^{-1})	37 n.s.	39 n.s.	48 n.s.	47 n.s.	51 n.s.
Total Al (g kg^{-1})	16 n.s.	18 n.s.	19 n.s.	20 n.s.	19 n.s.
Total Ca (mg kg^{-1})	121 c	253 bc	410 b	703 a	129 c
Total P (mg kg^{-1})	476 a	477 a	521 a	558 a	346 b

Lime (L); phosphogypsum (PG); lime + phosphogypsum (LPG); native vegetation (NV). Means followed by the same letter in the same row are not different by *Tukey* test at $p < 0.05$.

In the PG treatment, the absence of chemical reactions producing OH^- limited the pH increase in the soil, as observed in the treatments with lime. However, even so, the pH observed in PG was higher than that of the control treatment (Table 3). This may be related to the formation of the Al_3SO_4 ionic pair and consequently a decrease in the Al concentration that can undergo hydrolysis and generate H^+ in the soil (Zoca and Penn 2017). Although phosphogypsum has no direct effect on pH, the ligand exchange reactions of SO_4^{2-} with terminal hydroxides in Fe- and Al-(hydr)oxides may displace OH^- and support partial soil acidity neutralization (Bossolani et al. 2020).

The highest contents of Ca were found in the LPG treatments because this treatment received lime and phosphogypsum, both containing Ca. Calcium contents were low in sois samples from the control and NV, evidencing that the soil was naturally not rich in basic cations. Considering the amounts of Ca that were added in PG and L over the 18 years of experimentation, there was a difference of 250 kg ha^{-1} more than Ca in PG. However, the contents of exchangeable Ca in PG were 35% lower compared to L (Table 3). This probably occurred due to the lower mobility of $CaCO_3$ in the soil profile and consequent accumulation in most superficial layers of the soil, such as the 0-0.1 m layer from which the results contained in table 3 were obtained. The linear correlation between the contents of Ca^{2+} and SOM was low (r = -0.44), which may be

linked to the wide range in Ca^{2+} contents among the samples (e.g. high Ca^{2+} contents resulting from the amendment rates and low Ca^{2+} contents in the NV).

The total contents of Fe and Al did not differ ($p > 0.05$) among treatments. However, differences were found for the total contents of P and Ca in the soil and are related to the management practices carried out in the experimental area. The total contents of Ca followed the trend of rates and types of amendments used, while the lowest contents were expected in NV and in the control, because they did not receive lime and phosphogypsum. For P, a difference was observed only between the NV soil and the amended soils which, in turn, did not differ from each other but had 32% more total P contents than NV, on average.

The low values of Prem in the LPG and NV indicated greater potential for P fixation in these conditions compared to the others (Fig. 3). Although the pH of soil samples from the control did not differ from those found in NV, the levels of Al^{3+} and H+Al were higher in NV. The retention of P by Al-(hydr)oxides is a recurrent phenomenon in acidic soils and drastically reduces the bioavailability of P, especially by the adsorption in SRO Fe and Al mineral phases (McGahan et al. 2003). Paradoxically, the available P contents in the LPG treatment were the highest, about four times higher than those observed in NV.

The higher concentrations of H+Al and Al^{3+}, indicative of the presence of Al phases that are phosphate sinks, could explain the lower values of available P and P_{rem} in NV. Still, the low Prem contents in the LPG treatment are intriguing and may be related to the formation of Ca-phosphates in the slurry after the addition of 60 mg l^{-1} P (KH_2PO_4) solution, and consequent saturation of the medium with phosphate, to determine the Prem index. Another factor that was probably determinant for the low Prem contents in NV was SOM, which presented a linear correlation of -0.67 with the contents of P_{rem}. The higher P retention in conditions with a greater amount of SOM may be linked to those reported by McGahan et al. (2003), Grand and Lavkulich (2015) and Weng et al. (2020), who detected formation of SRO Fe and Al phases in soils with progressive acidification and increased OC contents.

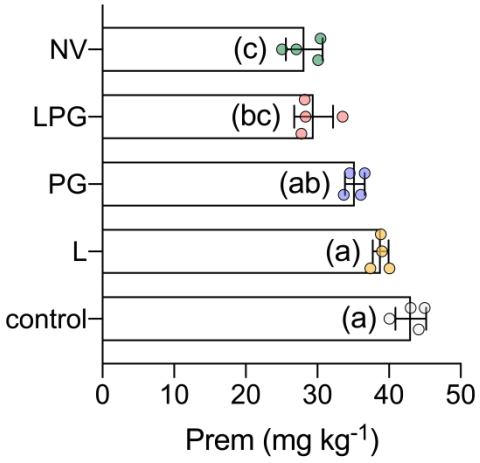

Figure 3. Remaining P (P_{rem}) index between 0-10 cm soil layer. Different letters in the columns indicate significant difference (*Tukey* test, $p < 0.05$, n = 4). Lime (L); phosphogypsum (PG); lime + phosphogypsum (LPG); native vegetation (NV).

3.3.3. Fe fractions

Treatments influenced all Fe fractions except om-Fe, which averaged 0.74 g kg^{-1} (Fig. 4). The tf-Fe fraction was higher in the lime-amended treatments and in the NV. The highest contents of c-Fe fraction were found in L and LPG treatments. On the other hand, for the nc-Fe fraction, the highest contents were found in L treatment and NV (Fig. 4). For re-Fe fraction the higher contents were found in the NV (Fig. 4).

Iron fractions concentrations decreased in the order tf-Fe > c-Fe > re-Fe ~ nc-Fe > om-Fe. Wang et al. (2019) evaluated the effect of 37-years fertilizer management on a sandy loam soil and found the same sequence. According to Wang et al. (2019), the long-term manure application may increase nc-Fe fraction, which binds to SOM in the form of macroaggregates. The reports of Wang et al. (2019) are in agreement with the results presented in Fig. 5a, in which nc-Fe exhibited a high positive correlation (R^2 = 0.81) with SOM contents from all treatments.

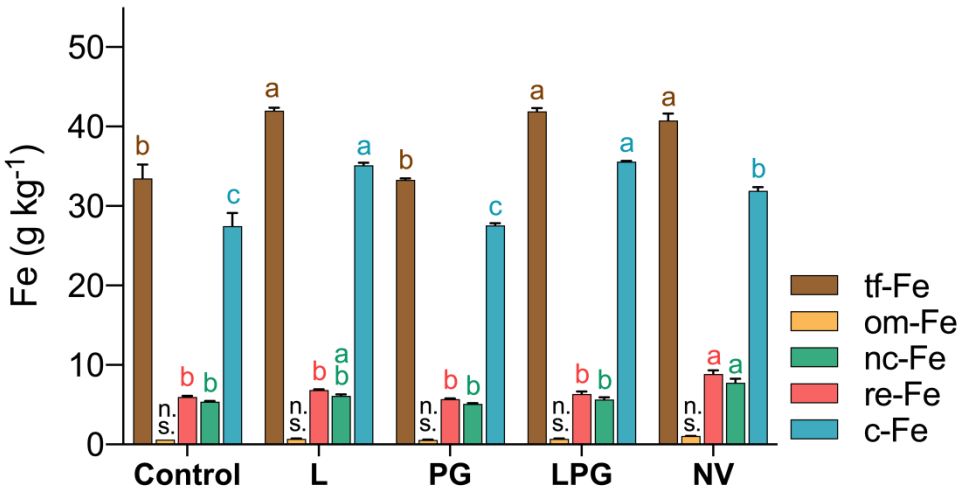

Figure 4. Concentrations of total free Fe (tf-Fe), organic matter bounded Fe (om-Fe), reactive Fe (re-Fe), non-crystalline Fe (nc-Fe) and crystalline Fe (c-Fe) under Al-suppressors treatments and native forest. Bars with the same letter at the top indicate no difference by *Tukey* test at p = 0.05 and n = 4. Lime (L); phosphogypsum (PG); lime + phosphogypsum (LPG); native vegetation (NV).

Despite the high positive correlations for re-Fe and om-Fe in relation to SOM, the use of lime or phosphogypsum had no noticeable effect on these Fe fractions. According to Wang et al. (2019), the formation of nc-Fe may increase the stabilization of SOC in soil aggregates of varying sizes. This process is favored when manures are applied to the soil. In our study, however, the prolonged use of lime did not increase the formation of nc-Fe forms associated with SOM, despite the positive effects of liming in increasing SOC contents (Carmeis Filho et al. 2017). These results suggest that the increase in quantity and quality of SOM promoted by liming could not stimulate the formation of ternary complexes with Fe-oxides, Ca^{2+} and SOM. However, the high R^2 of the linear model between SOM and re-Fe also indicates that these free Fe forms are associated with SOM stabilization, as reported by Wang et al. (2019).

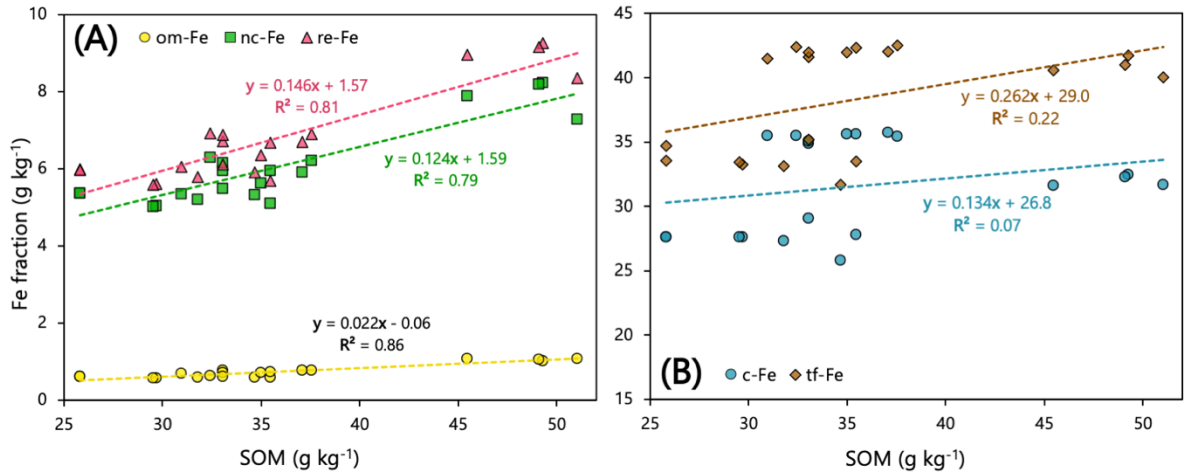

Figure 5. Linear models for the relationship between soil organic matter (SOM) and om-Fe; nc-Fe; re-Fe (**A**), and c-Fe; tf-Fe (**B**).

The increases in c-Fe and tf-Fe fractions in the lime-amended treatments reinforces that long-term lime broadcast affects crystalline Fe forms. However, based on the coefficients of determination of the linear models between SOM and c-Fe, and SOM and tf-Fe (Fig. 5b), it is possible to verify that there is a low association of these forms of Fe with SOM. This agrees with Kwon et al. (2014) and Wang et al. (2019), who highlighted that the stabilization of SOC is more closely linked to non-crystalline Fe forms in uppermost soil layers.

3.3.4. Fe-EXAFS

The long-term effects of lime and/or phosphogypsum broadcast on Fe-oxides properties was carried out by speciation of the *K*-edge of Fe in the XANES and EXAFS regions. For these analyzes, key samples were selected (control, LPG and NV) because they had the greatest variations in chemical and mineralogical attributes investigated so far.

In general, soil samples revealed spectra with hardly perceptible variations. However, the reference samples presented quite different spectra, especially in amplitudes and shapes between ~4.5 and ~10 Å (Fig. 6). The lower crystallinity and structural ordering of Fh promoted the formation of a flatter spectra, especially in

wavenumbers higher than 9 Å, in contrast to that observed for Fe-oxides of higher structural order (Hem and Gth) (Fig. 5).

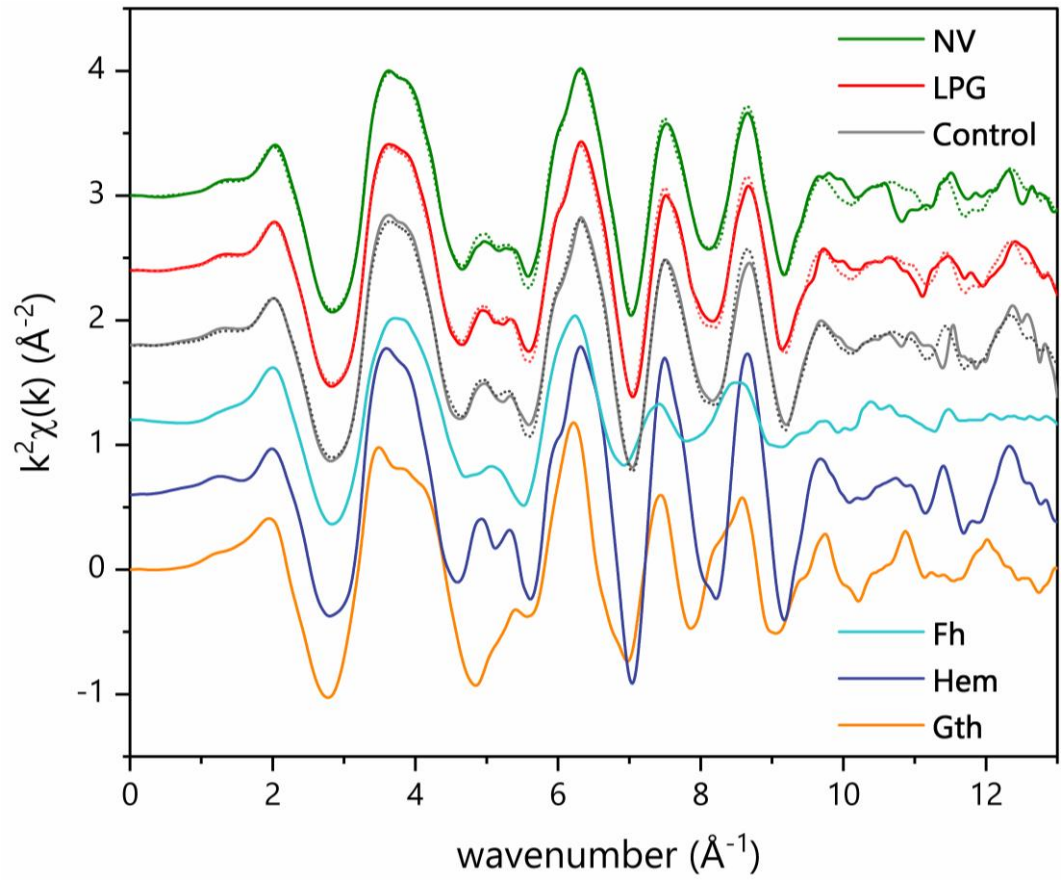

Figure 6. Iron *K*-edge EXAFS spectra for control, lime+phosphogypsum (LPG) and native vegetation (NV) soil samples and goethite (Gth), hematite (Hem) and ferrihydrite (Fh) reference samples. Soil samples data are overlaid by LCF spectra (dotted lines).

The mineralogical constitution of Oxisols is generally dominated by kaolinite, quartz, Fe- and Al-(hydr)oxides (Schaefer et al., 2008). The formation of Fh in well-drained tropical Oxisols is extremely rare. This is due to pedo-environmental conditions such as desilication, bioturbation and ferralitization that accelerate the transformation of Fh in Hem. Therefore, the reference sample Fh used in the Fe-EXAFS analyzes was inserted to represent Fe-oxides of lesser structural order or SRO Fe phases. The Hem-Fh association is atypical when compared to the Gth-Fh association (Parfitt et al., 1988) and shows that the transformation from Fh to Hem occurs fast.

The distribution patterns of Fe-species among the soil samples were the same in Fe-EXAFS and Fe-XANES, which reflects the quality of the LCF performed (Table 4). Low R-factors (~0.02 on average) and uncertainties (~3% on average) are acceptable for samples with a diverse composition as soils. Considering all data, the weighting factors summed up to 96-100% and were presented normalized to 100% (Table 4).

The LCF revealed that Hem and Fh contributed with the highest proportions of Fe-species. The highest proportions of Fh were found in the native forest soil (Table 4). Similar results were obtained by Antonangelo et al. (2020) in an Oxisol under long-term P rates management. For Antonangelo et al. (2020), the high proportions of Fh (> 50%) in the LCF was probably related to the presence of lesser structural ordered Fe-oxides. These Fe-oxides with less crystalline arrangement can be formed in Oxisols by association with organic acids, by complexation processes or by the action of microorganisms (Wagai and Mayer 2007; Hori et al. 2015). These results are in agreement with the high contents of SOM (Table 3), as well as the nc-Fe and re-Fe fractions (Fig. 4) observed in this study.

Table 4. Relative proportions of Fe-oxides (Hem, Fh and Gth) estimated by linear combination fitting analysis of the Fe-EXAFS and Fe-XANES data regions data.

sample	% Fe specie ± uncertainty			R-factor[1]	chi-squared
	Hem	Fh	Gth		
	Fe-EXAFS				
control	57±3	35±3	8±1	0.01206	0.6169
LPG	51±3	40±4	9±1	0.01599	0.8074
NV	40±3	48±3	12±2	0.01214	0.5978
	Fe-XANES[2]				
control	50±3	39±4	11±2	0.01451	0.01412
LPG	40±4	46±5	14±3	0.02538	0.02449
NV	18±3	61±6	21±4	0.04378	0.04272

[1] R-factor=$\sum[(data-fit)^2]/\sum(data^2)$ (Kelly et al., 2008).

[2] For Fe-XANES the first derivative of spectra was used during the LCF.

The low contribution of Gth to the LCF was expected due to its low expression in mineralogical analyzes (XRD and DRS). However, in the LCF of Fe-XANES in the native forest soil the Gth proportions were higher than those of Hem, which was not observed in the LCF of Fe-EXAFS (Table 4). Considering only the control and LPG samples, the use of amendments did not promote notable changes in the proportions of Hem and Fh in the LCF of Fe-EXAFS, but the participation of Fh increased in the LPG treatment. These results are not in line with the pattern of increased c-Fe fraction in LPG (Fig. 4) but serve as an indication that prolonged management with amendments can affect Fe-species.

3.4. Conclusions

The associations of Fe-oxides with SOM were not enhanced by liming. However, the P retention potential, estimated by Prem, may increase with the joint use of lime and phosphogypsum. Despite this, the P availability did not vary between treatments.

The dominant minerals in the clay fraction of the soil were hematite and goethite, the latter presenting greater substitution by Al in the native forest area.

Fractions of Fe were influenced by the long-term use of amendments, especially crystalline Fe fractions after the long-term use of lime and phosphogypsum combined.

Even with the variations in Fe fractions, solid state Fe-species obtained by XAS were not considerably influenced by amendments, and the most notable effects were observed in soil samples from the native forest, where lesser structural ordered species prevailed.

References

Alvarez V, Novais RF, Dias LE, Oliveira JA (2000) Determination and use of remaining phosphorus. Inf Bull Brazilian Soil Sci Soc 25:27–32

Antonangelo JA, Firmano RF, Zhang H, et al (2020) Phosphorus speciation by P-XANES in an Oxisol under long-term no-till cultivation. Geoderma 377:114580.

Aye NS, Sale PWG, Tang C (2016) The impact of long-term liming on soil organic carbon and aggregate stability in low-input acid soils. Biol Fertil Soils 52:697–709.

Bache BW, Williams EG (1971) A phosphate sorption index for soils. J Soil Sci 22:289–301.

Bahia ASRS, Marques Junior J, Siqueira DS (2015) Procedures using diffuse reflectance spectroscopy for estimating hematite and goethite in Oxisols of São Paulo, Brazil. Geoderma Reg 5:150–156.

Bertic B, Vukadinovic V, Kovacevic V, Juric I (1988) Influence of lime on soil acidity and iron availability. J Plant Nutr 11:1361–1367.

Bertsch PM, Bloom PR (1996) Aluminum. In: Sparks DL (ed) Methods of Soil Analysis Part 3 - Chemical Methods. pp 517–550

Bossolani JW, Crusciol CAC, Merloti LF, et al (2020) Long-term lime and gypsum amendment increase nitrogen fixation and decrease nitrification and denitrification gene abundances in the rhizosphere and soil in a tropical no-till intercropping system. Geoderma 375:114476.

Bottinelli N, Angers DA, Hallaire V, et al (2017) Tillage and fertilization practices affect soil aggregate stability in a Humic Cambisol of Northwest France. Soil Tillage Res 170:14–17

Briedis C, De Moraes Sá JC, Caires EF, et al (2012a) Changes in organic matter pools and increases in carbon sequestration in response to surface liming in an Oxisol under long-term no-till. Soil Sci Soc Am J 76:151–160.

Briedis C, Sá JC de M, Caires EF, et al (2012b) Soil organic matter pools and carbon-protection mechanisms in aggregate classes influenced by surface liming in a no-till system. Geoderma 170:80–88.

Brindley GW, Brown G (1980) Crystal structure of clay minerals and their X-ray identification. Mineralogical Society, London

Caires EF, Guimarães AM (2018) A novel phosphogypsum application recommendation method under continuous no-till management in Brazil. Agron J 110:1987–1995.

Caires EF, Haliski A, Bini AR, Scharr DA (2015) Surface liming and nitrogen fertilization for crop grain production under no-till management in Brazil. Eur J Agron 66:41–53.

Cantarella H, van Raij B, Quaggio JA (1998) Soil and plant analyses for lime and fertilizer recommendations in Brazil. Commun Soil Sci Plant Anal 29:1691–1706.

Carmeis Filho ACA, Crusciol CAC, Guimarães TM, et al (2018) Changes in soil physical properties and carbon protection mechanisms by surface application of lime in a tropical no-tillage system. Soil Sci Soc Am J 82:56–65.

Carmeis Filho ACA, Penn CJ, Crusciol CAC, Calonego JC (2017) Lime and phosphogypsum impacts on soil organic matter pools in a tropical Oxisol under long-term no-till conditions. Agric Ecosyst Environ 241:11–23.

Carvalho MCS, Van Raij B (1997) Calcium sulphate, phosphogypsum and calcium carbonate in the amelioration of acid subsoils for root growth. Plant Soil 192:37–48.

Castro GS a, Crusciol C a C, Calonego JC, Rosolem C a. (2015) Management impacts on soil organic matter of tropical soils. Vadose Zo J 1-8.

Colombo C, Palumbo G, He JZ, et al (2014) Review on iron availability in soil: Interaction of Fe minerals, plants, and microbes. J Soils Sediments 14:538–548.

Cornell RM, Schwertmann U (2003) The Iron Oxides

Costa CHM, Crusciol CC (2016) Long-term effects of lime and phosphogypsum application on tropical no-till soybean-oat-sorghum rotation and soil chemical properties. Eur J Agron 74:119–132.

Deshpande TL, Greenland DJ, Quirk JP (1964) Role of iron oxides in the bonding of soil particles. Nature 201:107–108.

Fageria NK, Baligar VC (2008) Ameliorating soil acidity of tropical Oxisols by liming for sustainable crop production. 99:345–399.

Feng W, Plante AF, Aufdenkampe AK, Six J (2014) Soil organic matter stability in organo-mineral complexes as a function of increasing C loading. Soil Biol Biochem 69:398–405.

Fernandes RBA, Barrón V, Torrent J, Fontes MPF (2004) Quantification of iron oxides in Brazilian Latosols by diffuse reflectance spectroscopy. Rev Bras Ciência do Solo 28:245–257.

Fitzpatrick R, Le Roux J, Schwertmann U (1978) Amorphous and crystalline iron-titanium oxides in synthetic preparation, at near ambient conditions, and soil clays. Clays Clay Miner 26:189–201

Gee GW, Bauder JW (1986) Particle-size analysis. In: Klute A (ed) Methods of soil analysis: Physical and Mineralogical Methods. American Society of Agronomy, Madison, pp 383–412

Gee GW, Or D (2002) Particle-size analysis. In: Dane JH, Toop GC (eds) Methods of soil analysis: physical methods. Soil Science Society of America, pp 255–293

GIle PL, Carrero JO (1920) Cause of lime-induced chlorosis and availability of iron in the soil. J Agric Res 33–61

Grand S, Lavkulich LM (2015) Short-range order mineral phases control the distribution of important macronutrients in coarse-textured forest soils of coastal British Columbia, Canada. Plant Soil 390:77–93.

Groppo JD, Lins SRM, Camargo PB, et al (2015) Changes in soil carbon, nitrogen, and phosphorus due to land-use changes in Brazil. Biogeosciences 12:4765–4780.

He H, Liu L, Munir S, et al (2019) Crop diversity and pest management in sustainable agriculture. J Integr Agric 18:1945–1952.

Heanes DLL (1984) Determination of total organic-C in soils by an improved chromic acid digestion and spectrophotometric procedure. Commun Soil Sci Plant Anal 15:1191–1213.

Hori T, Aoyagi T, Itoh H, et al (2015) Isolation of microorganisms involved in reduction of crystalline iron(III) oxides in natural environments. Front Microbiol 6.

Inagaki TM, de Moraes Sá JC, Caires EF, Gonçalves DRP (2017) Why does carbon increase in highly weathered soil under no-till upon lime and gypsum use? Sci Total Environ 599–600:523–532.

Jenkinson DS, Powlson DS (1976) The effects of biocidal treatments on metabolism in soil. Soil Biol Biochem 8:209–213.

Jiang Z, Liu Q, Colombo C, et al (2013) Quantification of Al-goethite from diffuse reflectance spectroscopy and magnetic methods. Geophys J Int 196:131–144.

Joris HAW, Caires EF, Scharr DA, et al (2016) Liming in the conversion from degraded pastureland to a no-till cropping system in Southern Brazil. Soil Tillage Res 162:68–77.

Kleber M, Eusterhues K, Keiluweit M, et al (2015) Mineral-Organic Associations: Formation, properties, and relevance in soil environments. Elsevier Ltd

Kubelka P, Munk F (1931) Ein beitrag zur optic der farbanstriche. Zeitschrift für Tech Phys 12:593–620

Kwon MJ, Boyanov MI, Antonopoulos DA, et al (2014) Effects of dissimilatory sulfate reduction on Fe_{III} (hydr)oxide reduction and microbial community development. Geochim Cosmochim Acta 129:177–190.

Lalonde K, Mucci A, Ouellet A, Gélinas Y (2012) Preservation of organic matter in sediments promoted by iron. Nature 483:198–200.

Lindsay WL (2001) Chemical equilibria in soils, 2nd edn. The Blackburn Press

Lindsay WL, Schwab AP (1982) The chemistry of iron in soils and its availability to plants. J Plant Nutr 5:821–840.

McDowell R, Condron L (2001) Influence of soil constituents on soil phosphorus sorption and desorption. Commun Soil Sci Plant Anal 32:2531–2547.

McGahan DG, Southard RJ, Zasoski RJ (2003) Mineralogical comparison of agriculturally acidified and naturally acidic soils. Geoderma 114:355–368.

McKeague JA, Day JH (1966) Dithionite and oxalate Fe and Al as aids in differentiating various classes of soils. Can J Soil Sci 46:13–22

Mehlich A (1957) Aluminum, iron, and pH in relation to lime induced manganese deficiencies. Soil Sci Soc Am J 21:625–628.

Mehra OP, Jackson ML (1960) Iron oxide removal from soils and clays by a dithionite–citrate system buffered with sodium bicarbonate. In: Clays and clay minerals: proceedings of the Seventh National Conference. pp 317–327

Murphy J, Riley JP (1962) A modified single solution method for the determination of phosphate in natural waters. Anal Chim Acta 27:31–36.

Norse D (2012) Low carbon agriculture: Objectives and policy pathways. Environ Dev 1:25–39.

Oates KM, Caldwell AG (1985) Use of by-product gypsum to alleviate soil acidity. Soil Sci Soc Am J 49:915–918.

Rosolem C, Li Y, Garcia R (2016) Soil carbon as affected by cover crops under no-till under tropical climate. Soil Use Manag 32:495–503.

Rowley MC, Grand S, Verrecchia ÉP (2018) Calcium-mediated stabilisation of soil organic carbon. Biogeochemistry 137:27–49.

Sá JC de M, Lal R, Cerri CC, et al (2017) Low-carbon agriculture in South America to mitigate global climate change and advance food security. Environ Int 98:102–112.

Sanaullah M, Usman M, Wakeel A, et al (2020) Terrestrial ecosystem functioning affected by agricultural management systems: A review. Soil Tillage Res 196:104464.

Sanderman J, Maddern T, Baldock J (2014) Similar composition but differential stability of mineral retained organic matter across four classes of clay minerals. Biogeochemistry 121:409–424.

Sayin M, Jackson ML (1979) Size and shape of fine quartz in the clay fraction of soils and geological materials. Zeitschrift für Pflanzenernährung und Bodenkd 142:865–873.

Schaefer C, Fabris JD, Ker JC (2008) Minerals in the clay fraction of Brazilian Latosols (Oxisols): a review. Clay Miner 43:137–154.

Scheinost AC, Schulze DG, Schwertmann U (1999) Diffuse reflectance spectra of A1 substituted goethite: A ligand field approach. Clays Clay Miner 47:156–164.

Schwertmann U, Murad E (1983) Effect of pH on the formation of goethite and hematite from ferrihydrite. Clays Clay Miner 31:277–284.

Schwertmann U, Taylor RM (1989) Iron oxides. In: Dixon JB, Weed SB (eds) Minerals in soil environments, 2nd edn. Soil Science Society of America, Madison, pp 379–438

Sherman D, Waite T (1985) Electronic spectra of Fe^{3+} oxides and oxide hydroxides in the near IR to near UV. Am Mineral 70:1262–1269

Shoemaker HE, McLean EO, Pratt PF (1961) Buffer methods for determining lime requirement of soils with appreciable amounts of extractable aluminum. Soil Sci Soc Am J 25:274–277.

Simonsson M, Östlund A, Renfjäll L, et al (2018) Pools and solubility of soil phosphorus as affected by liming in long-term agricultural field experiments. Geoderma 315:208–219.

Singh B, Gilkes RJ (1991) Concentration of iron oxides from soil clays by 5 M NaOH treatment: the complete removal of sodalite and kaolin. Clay Miner 26:463–472.

Soil Survey Staff (2014) Keys to Soil Taxonomy, 12th edn. USDA - Natural resources conservation service, Washington, DC

Torrent J, Barrón V (2003) The visible diffuse reflectance spectrum in relation to the color and crystal properties of hematite. Clays Clay Miner 51:309–317.

USPEA (1996) Soil screening guidance: technical background document, 2nd ed. United States Government Publishing Office, Washington, United States of America

Vaezi AR, Zarrinabadi E, Auerswald K (2017) Interaction of land use, slope gradient and rain sequence on runoff and soil loss from weakly aggregated semi-arid soils. Soil Tillage Res 172:22–31

van Raij B, Andrade JC, Cantarella H, Quaggio JA (2001) Chemical analysis for fertility evaluation of tropical soils (in Portuguese). Campinas

van Raij B, Cantarella H, Quaggio JA, Furlani AMC (1996) Fertilization and liming recommendations for São Paulo Sate, Brazil (*in portuguese*). Campinas

Veneranda M, Aramendia J, Bellot-Gurlet L, et al (2018) FTIR spectroscopic semi-quantification of iron phases: A new method to evaluate the protection ability index (PAI) of archaeological artefacts corrosion systems. Corros Sci 133:68–77.

Wagai R, Mayer LM (2007) Sorptive stabilization of organic matter in soils by hydrous iron oxides. Geochim Cosmochim Acta 71:25–35.

Wang P, Wang J, Zhang H, et al (2019) The role of iron oxides in the preservation of soil organic matter under long-term fertilization. J Soils Sediments 19:588–598.

Weng YT, Rathod J, Liang B, et al (2020) Black carbon enriches short-range-order ferrihydrite in Amazonian Dark Earth: Interplay mechanism and environmental implications. Sci Total Environ 725.

Whitting LD, Allardice WR (1986) X-ray diffraction techniques. In: Klute A (ed) Methods of soil analysis: Part 1 - Physical and mineralogical methods, 2nd edn. American Society of Agronomy, Madison, p 1358.

Wilfert P, Kumar PS, Korving L, et al (2015) The relevance of phosphorus and iron chemistry to the recovery of phosphorus from wastewater: a review. Environ Sci Technol 49:9400–9414.

Zoca SM, Penn C (2017) An important tool with no instruction manual: A review of gypsum use in agriculture, 1st edn. Elsevier Inc.

4. PHOSPHORUS SPECIATION AND DISTRIBUTION IN AN OXISOL AMENDED WITH LIME AND PHOSPHOGYPSUM IN A LONG-TERM FIELD EXPERIMENT

ABSTRACT

Long-term management with lime and/or phosphogypsum in tropical soils can change phosphorus (P) forms across the soil profile. Synchrotron-based spectroscopy and sequential chemical fractionation were used to investigate P chemical species after long-term (18 years) amendments' application in an Oxisol. The availability of nutrients increased with the combined use of lime and phosphogypsum, and a stratification of attributes was identified due to long-term broadcast applications. The X-Ray Absorption Near Edge Structure (XANES) spectra profile revealed the predominance P adsorbed to Fe- and Al-mineral species, and also P bounded to kaolinite. Low concentrations of calcium-phosphates in the uppermost soil layer (0-5 cm) were found in the treatment that received high inputs of calcium (Ca) by lime and phosphogypsum broadcast. Few correlations were identified between the proportions of P species obtained by XANES and P fractions operationally defined by sequential chemical fractionation (SF). Still, our results suggest that P-species bound to kaolinite can store stable P forms, which correlate with the residual P fractions obtained by SF and highlight the importance of kaolinite as a legacy P store in Oxisols.

Keywords: P fertilization; P fractions; Solid state XAS; Fe oxides; Kaolinite

4.1. Introduction

Because of the abundance of Fe-, Al- and Mn-(hydr)oxides and the low pH_{H_2O} (between 4.0-5.5), soils from the inter-tropical region adsorb high amounts of orthophosphate (HPO_4^{2-}; $H_2PO_4^-$). Thus, phosphorus (P) availability to plants and P-fertilization efficiency are reduced, impacting food, fuel and fiber production chains. In South America, ~85% of the soils can be considered acid (Fageria and Baligar, 2008). In this scenario, the neutralization of soil acidity by liming reduces the need to open new areas for agriculture and stabilizes food security in developing countries (Godfray et al., 2010).

The adoption of soil cultivation practices that could lower P retention such as no-tillage (NT) has greatly increased in South American Oxisols and Ultisols in the last three decades (Caires et al., 2017; Tiecher et al., 2017). In these management systems, lime (Ca, $MgCO_3.H_2O$) is broadcasted to raise the low pH, the low cation exchange capacity (CEC) and the low bases saturation (BS) of these soils, and to lessen reactive forms of aluminum (Al). Another way for decreasing reactive Al forms is the addition of phosphogypsum (PG), ($CaSO_4.2H_2O$), that does not contain carbonate ions (CO_3^{2-}) for decreasing soil acidity, but contains sulfate (SO_4^{2-}), that binds to Al^{3+} and limits its availability to plants. The concentration of P in phosphogypsum generally does not exceed 1%.

Improvements in soil quality, carbon (C) storage and microbiological activity has been reported frequently in areas under no-till (NT) (Aziz et al., 2013; Castro et al., 2015; Deng and Tabatabai, 1997; Ogle et al., 2012). Likewise, similar effects have been reported in tropical and subtropical soils that receive lime throughout the crops (Briedis et al., 2012; Carmeis Filho et al., 2017; Inagaki et al., 2017). In these environments, the increase in soil organic carbon (SOC) levels and quality can have positive effects on soil P chemistry.

In Brazil, more than 30 million ha are cultivated with soybeans (*Glycine max* L.) and corn (*Zea mays* L.) annually under NT (Freitas and Landers, 2014). The P placement in these areas is usually done at the sowing time, in the rows on which the plants will grow. The efficiency of P-fertilization and the organic P cycling are typically high under NT (Caires et al., 2017; Rodrigues et al., 2016). However, several researchers highlighted the possibility of P stratification in NT systems (Cade-Menun et al., 2010; Mackay et al., 1987; Rehm et al., 1995; Wei et al., 2018).

As lime or phosphogypsum are applied in the soil surface, a microenvironment for the reaction between P and these amendments is created in the first soil centimeters. In this sense, a better understanding of the interactions between P chemistry and these amendments can be useful to optimize NT management practices in highly weathered soils.

Phosphorus speciation in solid samples by X-Ray Absorption Near Edge Structure (XANES) spectroscopy at the P *K*-edge has been effectively employed in soil chemistry studies. By investigating the X-ray absorption spectra and comparing their similarities with reference samples spectra, it is possible to assess which P-bearing species (*i.e.* Ca-, Al-, Fe_{III}-, C-) are prevailing in the sample, and whether or not the P species vary due to the soil management. In recent years, studies associating X-Ray Absorption Spectroscopy (XAS) and soil P sequential chemical fractionation analysis have provided novel agro-environmental insights (Acksel et al., 2019; Gu and Margenot, 2020; Koch et al., 2018; Liu et al., 2013; Luo et al., 2017).

There are few studies about how P-bearing species are affected by soil management practices such as liming and phosphogypsum broadcast in a long-term. In the same way, studies involving speciation of P in soil samples by XAS in different soil layers are also not common. Hence, we used soil samples of a long-term field experiment carried out since 2002 in southeastern Brazil, to ascertain the effects of lime and, or, phosphogypsum broadcasting in a diversified crop rotation under long-term NT. Hence, the general objective was to associate conventional soil analysis with P *K*-edge XANES and P sequential chemical fractionation to evaluate the effects of lime and phosphogypsum on P speciation in an Oxisol under NT.

4.2. Material and methods

4.2.1. Experimental site and treatments

A long-term field experiment has been carried out since 2002 on a Typic Haplorthox (Soil Survey Staff, 2014) in southwestern Brazil (48º 23' W; 22º 51' S; 765 m a.s.l.). The region has a dry winter and a hot wet summer, with the climate classified as subtropical humid. The average minimum and maximum temperatures are 15.3ºC and 26.1ºC, respectively, with an average annual rainfall of ~1,360 mm. The experiment design is a randomized complete block (RCB) with four replications and experimental units (plots) with 48.6 m^2 (5.4 m x 9.0 m). Before the establishment of the field

experiment, some soil chemical attributes in the 0-0.2 m layer were determined (Table 1).

Table 1. Selected soil chemical properties before the installation of the experiment (year 2001).

pH [a]	SOC [b]	P [c]	$_{EX}$Ca [d]	$_{EX}$Mg	$_{EX}$K	$_{EX}$Al
	g dm^{-3}	*mg dm^{-3}*		——— *mmol$_c$ dm^{-3}* ———		
4.2	12	9	14	5	1.2	2.3
H+Al [e]	*e*CEC	*t*CEC [f]	BS	Clay	Silt	Sand
——— *mmol$_c$ dm^{-3}* ———			*%*	——— *g kg^{-1}* ———		
37	23	58	35	347	108	545

[a] pH obtained in 1:2.5 soil:0.01 mol l^{-1} $CaCl_2$ ratio;
[b] Soil Organic Carbon, extracted by chromic acid digestion (Heanes, 1984);
[c] P (phosphorus), extracted with anion exchange resin (van Raij et al., 1986);
[d] $_{EX}$Ca (exchangeable calcium), $_{EX}$Mg (exchangeable magnesium), $_{EX}$K (exchangeable potassium) and $_{EX}$Al (exchangeable aluminum), extracted with ion exchange resin (van Raij et al., 2001);
[e] Potential acidity at pH 7.0, estimated after extraction with SMP solution (Shoemaker et al., 1961);
[f] *t*CEC (total cation exchange capacity), [$_{EX}$Ca+$_{EX}$Mg+(H+Al)+$_{EX}$K]; and *e*CEC (effective cation exchange capacity), ($_{EX}$Ca+$_{EX}$Mg+$_{EX}$K+$_{EX}$Al); and BS (base saturation), [($_{EX}$Ca+$_{EX}$Mg+$_{EX}$K)*100/*t*CEC];

The following treatments were evaluated: (**i**) control (no lime and no phosphogypsum); (**ii**) lime (L); (**iii**) phosphogypsum (PG); and (**iv**) lime and phosphogypsum (LPG). The lime rate was defined according to the chemical analysis of the topsoil (0-0.2 m) to raise 70% of BS (Cantarella et al., 1998); thereby 2700 kg ha-1 of lime were applied in 2002. The rate of phosphogypsum was calculated according to van Raij et al. (1996), with 2100 kg ha^{-1} applied in 2002.

Lime and phosphogypsum applications were performed again when the lime treatment reached ≤50% of BS (which was verified annually). Therefore, when lime reapplication was needed, the phosphogypsum (2100 kg ha^{-1}) was also reapplied. In addition to the initial application of treatments in 2002, there was one application in 2004 and another in 2010, each with 2000 kg ha^{-1} of lime and 2100 kg ha^{-1} of phosphogypsum.

The lowest lime rates in 2004 and 2010 was due to the increased soil BS over time in the experiment (Costa and Crusciol, 2016). There was a need for lime again in 2016, however, the recommendation methods this year were ameliorated. This change

is due to an emerging trend in updating the amendments recommendation in Brazil. For lime, the procedure proposed by Caires et al. (2015) and Joris et al. (2016) was used. The rate of phosphogypsum was calculated based on the recommendation described in Caires and Guimarães (2018). All applications were broadcasted because the experiment is conducted under NT.

The lime was an anhydrous carbonate mineral grounded with 16.6% Ca and 10.5% MgO. The phosphogypsum was a by-product of the manufacture of acidulated phosphate fertilizers, containing 20% Ca, 15% S, <0.1% P and fluorine (F). Throughout the 18 years the experiment has gone through more than 30 crops, being cultivated with several species as detailed by Carmeis Filho et al. (2017) and by Costa and Crusciol (2016). Phosphorus rates were equal for all treatments in all years, varying with the species requirement in each crop. The applications of P were carried out in the sowing line of cultivated species with soluble P-fertilizers such as simple superphosphate (8% P, 16% Ca, 9% S) or triple superphosphate (20% P, 10% Ca).

4.2.2. Soil sampling

Soil samples were collected from 0-0.05 m, 0.05-0.1 m and 0.1-0.2 m soil layers with a soil probe (80-mm diameter) in 2018 during the soybean full bloom (R2 phenological stage). The sampling was performed during R2 because of the higher P absorption rates per soybean plants at this stage. The distance between soybean sowing lines was 0.45 m. Each composite sample was composed of two subsamples in the sowing line, four to 11 cm from the sowing line and four to 22 cm from the sowing line. After collecting ten subsamples per plot, equal volumes were mixed to form a final composite sample. The justification of the sampling procedure is due to the probable overestimation of P contents in a sampling made exclusively at the sowing line.

Plants do not absorb P present only in the sowing line, and any sampling made only in the interline region would underestimate the P contents in the plots as well. Another reason that led us to opt for this sampling method was the fact that the sowing lines were not positioned in the same places over the years and as it is sought to

evaluate the effect of a prolonged management. The soil sampling procedure chosen covered a space close to 0.45 m, coincident with the soybean spacing and covering the surface that received broadcast application of lime and, or phosphogypsum. An isolation of 0.5 m from the edges to the interior of the plots was preserved during the sampling.

Soil samples from native vegetation (NV) located ~100 m from the experimental area were also collected to be used as a reference environment (without direct anthropic interferences) during the investigation. In the NV, ten sampling points were randomly selected in an area of 225 m^2 inside the forest.

4.2.3. Soil chemical properties analysis

Soil samples 2 mm-sieved and air dried has the following soil attributes determined: (**i**) pH in 1:2.5 ratio of soil:0.01 mol l^{-1} $CaCl_2$ solution with a glass electrode; (**ii**) organic carbon extracted by $K_2Cr_2O_7$ (Heanes, 1984); (**iii**) exchangeable Al ($_{EX}$Al) extracted by 1 mol l^{-1} KCl and quantified by the titrimetric method with 0.025 mol l^{-1} NaOH (Bertsch and Bloom, 1996); (**iv**) exchangeable Ca ($_{EX}$Ca) and magnesium ($_{EX}$Mg) extracted by ion exchange resin, according to van Raij et al. (2001) and determined by Atomic Absorption Spectroscopy (AAS) in a Perkin-Elmer 1100B; (**v**) plant-available P extracted by Mehlich-1 solution (0.0125 mol l^{-1} H_2SO_4 + 0.05 mol l^{-1} HCl) (Mehlich, 1953) and by Mehlich-3 solution (0.2 mol l^{-1} CH_3COOH + 0.25 mol l^{-1} NH_4NO_3 + 0.015 mol l^{-1} NH_4F + 0.013 mol l^{-1} HNO_3 + 0.001 mol l^{-1} EDTA) (Mehlich, 1984), with colorimetric quantification according to Murphy and Riley (1962) in a Bel Photonics UV-M51 spectrophotometer; (**vi**) Fe contents in crystalline ("free") oxides ($_{DCB}$Fe), determined after extraction with sodium dithionite-citrate-bicarbonate (Mehra and Jackson, 1960); and (**vii**) Fe contents in less crystalline ("amorphous") oxides, extracted with oxalic acid + ammonium oxalate ($_{OX}$Fe) (Loeppert and Inskeep, 1996).

The pseudototal contents of Al, P, S, Ca and Mg were extracted by microwave assisted acid digestion with concentrated HCl, HNO_3 and HF acids (method EPA 3052) (USEPA, 1996) and determined by Inductively Coupled Plasma Optical Emission

Spectrometry (ICP-OES) in a Thermo Scientific iCAP 6200 working under 1150 W, with 0.5 and 0.7 L min^{-1} of auxiliary and nebulizer gas flow, with yttrium (Y) as internal standard.

4.2.4. Sequential phosphorus fractionation

The soil P fractions were obtained using the Hedley et al. (1982) chemical fractionation procedure with adaptations described by Condron et al. (1985). Triplicate 0.5 g of <2 mm-sieved soil samples were placed into 15-ml screw-cap centrifuge tubes and extracted with: (*i*) anion exchange resin membrane strip (AER) charged by 0.5 $NaHCO_3$ (pH 8.5) in 10 ml of ultrapure water, named $Pi\text{-}_{Resin}$ (end-over-end shaken for 16 h at 25ºC with P desorption from the AER made by 15 ml of 0.5 mol l^{-1} HCl under end-over-end shaken for 2 h at 25ºC); (*ii*) 10 ml of 0.5 mol l^{-1} $NaHCO_3$ (pH 8.5), named $Pi\text{-}_{Bic}$ or $Po\text{-}_{Bic}$; (*iii*) 10 ml of 0.1 NaOH (13.0 pH), named $Pi\text{-}_{NaOH01}$ or $Po\text{-}_{NaOH01}$; (*iv*) 10 ml of 1 mol l^{-1} HCl, named $Pi\text{-}_{HCl}$; (*v*) 10 ml of 0.5 mol l^{-1} NaOH (13.7 pH), named $Pi\text{-}_{NaOH05}$ or $Po\text{-}_{NaOH05}$. The residual P was extracted by H_2SO_4 + H_2O_2 + $MgCl_2$ digestion in the soil remaining after the 0.5 mol l^{-1} NaOH extraction (Brookes et al., 1982), named $P\text{-}_{Residual}$. A blank (no soil) and a standard sample were included within each run and the soil suspensions were centrifuged for 25 min at 2500×g after each extraction.

Total P, composed of inorganic P (Pi) + organic P (Po), was determined from $NaHCO_3$ and NaOH extracts after acidified ammonium persulfate digestion (USPEA, 1993). The Pi was measured in acid extracts by colorimetry, according to Murphy and Riley (1962), and in alkaline extracts, according to Dick and Tabatabai (1977). The Po in extracts was estimated considering the P determined in the extract from total digestion (Pi + Po) minus Pi directly determined in the extract, making it possible to obtain $Po\text{-}_{Bic}$, $Po\text{-}_{NaOH01}$ and $Po\text{-}_{NaOH05}$ fractions. The sum of all Pi and Po fractions including residual P was named $P\text{-}_{fracTotal}$.

Furthermore, P fractions were grouped by relative lability to plants in: (*i*) labile P pool, consisted of $Pi\text{-}_{Resin}$ + $Pi\text{-}_{Bic}$ + $Po\text{-}_{Bic}$ fractions (Tiessen and Moir, 1993); (*ii*) moderately labile P pool, consisted of $Pi\text{-}_{NaOH01}$ + $Po\text{-}_{NaOH01}$ + $Pi\text{-}_{HCl}$ fractions (Hedley

et al., 1982); and (*iii*) non-labile P pool, consisted of $Pi\text{-}_{NaOH05}$ + $Po\text{-}_{NaOH05}$ + $Pi\text{-}_{Residual}$ fractions (Condron et al., 1985). The P fractions grouping scheme proposed by Cross and Schlesinger (1995) was also carried out by dividing the fractions into a biological P pool ($Po\text{-}_{Bic}$ + $Po\text{-}_{NaOH01}$ + $Po\text{-}_{NaOH05}$) and a geochemical P pool ($Pi\text{-}_{Resin}$ + $Pi\text{-}_{Bic}$ + $Pi\text{-}_{HCl}$ + $Pi\text{-}_{NaOH01}$ + $Pi\text{-}_{NaOH05}$ + $P\text{-}_{Residual}$).

4.2.5. Phosphorus *K*-edge XANES spectroscopy

The spectral data were collected at SXS beamline of the Brazilian Synchrotron Light Laboratory. The beamline, equipped with a Si(111) monochromator, was operated in fluorescence mode under vacuum and 1.37 GeV of electron beam energy. The XANES data were collected straight on air-dried 150 µm-sieved samples. Three soil layers (0-0.05, 0.05-0.10 and 0.10-0.20 m) were investigated. The samples used were formed by the blending of equal masses of four composite samples (field replicates).

As reference materials we selected ten chemical compounds: amorphous calcium phosphate; ß-tri-calcium phosphate, brushite ($CaHPO_4ú2H_2O$), DNA, potassium dihydrogen phosphate (KH_2PO_4), lecithin, octa-calcium phosphate [$Ca_8H_2(PO_4)_{\cdot}6.5H_2O$], monetite ($CaHPO_4$), hydroxyapatite-[$Ca_5(PO_4)_3OH$] and Na-phytate ($C_6H_{18}O_{24}P_6$), and six P-sorbed to mineral samples: gibbsite (Al_2O_3), goethite (α-FeOOH), hematite (α-Fe_2O_3), kaolinite, variscite, and ferrihydrite. The P source in the sorption process was K_2HPO_4. The mineral species that underwent P adsorption are supposed to represent the major minerals present in the studied soil that interact expressively with the P. A detailed description of the reference materials origins and P adsorption procedure can be found in Antonangelo et al. (2020).

The samples were diluted to ~0.15% P (m/m) with boron nitride to avoid self-absorption effects. A thin layer of either samples or reference compounds were spread on double coated carbon tape (P-free) and mounted on a stainless-steel sample holder. All samples and reference materials were assigned a reference energy (defined as E0 for data normalization) by setting the maximum of the first derivative spectrum of Ca-phosphate (E_0 = 2150.8 eV). Thereby, any spectral differences in the first derivative

maxima should be spectral shifts attributable to local molecular bonding. The P *K*-edge XANES spectra were collected from 2120 to 2300 eV and the step sizes were 1 eV (2120-2145 eV), 0.2 eV (2145.2-2180 eV), 1 eV (2181-2220 eV), and 3 eV (2223-2300 eV). To improve the signal-to-noise ratio, ~15 scans per sample were performed and merged.

4.2.6. Data analysis

The data homogeneity was previously checked using the *Shapiro-Wilk* test and analyzed considering their replication. Soil chemical attributes and P fractions were subjected to two-way analyses of variance (ANOVA) to reveal the effects of amendment conditions (control, L, PG, LPG and NV), soil layers (0-5 cm; 5-10 cm; 10-20 cm) and their interaction. In the case of sufficiently low *p* values (< 0.05), means were separated by *Tukey* test.

Simple *Pearson's* correlations were performed among P fractions obtained from sequential fractionation (SF) and P-species associated with iron (Fe-P), Al (Al-P) or Kln (Kln-P) obtained from XANES. The data analyzes were performed on IBM SPSS Statistics Desktop version 22 (Armonk, NY, USA) and the preparation of figures on GraphPad Prism 8.0 (San Diego, CA, USA).

The XANES data processing was performed in the Athena software (Ravel and Newville, 2005) with figures prepared on Origin version 2020 (Northampton, MA, USA). All merged spectra were calibrated setting de edge reference energy (E0) at the maximum of the first derivative and then normalized setting the background pre-edge range from E0 -30 to E0 -10 eV, and the normalization range from E0 +35 to E0 +140 eV. The linear combination fitting (LCF) was preceded by a visual inspection of the main features in reference samples. The LCF was performed over the -10 to +45 eV energy range relative to E0 and carried out according to Colzato et al. (2017), employing two approaches that converged to the same results.

4.3. Results and discussion

4.3.1. Soil chemical attributes

Considering the comparisons among treatments on specific soil layers, CEC*t*, $_{EX}$Mg, $_{DCB}$Fe, pseudo-total P and pseudo-total Al were not affected (p > 0.05) by amendments broadcast, especially in the 10-20 cm soil layer (Table 2). Expressive increases in $_{EX}$Ca and pseudo-total Ca contents were expected in L, PG and LPG treatments due to the Ca concentrations in lime and phosphogypsum. The same was observed for $_{EX}$Mg and pseudo-total Mg, although the contents remained low in PG treatment, similar to those of the control and native vegetation, as a result of the Mg absence in the phosphogypsum (Table 2).

The high Ca contents can potentially increase the leaching loss of $_{EX}$Mg to deep layers after PG applications (Zoca and Penn, 2017). Due to the presence of SO_4^{2-}, the S buildup was observed in PG and LPG treatments between 0 to 5 cm soil layer, in which pseudo-total S contents were higher. The pseudo-total S contents equalization in the deeper soil layers is probably related to previous phosphogypsum applications in the experiment.

The NV exhibited the highest CEC*t*, ~44% higher than those found in the control, which is largely due to the high OC contents found in the NV samples (Table 2). The $_{OX}$Fe contents were also higher in the NV, probably as a result of the continuous stock of organic materials on the soil surface and of the activity of living roots. However, the highest Al^{3+} and H+Al contents were also found in NV, as well as the low pH values, indicating strong soil acidity which is common in tropical humid forest soils (Motavalli et al., 1995). In L and LPG treatments the acidity neutralization was evidenced by high pH values, Al^{3+} contents close to zero and H+Al contents ~71% lower than those found in the control.

Despite the higher contents of OC in the forest soil, the association of lime with phosphogypsum was effective to increase OC in relation to the control from 0 to 5 cm (Table 2). These results are in agreement with Inagaki et al. (2016), who found that the

efficiency of lime can be increased in humid tropical soils when applied with phosphogypsum. Also, the lime-amended treatments proved effective in increasing OC contents in the 10-20 cm soil layer. Comparing the lime-amended treatments across soil layers, it is possible to observe the least effect of lime in depth, with pH values and H+Al contents close to those of control and PG (Table 2).

Table 2. Selected properties of the soil samples studied.

attribute	treatment														
	0-5 cm					**5-10 cm**					**10-20 cm**				
	C [a]	**L**	**PG**	**LPG**	**NV**	**C**	**L**	**PG**	**LPG**	**NV**	**C**	**L**	**PG**	**LPG**	**NV**
pH 0.01 mol l^{-1} $CaCl_2$	4.0 cNS [b]	5.7 aA	4.5 bA	5.8 aA	3.9 cNS	4.0 bNS	4.8 aB	4.1 bB	5.0 aB	3.9 bNS	4.0 bNS	4.5 aC	4.1 bB	4.6 aC	3.8bNS
OC (g dm^{-3})	21 cA	25 bcA	24 bcA	26 bA	36 aA	13 bB	15 bB	13 bB	14 bB	20 bA	9 cC	12 bB	9 cB	12 bB	16 aC
Al^{3+} ($mmol_c$ dm^{-3})	9 bB	1 cB	6 bB	1 cNS	19 aNS	14 bA	2 cAB	10 bA	2 cNS	20 aNS	16 abA	5 cA	13 bA	3 cNS	19 aNS
H+Al ($mmol_c$ dm^{-3})	67 bNS	20 dB	51 cNS	18 dB	130 aA	66 bNS	39 cA	60 bNS	33 cA	96 aB	58 bNS	42 bcA	53 bNS	35 cA	80 aC
CEC_t ($mmol_c$ dm^{-3})	81 bNS	142 aA	82 bA	134 aA	146 aA	74 bNS	69 bB	80 abA	65 bB	104 aB	71 nsNS	62 nsB	61 nsB	61 nsB	84 nsB
$_{EX}Ca$ ($mmol_c$ dm^{-3})	7 dNS	64 bA	27 cA	80 aA	10 dNS	4 cNS	18 abB	10 bcB	24 aB	4 cNS	10 abNS	12 abB	6 abB	19 aB	2 bNS
$_{EX}Mg$ ($mmol_c$ dm^{-3})	5 cNS	56 aA	2 cNS	34 bA	4 cNS	2 bNS	10 aB	2 bNS	7 abB	2 bNS	2 nsNS	6 nsB	1 nsNS	5 nsB	1 nsNS
$_{M\text{-}1}$ P (mg kg^{-1})	53 cA	42 dA	96 aA	80 bA	7 eNS	56 bA	48 bA	76 aB	56 bB	4 cNS	24 bB	19 bB	35 aC	20 bC	3 cNS
$_{M\text{-}3}$ P (mg kg^{-1})	79 bA	53 dA	117 aA	68 cA	14 eA	81 bA	56 dA	100 aB	64 cA	10 eB	35 bB	27 cB	49 aC	25 cB	6 dC
$_{DCB}Fe$ (g kg^{-1})	50 nsNS	50 nsNS	51 nsNS	56 nsAB	50 nsNS	51nsNS	56nsNS	56nsNS	62aNS	49nsNS	46 nsNS	51 nsNS	49 nsNS	53 nsB	49 nsNS
$_{OX}Fe$ (g kg^{-1})	2.2 bNS	2.3 bNS	2.2 bB	2.3 bNS	3.7 aA	2.4 bNS	2.5 bNS	2.6 bA	2.5 bNS	3.4 aA	2.3 bNS	2.4 bNS	2.4 bAB	2.4 bNS	3.4 aB
pseudo-total P	475 bNS	529 abA	541 abA	586 aA	348 cNS	478 aNS	512 aA	413 aA	530 aA	344 bNS	413 nsNS	448 nsB	421 nsB	441 nsB	379 nsNS
pseudo-total Al	15 nsNS	17 nsNS	16 nsNS	18 nsNS	20 nsNS	16 nsNS	20 nsNS	18 nsNS	20 nsNS	19 nsNS	19 nsNS	20 nsNS	20 nsNS	21 nsNS	22 nsNS
pseudo-total Ca	186 dNS	1471 bA	604 cA	2127 aA	187 dNS	126 bNS	411 abB	254 bB	703 aB	130 bNS	62 bNS	291 abB	169 abB	530 aB	150 abNS
pseudo-total Mg	249 bNS	970 aA	214 bNS	920 aA	236 bNS	214 bNS	447 aB	204 bNS	361 aB	263 abNS	235 bNS	344 abB	218 bNS	386 aB	233 bNS
pseudo-total S	249 bcNS	305 bNS	349 abNS	433 aA	185 cNS	239 abNS	262 abNS	275 abNS	317 aB	168 bNS	243 abNS	267 abNS	298 aNS	322 aB	184 bNS

[a] control (C), lime (L), phosphogypsum (PG); lime+phosphogypsum (LPG), native vegetation (NV).

[b] Different lowercase letters in the same line indicate difference between treatments in each soil layer, and different uppercase letters in the same line indicate difference for each treatment between soil layers (*Tukey* test, $p<0.05$, n = 4). The letters 'ns' indicate absence of *p*-value high enough to means comparison (no difference)

4.3.2. Bioavailable P

Regardless the extractant, the bioavailable contents of P were higher in the PG treatment in all investigated layers. On average, P contents extracted by Mehlich-3 were 21% higher than those extracted Mehlich-1 (Table 2). A possible reason is that the acidity of Mehlich-3 is less neutralized by soil carbonates than Mehlich-1 (Tran and Simard, 1993). As a result, the strength of Mehlich-1 extraction may have been reduced. Another reason may be the forms of P that the extractor accessed. Mehlich-1 extracts exclusively inorganic forms, while Mehlich-3 can have a combined action, extracting organic and inorganic forms of P (Gatiboni et al., 2005).

The other treatments (control, L and LPG) had similar available P contents across the soil layers, and the NV had the lowest content, as expected because of the absence of P-fertilization. Oliveira et al. (2000) compared Mehlich-1 and anion exchange resin to estimate the availability of P in tropical soils with contrasting P buffer capacities and observed that variations in the amounts of P extracted and in the critical levels of P between soils were higher when Mehlich-1 as the extractor.

The highest contents of available P in the PG-amended treatments may be related to the low P concentrations in phosphogypsum (~0.1-0.3%). However, the LPG treatments exhibited lower bioavailable P contents than PG in all soil layers. This in turn may be associated with the formation of Ca-phosphates, or with the high base saturation in the lime-amended treatments, partially neutralizing the acidity of acid of Mehlich-1 and Mehlich-3 and consequently its P extraction strength (Lins and Cox, 1989).

Although separate applications of either phosphogypsum or lime have been effective in improving some soil fertility attributes, the greatest effects were observed with the joint use of these amendments, as reported by Bossolani et al. (2020), Inagaki et al. (2016) and Zoca and Penn (2017). These benefits in soil fertility were reflected in higher corn yields and nutrient contents in index corn leaves (*supplementary material*).

4.3.3. Soil P fractions

Regardless the P fraction, the uppermost soil layers (0-5 cm and 5-10 cm) had highest P contents (Table 3). The higher concentrations of P in uppermost soil layers are the result of the low P mobility in the soil profile, evidenced in labile and moderately labile P pools (Fig. 1a; 1b) that remained higher in 0-5 cm and 5-10 cm soil layers, irrespective of the treatment. This was linked to the high P adsorption capacity of the studied soil and reinforced by the highest pseudo-total P contents in 0-5 cm (Table 2). The P buildup in the topsoil layers is a common process in long-term P-fertilized soils (Annaheim et al., 2014; Schmieder et al., 2018). This pattern was also observed by Pavinato et al. (2009) in samples from an Oxisol under NT and was related to the lack of soil disturbance.

Plants' straw and fertilizer inputs stimulate the increase of P in uppermost Oxisols layers (Pavinato et al., 2009; Selles et al., 1997). However, the non-labile P pools were homogeneous throughout the soil layers (Fig. 1c), which suggests a weak relationship between recalcitrant P forms and the performed fertilization. This may be related to the continuous removal of P by crops throughout the experiment. Another factor is the low P rates applied annually, not exceeding 60 kg ha^{-1}. The P pools accumulation reported by Menezes-Blackburn et al. (2018) for excessively fertilized European soils may occur more slowly in tropical Oxisols.

Considering all samples, the majority of P was found as a non-labile P pool, accounting for 59% of $P\text{-}_{fracTotal}$, on average. The lowest contribution was from the labile pool, that accounted for 20% of $P\text{-}_{fracTotal}$. The high plant-available P contents found in PG (Table 2) were in agreement with the high contents of labile P in the uppermost soil layer (0-5 cm) found in PG treatment (Table 3). However, considering the moderately labile forms, which are typically associated with P forms bounded to Fe, Al or Ca (Cross and Schlesinger, 1995), soil samples from the LPG treatment had the highest contents in the 0-5 cm and 5-10 cm soil layers, which indicates more P retention in forms not readily available to plants.

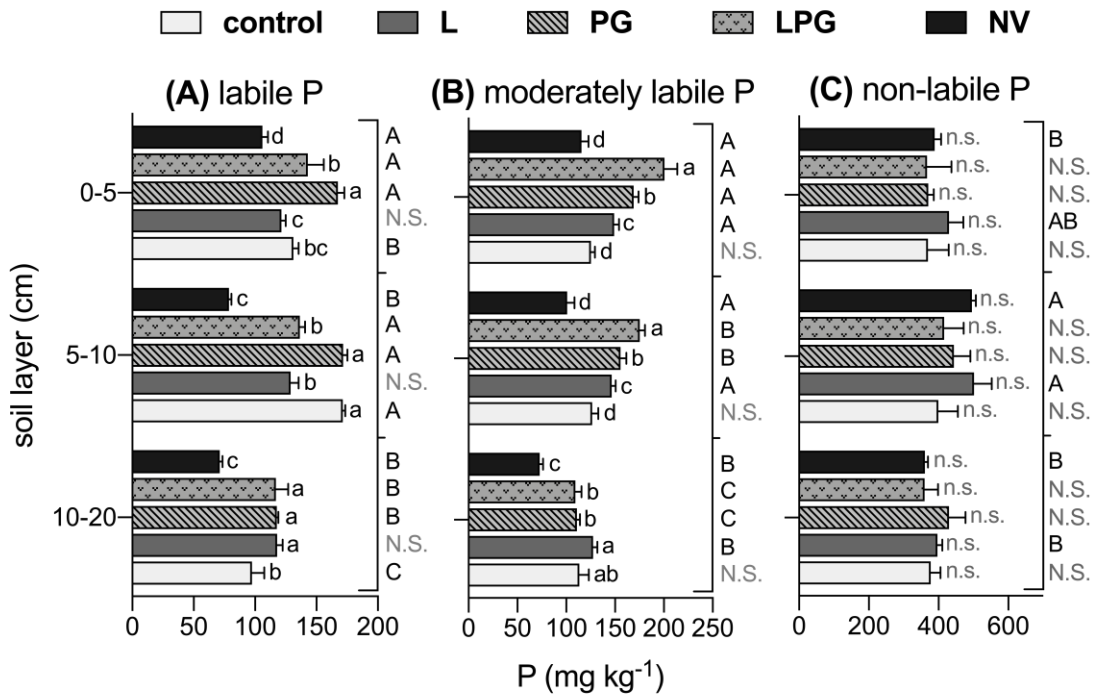

Figure 1. Labile ($Pi\text{-}_{Resin}$ + $Pi\text{-}_{Bic}$ + $Po\text{-}_{Bic}$) (**A**), moderately labile ($Pi\text{-}_{NaOH01}$ + $Po\text{-}_{NaOH01}$ + $Pi\text{-}_{HCl}$) (**B**) and non-labile P ($Pi\text{-}_{NaOH05}$ + $Po\text{-}_{NaOH05}$ + $Pi\text{-}_{Residual}$) (**C**) pools at 0-5 cm, 5-10 cm and 10-20 cm soil layers. Bars represent the standard deviation of the mean values (n = 3). Different lowercase letters indicate difference between treatments in the same soil layer, and different uppercase letters indicate difference between soil layers in the same treatment (*Tukey* test, $p < 0.05$). Lime (L); phosphogypsum (PG); lime + phosphogypsum (LPG); native vegetation (NV).

Table 3. Soil P fractions sequentially extracted.

P fraction	Treatment														
	0-5 cm					5-10 cm					10-20 cm				
	C [a]	L	PG	LPG	NV	C	L	PG	LPG	NV	C	L	PG	LPG	NV
Pi_{Resin}	37 bB [b]	33 bA	52 aA	39 bA	13 cA	54 aA	34 bA	53 aA	33 bB	9 cAB	24 abC	19 bB	27 aB	17 bC	6 cB
Pi_{Bic}	31 bB	33 bA	40 aB	35 abB	23 cA	42 bcA	37 cA	51 aA	44 bA	18 dB	35 aB	26 bB	33 aC	19 cC	14 cB
Po_{Bic}	64 nsA	56 nsNS	80 nsNS	70 nsAB	70 nsNS	76 aA	58 abNS	68 abNS	59 abB	52 bNS	38 cB	73 abNS	58 bcNS	82 aA	52 cNS
$Pi_{NaOH0.1}$	30 bB	74 aA	68 aA	71 aA	15 bNS	47 aA	41 aB	38 aB	50 aB	11 bNS	49 aA	24 bB	26 bB	16 bC	10 bNS
$Po_{NaOH0.1}$	77 abA	49 cB	62 bcB	63 bcB	90 aA	61 bAB	83 abA	93 aA	100 aA	81 abA	49 cB	90 aA	71 abB	78 abB	59 bcB
Pi_{HCl}	19 cdNS	27 cA	39 bA	66 aA	10 dNS	19 aNS	22 aA	25 aB	25 aB	10 bNS	16 nsNS	14 nsB	15 nsC	15 nsC	8 nsNS
$Pi_{NaOH0.5}$	147 nsNS	135 nsNS	163 nsNS	114 nsNS	137 nsNS	143 nsNS	190 nsNS	164 nsNS	129 nsNS	152 nsNS	92 nsNS	165 nsNS	176 nsNS	155 nsNS	135 nsNS
$Po_{NaOH0.5}$	13 bB	21 abNS	21 abNS	36 aA	33 aA	32 nsA	24 nsNS	22 nsNS	14 nsB	26 nsA	10 nsB	11 nsNS	12 nsNS	13 nsB	4 nsB
$P_{Residual}$	209 abNS	264 aAB	187 bA	217 abAB	219 abB	225 bNS	298 abA	257 abB	274 abA	317 aA	265 nsNS	221 nsB	243 nsB	192 nsB	222 nsB
$P_{fracTotal}$	627 nsNS	701 nsAB	707 nsNS	711 nsA	611 nsAB	698 nsNS	788 nsA	772 nsNS	728 nsA	676 nsA	588 abNS	643 abB	659 aNS	586 bB	506 bB

[a] control (C), lime (L), phosphogypsum (PG); lime+phosphogypsum (LPG), native vegetation (NV).

[b] different lowercase letters in the same line indicate difference between treatments in each soil layer, and different uppercase letters in the same line indicate difference for each treatment between soil layers (*Tukey* test, $p < 0.05$, n = 4). The letters 'ns' indicate absence of *p*-value high enough to means comparison (no difference).

The exchangeable $Pi\text{-}_{Resin}$ was affected by treatments ($p < 0.05$), with higher contents in 0-5 cm and 5-10 cm soil layers (Table 3). The PG treatment had the highest $Pi\text{-}_{Resin}$ contents, while the NV had the lowest contents, following the pattern observed with the other bioavailable P extractants, Mehlich-1 and Mehlich-3 (Table 2). Likewise, samples from the PG treatment had the highest $Pi\text{-}_{Bic}$ contents among the treatments in all studied soil layers. However, $Po\text{-}_{Bic}$ contents in 0-5 cm were not affected by the treatments ($p > 0.05$) (Table 3).

Samples from the NV had the lowest $Po\text{-}_{Bic}$ contents, which indicates that cropping and management in the experimental area may have enhanced the buildup of labile Po forms. Bossolani et al. (2020) observed an increase in the N biological fixation, as well as total archaea and bacteria with the long-term use of lime and phosphogypsum in the same experiment of the present study. The joint application of lime and phosphogypsum benefits soil quality and fertility, leading to greater N absorption by plants (Bossolani et al., 2020). These results are in agreement with those obtained by Carmeis-Filho et al. (2017), in which the largest pools of C were found where lime was applied with phosphogypsum in a tropical intercropping NT system.

The $Pi\text{-}_{NaOH0.1}$ and $Po\text{-}_{NaOH0.1}$ fractions are considered poorly available to plants, possibly associated with Fe-(hydr)oxides (Cross and Schlesinger, 1995). The $Pi\text{-}_{NaOH0.1}$ contents were higher in samples from the field experiment than in the NV samples (Table 3). However, the $Po\text{-}_{NaOH0.1}$ contents in the NV were close to those found in the experiment samples, especially in the 0-5 cm and 5-10 cm soil layers. Major proportions of $P\text{-}_{NaOH01}$ and $P\text{-}_{NaOH05}$ are usually found in more uppermost soil layers and are typical of tropical and subtropical Oxisols with abundance of Fe- and Al-(hydr)oxides, kaolinite and organic compounds (Lilienfein et al., 2000; Pavinato et al., 2009).

No differences among treatments or soil layers were found for $Pi\text{-}_{NaOH05}$ (Table 3), whereas samples from the NV and the LPG treatments presented the highest contents of $Po\text{-}_{NaOH05}$ between 0 to 5 cm (Table 3). These results are consistent with the findings of Carmeis Filho et al. (2017) who reported high concentrations of soil

particulate C, total C and mineral-associated C between 0 to 5 cm in the lime-amended treatments of the same experiment used in the present study.

The LPG treatment exhibited a strong gradient among $Pi\text{-}_{HCl}$ contents. This is probably linked with the highest contents of $_{EX}Ca$ and pseudo-total Ca in the soil amended with lime + phosphogypsum, since the $P\text{-}_{HCl}$ fraction is usually associated with Ca-bounded stable P forms, considered non-available to plants (McKenzie et al., 1992). There was no variation in $P\text{-}_{HCl}$ across soil layers in the control treatment and NV (Table 3). For L and PG, the highest contents of $Pi\text{-}_{HCl}$ were concentrated in the uppermost soil layers.

The $P\text{-}_{Residual}$ contents varied among treatments in the 0-5 cm layer, in which PG had the lowest contents, and in the 5-10 cm layer, in which the lowest contents were found in the control treatment (Table 3). The highest contents of $P\text{-}_{Residual}$ were found in the NV soil, between 5 and10 cm. Therefore, it is difficult to assume that treatments had direct effects on this fraction because it is considered the least bioavailable and most stable P form (Cross and Schlesinger, 1995).

The $P\text{-}_{fracTotal}$ contents did not differ among treatments when compared in each soil layer. These results were expected since the P rates were the same in all treatments in all years of experimentation. The $P\text{-}_{fracTotal}$ were between 506 and 788 mg kg^{-1} (Table 3) that, on average, were 31% higher than the pseudo-total P contents obtained by acidic digestion in microwave (Table 2). However, the differences among means were similar in both pseudo-total P and $P\text{-}_{fracTotal}$ contents, with lower P contents in the 10-20 cm soil layers.

Taking all soil layers into account, the geochemical P was, on average, 70% higher than biological P (Fig. 2), and there was no variation across soil layers for samples from control and PG treatments. However, for L and LPG, the highest contents of geochemical P were found in 0-5 cm and 5-10 cm layers, which indicates the effect of lime in this fraction. As for biological P, there were no differences among treatments in the 5-10 cm soil layer ($p < 0.05$).

In the 0-5 cm soil layer, the NV had the highest contents of biological P, followed by LPG treatment. Interestingly, lime-amended treatments had high contents of biological P between 10 and 20 cm, which is a possible evidence of the accumulation of SOC in this layer. These results converge with the findings of Carmeis Filho et al. (2017) and Inagaki et al. (2016), who emphasize the beneficial effects of liming in increasing the quantity and quality of organic matter in tropical soils over time.

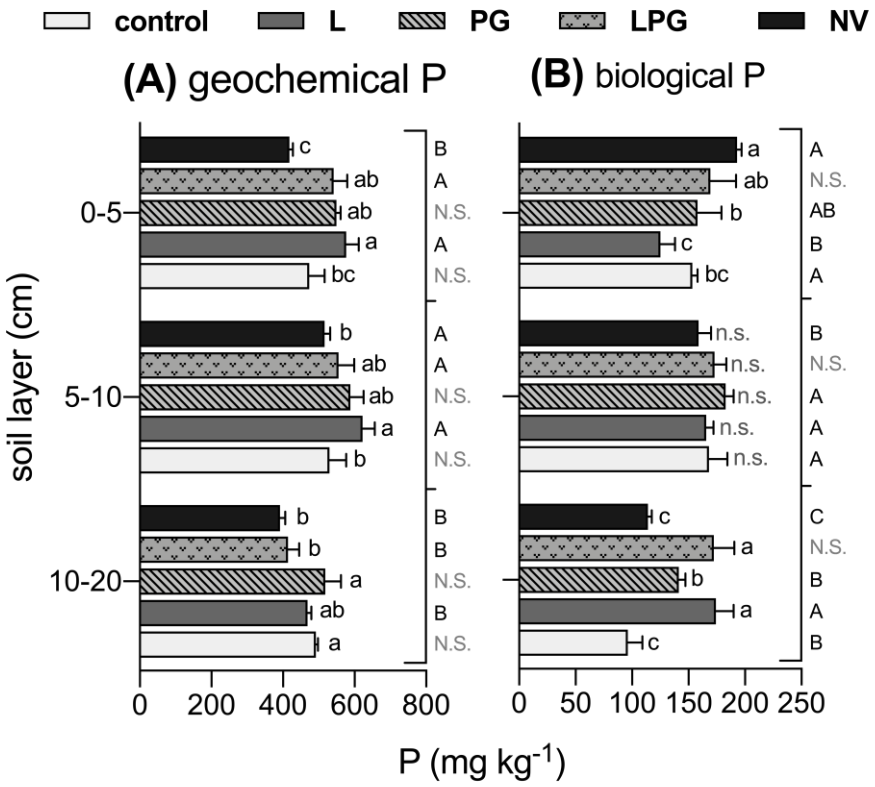

Figure 2. Geochemical P ($Pi\text{-}_{Resin}$ + $Pi\text{-}_{Bic}$ + $Pi\text{-}_{HCl}$ + $Pi\text{-}_{NaOH01}$ + $Pi\text{-}_{NaOH05}$ + $P\text{-}_{Residual}$) (**A**) and biological P ($Po\text{-}_{Bic}$ + $Po\text{-}_{NaOH01}$ + $Po\text{-}_{NaOH05}$) (**B**) phosphorus pools at 0-5 cm, 5-10 cm and 10-20 cm soil layers. Bars represent the standard deviation of the mean values (n = 3). Different lowercase letters indicate difference between treatments in the same soil layer, while different uppercase letters indicate difference between soil layers in the same treatment by *Tukey* test ($p < 0.05$). Lime (L); phosphogypsum (PG); lime + phosphogypsum (LPG); native vegetation (NV).

4.3.4. P *K*-edge XANES

All soil samples exhibit strong spectral features consistent with P-bounded to Fe-(hydr)oxides, especially hematite (P-Hm), Al-(hydr)oxides, and phyllosilicates as kaolinite (P-Kln) (Fig. 3). This was expected due to the abundance of iron oxides and

kaolinite in subtropical Oxisols (Schaefer et al., 2008). Our results are in agreement with studies that stressed the importance of Fe in the P chemistry of agricultural soils (Antonangelo et al., 2020; Eriksson et al., 2015; Liu et al., 2014; Rivard et al., 2016).

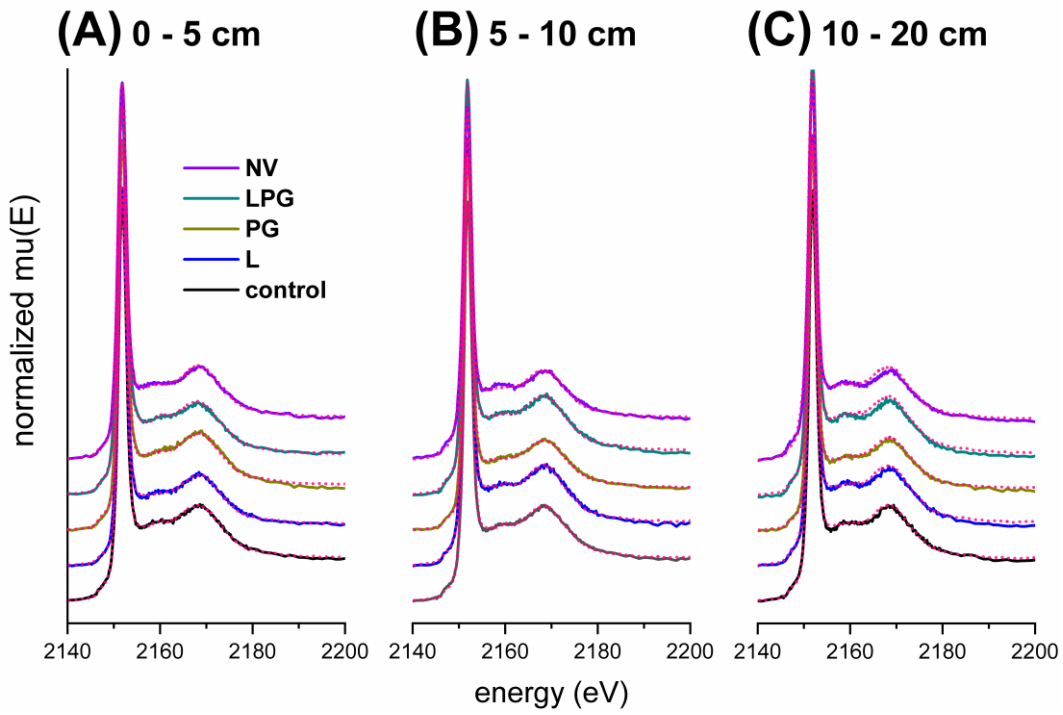

Figure 3. Linear combination fit (dot lines) of phosphorus *K*-edge XANES spectra (solid lines) of soil samples for the treatments: control, lime (L), phosphogypsum (PG), lime+phophogypsum (LPG) and native vegetation (NV) from 0-5 cm (**A**), 5-10 cm (**B**) and 10-20 cm (**C**) soil layers.

A slight pre-edge feature was observed in all samples (Fig. 3), especially in 5-10 cm and 10-20 cm soil layers, indicating the association between P and Fe-(hydr)oxides, as reported by Antonangelo et al. (2020) and Abdala et al. (2015). More specifically, this pre-edge extends from 2148–2152 eV in the spectra and is associated with inorganic P forms (Hesterberg et al. 1999). This pre-edge feature is formed by P 1*s* to Fe(4*p*)-O(2*p*) electronic transitions and denotes covalent bonds in Fe_{III}-phosphate minerals (Prietzel and Klysubun, 2018).

In the post-edge region, no strong distinctive features were identified among the samples, what is coherent with the low number of reference materials that composed the LCF analysis (Table 4). The R-factor values found, R-factor = ∑[(data-

fit)^2]/∑(data^2), varied from 0.000411 to 0.001783, which represents a good fit of the data. The weighting factors did not exceed the predetermined range (95 to 105%), concentrating from 97 to 101%.

Table 4. Relative proportions of reference P-bounded minerals based on linear combination fitting analysis of P XANES data.

sample	P-Hm	P-Kln	P-Gt	P-Gb	P-nc Fe	P-nc Al	P-oct Ca	R-factor [a]
	% P specie (uncertainty) [b]							
control								
0 – 5 cm	50.5 (1.7)	21.1 (2.1)	16.5 (1.5)	--	--	11.9 (1.2)	--	0.000411
5 – 10 cm	44.1 (2.0)	26.3 (2.4)	10.4 (1.3)	--	--	19.2 (1.4)	--	0.000539
10 – 20 cm	39.3 (3.6)	41.3 (3.5)	19.3 (3.5)	--	--	--	--	0.001321
L								
0 – 5 cm	35.0 (3.7)	24.9 (3.6)	40.0 (2.4)	--	--	--	--	0.000639
5 – 10 cm	44.4 (2.4)	49.2 (2.5)	--	--	6.3 (0.5)	--	--	0.000693
10 – 20 cm	51.8 (3.1)	48.2 (3.2)	--	--	--	--	--	0.001372
PG								
0 – 5 cm	62.7 (3.4)	16.0 (5.2)	13.9 (3.2)	7.4 (3.1)	--	--	--	0.001371
5 – 10 cm	67.2 (3.1)	12.0 (4.5)	5.7 (0.1)	15.1 (3.7)	--	--	--	0.001071
10 – 20 cm	41.7 (2.7)	27.0 (3.4)	--	--	--	31.3 (2.0)	--	0.001344
LPG								
0 – 5 cm	59.9 (2.5)	23.8 (2.6)	--	--	--	--	16.2 (0.5)	0.000760
5 – 10 cm	38.5 (3.2)	36.1 (2.5)	16.0 (5.1)	--	9.3 (1.7)	--	--	0.000655
10 – 20 cm	64.7 (3.8)	35.3 (3.9)	--	--	--	--	--	0.001783
NV								
0 – 5 cm	36.3 (1.9)	32.1 (2.3)	9.4 (1.1)	--	--	22.2 (1.4)	--	0.000537
5 – 10 cm	36.8 (4.1)	34.5 (3.1)	18.4 (2.4)	--	10.3 (0.9)	--	--	0.000978
10 – 20 cm	41.0 (3.4)	46.8 (3.6)	--	--	12.3 (0.7)	--	--	0.001780

[a] R-factor = ∑[(data-fit)^2]/∑(data^2) (Kelly et al., 2008).
[b] data have been re-normalized to sum 100% with uncertainties calculated in Athena; numbers in parentheses represent the uncertainties of the values.

The reference materials exhibited contrasting shapes (Fig. S3). In addition to the typical pre-edge feature at 2149 eV of P-Fe species, another features like a shoulder at the higher energy side of the white line peak at 2161 eV from P-Ca species were identified in the reference materials (*e.g.* amorphous-Ca phosphate, octa-calcium phosphate, brushite and ß-tri-calcium phosphate) (Fig. S3), but not in the samples (Fig. 3). The low degree of crystallinity of Fe-P forms (*e.g.* P-nc-Fe and P-Fh) presented prominent characteristics in the pre-edge region, as reported by Hesterberg et al.

(1999) and a featureless post-edge. The opposite was observed for the reference mineral P-Kln that presented a pronounced feature around 2170 eV in the post-edge region (Fig. S3), which is also in accordance with Antonangelo et al. (2020).

Organic patterns had spectra with varying intensities and pre- and post-edge patterns similar to those observed by other authors (Antonangelo et al., 2020; Liu et al., 2013; Schmieder et al., 2020). However, they did not make up the LCF due to the low proportion of these species and their structural complexity. In general, the set of reference materials represented the samples well and indicated that overall P compositions among treatments could be described with no more than four compounds (Table 4; Fig. 4).

Despite no visible spectral differences between topsoil and subsoil (Fig. 3), different LCF results were found across soil layers (Table 4). Soil samples from lime-amended treatments (L and LPG) were the only ones that did not exhibited P-species bounded to Al, either P-bounded to Gibbsite (P-Gb) or P-bounded to low-crystalline Al-hydroxides (P-nc-Al) (Fig. 4). This may be related to the pH elevation that neutralized Al^{3+} and produced stable forms of Al that were not associated with P. However, higher values of potential acidity (H+Al) and $_{EX}$Al were found in soil samples from the native vegetation and the control (Table 2). These values are related to the greatest Al activity under these conditions and are probably linked to the presence of P-Al species obtained from XANES (Fig. 4, Table 4). This pattern was not observed for Fe-P species, probably due to the lower susceptibility to solubilization that pedogenic Fe_{III}-minerals have in relation to Al-(hydr)oxides under pH conditions above 5.0.

As for the soil Al chemistry, the two key chemical processes that occur in the soil as a result of phosphogypsum application are: **i**) the complexation of Al^{3+} by SO_4^{2-} ions, forming $AlSO_4^{+}{}_{(aq)}$; and **ii**) the increase in $Al(OH)_{3(s)}$ solubility in the presence of H^+ and SO_4^{2-}, also forming $AlSO_4^{+}{}_{(aq)}$ (Zoca and Penn, 2017). Shainberg et al. (1989) also highlighted the formation of mineral complexes composed of $Al_2(SO_4)_3$ in soils after phosphogypsum application.

It is possible that orthophosphate ions reacted with these complexes during their formation, as the phosphogypsum was solubilized in the soil and this association resulted in the presence of P-species bounded to Al in the XAS. Interestingly, less crystalline Al-species were found in the 10-20 cm layer, which presented low OC contents (Table 2). This can be explained by the greater presence of roots and consequently organic acids in this layer (Boddey et al., 2010; Nwoke et al., 2008) since the soil sampling was done during the soybean cycle.

The association with P-Al in the soil samples from the control treatment occurred with less crystalline forms of Al, similar to that observed in NV (Fig. 4; Table 4). Therefore, the hypothesis that the species identified as P-nc-Al may be P adsorbed to gibbsite of reduced structural order remains. Something similar has been reported by Antonangelo et al. (2020) for P-Hm and P-ferrihydrite (P-Fh) species. For Antonangelo et al. (2020) fitting with P-Fh in Oxisols that do not have

Ferrihydrite identified by X-ray diffraction (XRD) can be P-Hm species with low structural order. This misunderstanding during the LCF probably occurs due to the striking pre-edge that low crystalline Fe-P species present (Hesterberg et al., 1999). The explanation of Antonangelo et al. (2020) is based on the rare formation of Fh in Oxisols of tropical regions, since soil-environment conditions as low amounts of OC and low silica activity in solution promotes Fh alteration to Hm through internal rearrangement and dehydration (Schaefer et al., 2008). However, for Al-P species, the difference in crystallinity leaves no marked differences in the shapes of the spectra, with the exception of slight variations between 2155-2159 eV (Fig. S3).

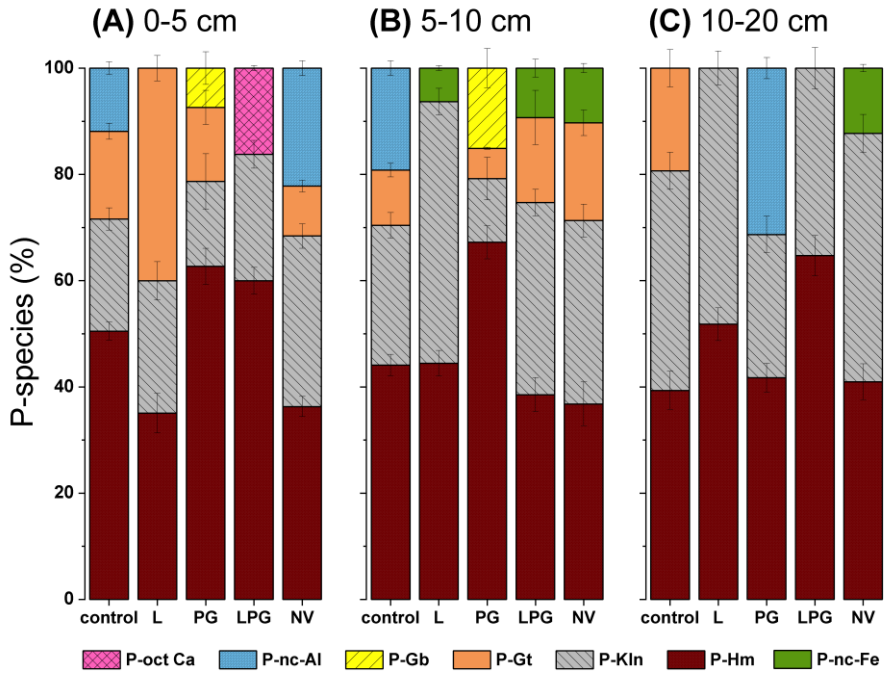

Figure 4. Proportions among P-species in the linear combination fitting (LCF) of soil samples spectra for the treatments: control, lime (L), phosphogypsum (PG), lime+phophogypsum (LPG) and native vegetation (NV) in three soil layers (0-5 cm, 5-10 cm and 10-20 cm). The P-species were P adsorbed to hematite (P-Hm), P adsorbed to kaolinite (P-Kln), P adsorbed to goethite (P-Gt), P adsorbed to Gibbsite (P-Gb), P adsorbed to non-crystalline Fe-hydroxide (P-nc Fe), P adsorbed to non-crystalline Al-hydroxide (P-nc Al) and octa-Ca phosphate (P-Oct Ca).

The LPG treatment was the only one to present octa-calcium phosphate in the LCF in the 0-5 cm layer. This may be related to the huge amount of amendments applied in this treatment in 2016 (10 t ha^{-1} of limestone and 6 t ha^{-1} of phosphogypsum). With that, a more favorable environment for the formation of Ca-phosphates has probably been formed, as identified as P-oct Ca in XANES (Fig. 3). This hypothesis is reinforced by the strong gradient of $Pi\text{-}_{HCl}$ contents across soil layers obtained in the SF for this treatment (Table 3), which mainly derive from P species bounded to Ca (Cross and Schlesinger, 1995).

The SF has the benefit of estimating organic and inorganic fractions of P bounded to Fe. However, the specific distinction of mineral species that are associated with P can only be observed with XANES. There were forms of P adsorbed to different Fe-oxides, like Hm and Gt, in addition to low crystalline Fe-oxides. The same occurred

for Al-bounded P species, which were identified as P adsorbed to gibbsite and as P adsorbed to low-crystalline Al-hydroxides (Fig. 4). It is not possible to obtain this type of information with the SF. However, examining the correlations between proportions of P fractions from SF and proportions of P-species from XANES, it was possible to find correlations between P-Hm and P-Kln species and P fractions (Fig. 5).

The association between P and Fe-(hydr)oxides was expected due to the high degree of weathering and Fe-minerals. However, despite the Pi-$_{NaOH0.1}$ fraction obtained by SF is assumed to be mostly associated with Fe- and Al-(hydr)oxides (Beauchemin et al., 2003), the proportions of Fe-P obtained by LCF analysis from XANES were ~7 times higher than Pi-$_{NaOH01}$. Even so, the proportions of Pi-$_{NaOH01}$ versus the proportions Fe-P from XANES revealed a correlation coefficient of 0.51 (Fig. 5a).

The higher proportions of Fe-P from XANES in relation to those obtained by NaOH extraction in the SF were also reported by Liu et al. (2013) in Chinese Ultisols. The high proportions of Fe-P species by XANES may occur due to the limited number of reference samples (Liu et al., 2013). This was probably not the case in our study, as we had four reference materials for Fe-P species. However, as there were adjustments with more than one Fe-P species in general in the samples, the sum of the proportions makes the contribution of Fe-P species high. Beauchemin et al. (2003) and Hunger et al. (2005) also found similar results and suggested that was probably related with the lack of specificity in SF procedures.

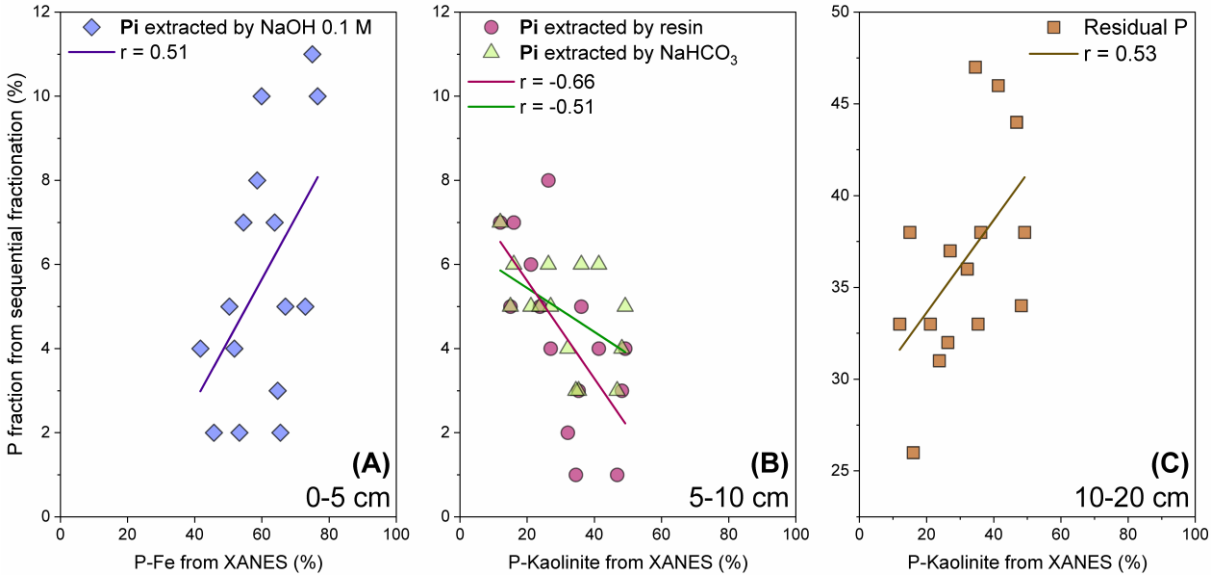

Figure 5. Correlations between iron-associated phosphorus and kaolinite-associated phosphorus from X-ray absorption near edge structure (XANES) analysis versus phosphorus fractions from sequential fractionation ($Pi\text{-}_{NaOH01}$; $Pi\text{-}_{Resin}$; $Pi\text{-}_{Bic}$; $P\text{-}_{Residual}$). The Fe-P proportions were calculated by summing P-Hm + P-Gt + P-nc-Fe obtained in the LCF analysis from XANES data.

4.4. Environmental remarks

The results of the present study are in line with those obtained by Alotaibi et al. (2018), Liu et al. (2013), and Luo et al. (2017), which suggest the use of more than one analytical technique to investigate phenomena related to P chemistry in soils. The Hedley fractionation provides operationally defined P fractions obtained that are not specific to one particular chemical species (Hunger et al., 2005). These fractions, however, can be lability indicators and, sometimes, complement the results obtained by other analytical means.

Phosphorus-Kln species obtained by XANES had low lability, since negative correlations were identified with $Pi\text{-}_{Resin}$ and $Pi\text{-}_{Bic}$, and positive with $P\text{-}_{Residual}$. This can be related with intense PO_4 penetration into Kln adsorption sites at the silicate structure, *i.e.* inter-lamellar or amorphous regions, as suggested by Muljadi et al. (1966), that evaluated high PO_4 loadings. In addition, the diffusion of PO_4 within Kln micro-structures and even into the solid phase seems to be a fast process with lasting effects (Gérard, 2016).

The abundance of Hm and Kln, typical minerals of highly weathered soils, caused most of the P species identified to be associated with these minerals. Our results highlighted the importance of P adsorption by Kln particles, as pointed out by Gérard (2016). In addition, we observed that P was associated with Fe and Al forms with different structural orders. Antonangelo et al. (2020) noted that P-Hm species with less organized three-dimensional arrangement may be fitted as P-Fh during the LCF in Oxisols. We inferred something similar for P-Al species in our study, in which P forms adsorbed to Al-hydroxides could be less structurally ordered gibbsite minerals. Anyway, XANES continues to be a unique technique for evaluating inorganic forms of P in the soil and has its potential increasing when associated with other analytical methods of investigation.

References

Abdala, D.B., da Silva, I.R., Vergütz, L., Sparks, D.L., 2015. Long-term manure application effects on phosphorus speciation, kinetics and distribution in highly weathered agricultural soils. Chemosphere 119, 504–514.

Acksel, A., Baumann, K., Hu, Y., Leinweber, P., 2019. A critical review and evaluation of some P-research methods. Commun. Soil Sci. Plant Anal. 50, 2804–2824.

Alotaibi, K.D., Schoenau, J.J., Kar, G., Peak, D., Fonstad, T., 2018. Phosphorus speciation in a prairie soil amended with MBM and DDG ash: Sequential chemical extraction and synchrotron based XANES spectroscopy investigations. Sci. Rep. 8, 1–9.

Annaheim, K.E., Doolette, A.L., Smernik, R.J., Mayer, J., Oberson, A., Frossard, E., Bunemann, E.K., 2014. Long-term addition of organic fertilizers has little effect on soil organic phosphorus as characterized by ^{31}P NMR spectroscopy and enzyme additions. Geoderma 257–258, 1–11.

Antonangelo, J.A., Firmano, R.F., Zhang, H., Colzato, M., Abdala, D.B., Carvalho, H.W.P., de Oliveira Junior, A., Alleoni, L.R.F., 2020. Phosphorus speciation by P-XANES in an Oxisol under long-term no-till cultivation. Geoderma 377, 114580.

Aye, N.S., Sale, P.W.G., Tang, C., 2016. The impact of long-term liming on soil organic carbon and aggregate stability in low-input acid soils. Biol. Fertil. Soils 52, 697–709.

Aziz, I., Mahmood, T., Islam, K.R., 2013. Effect of long-term no-till and conventional tillage practices on soil quality. Soil Tillage Res. 131, 28–35.

Beauchemin, S., Hesterberg, D., Chou, J., Beauchemin, M., Simard, R.R., Sayers, D.E., 2003. Speciation of phosphorus in phosphorus-enriched agricultural soils using X-ray absorption near-edge structure spectroscopy and chemical fractionation. J. Environ. Qual. 32, 1809–1819.

Bertsch, P.M., Bloom, P.R., 1996. Aluminum, in: Sparks, D.L. (Ed.), Methods of Soil Analysis Part 3 - Chemical Methods. pp. 517–550.

Boddey, R.M., Jantalia, C.P., Conceiçao, P.C., Zanatta, J.A., Bayer, C., Mielniczuk, J., Dieckow, J., Dos Santos, H.P., Denardin, J.E., Aita, C., Giacomini, S.J., Alves, B.J.R.,

Urquiaga, S., 2010. Carbon accumulation at depth in Ferralsols under zero-till subtropical agriculture. Glob. Chang. Biol. 16, 784–795.

Bossolani, J.W., Crusciol, C.A.C., Merloti, L.F., Moretti, L.G., Costa, N.R., Tsai, S.M., Kuramae, E.E., 2020. Long-term lime and gypsum amendment increase nitrogen fixation and decrease nitrification and denitrification gene abundances in the rhizosphere and soil in a tropical no-till intercropping system. Geoderma 375, 114476.

Briedis, C., De Moraes Sá, J.C., Caires, E.F., De Fátima Navarro, J., Inagaki, T.M., Boer, A., De Oliveira Ferreira, A., Neto, C.Q., Canalli, L.B., Dos Santos, J.B., 2012. Changes in organic matter pools and increases in carbon sequestration in response to surface liming in an Oxisol under long-term no-till. Soil Sci. Soc. Am. J. 76, 151–160.

Brookes, P.C., Powlson, D.S., Jenkinson, D.S., 1982. Measurement of microbial biomass phosphorus in soil. Soil Biol. Biochem. 14, 319–329.

Cade-Menun, B.J., Carter, M.R., James, D.C., Liu, C.W., 2010. Phosphorus forms and chemistry in the soil profile under long-term conservation tillage: A phosphorus-^{31} nuclear magnetic resonance study. J. Environ. Qual. 39, 1647–1656.

Caires, E.F., Guimarães, A.M., 2018. A novel phosphogypsum application recommendation method under continuous no-till management in Brazil. Agron. J. 110, 1987–1995.

Caires, E.F., Haliski, A., Bini, A.R., Scharr, D.A., 2015. Surface liming and nitrogen fertilization for crop grain production under no-till management in Brazil. Eur. J. Agron. 66, 41–53.

Caires, E.F., Sharr, D.A., Joris, H.A.W., Haliski, A., Bini, A.R., 2017. Phosphate fertilization strategies for soybean production after conversion of a degraded pastureland to a no-till cropping system. Geoderma 308, 120–129.

Cantarella, H., van Raij, B., Quaggio, J.A., 1998. Soil and plant analyses for lime and fertilizer recommendations in Brazil. Commun. Soil Sci. Plant Anal. 29, 1691–1706.

Carmeis-Filho, A.C.A.C., Crusciol, C.A.C., Castilhos, A.M., 2017. Liming demand and plant growth improvements for an Oxisol under long-term no-till cropping. J. Agric. Sci. 155, 1093–1112.

Carmeis Filho, A.C.A., Penn, C.J., Crusciol, C.A.C., Calonego, J.C., 2017. Lime and phosphogypsum impacts on soil organic matter pools in a tropical Oxisol under long-term no-till conditions. Agric. Ecosyst. Environ. 241, 11–23.

Castro, G.S., Crusciol, C. a C., Calonego, J.C., Rosolem, C. a., 2015. Management impacts on soil organic matter of tropical soils. Vadose Zo. J. 1-8.

Colzato, M., Kamogawa, M.Y., Carvalho, H.W.P.P., Alleoni, L.R.F.F., Hesterberg, D., 2017. Temporal Changes in Cadmium Speciation in Brazilian Soils Evaluated Using Cd L_{III}–Edge XANES and Chemical Fractionation. J. Environ. Qual. 0316.

Condron, L.M., Goh, K.M.K., Newman, R.H., 1985. Nature and distribution of soil phosphorus as revealed by a sequential extraction method followed by ^{31}P nuclear magnetic resonance analysis. J. Soil Sci. 36, 199–207.

Costa, C.H.M., Crusciol, C.C., 2016. Long-term effects of lime and phosphogypsum application on tropical no-till soybean-oat-sorghum rotation and soil chemical properties. Eur. J. Agron. 74, 119–132.

Cross, A.F., Schlesinger, W.H., 1995. A literature review and evaluation of the Hedley fractionation: Applications to the biogeochemical cycle of soil phosphorus in natural ecosystems. Geoderma 64, 197–214.

Deng, S.P., Tabatabai, M.A., 1997. Effect of tillage and residue management on enzyme activities in soils: III. Phosphatases and arylsulfatase. Biol. Fertil. Soils 24, 141–146.

Dick, W. a., Tabatabai, M. a., 1977. Determination of orthophosphate in aqueous solutions containing labile organic and inorganic phosphorus compounds. J. Environ. Qual. 6, 82.

Eriksson, A.K., Gustafsson, J.P., Hesterberg, D., 2015. Phosphorus speciation of clay fractions from long-term fertility experiments in Sweden. Geoderma 241–242, 68–74.

Fageria, N.K., Baligar, V.C., 2008. Ameliorating soil acidity of tropical Oxisols by liming for sustainable crop production 99, 345–399.

Freitas, P., Landers, J., 2014. The transformation of agriculture in Brazil through development and adoption of zero tillage conservation agriculture. Int. Soil Water Conserv. Res. 2, 35–46.

Gatiboni, L.C., Kaminski, J., Santos, D.R. dos, 2005. Alterations in soil phosphorus forms after successive extractions with Mehlich-1, Mehlich-3 and anion exchange resin methods. Rev. Bras. Ciência do Solo 29, 363–371.

Gérard, F., 2016. Clay minerals, iron/aluminum oxides, and their contribution to phosphate sorption in soils - A myth revisited. Geoderma 262, 213–226.

Godfray, H.C.J., Beddington, J.R., Crute, I.R., Haddad, L., Lawrence, D., Muir, J.F., Pretty, J., Robinson, S., Thomas, S.M., Toulmin, C., 2010. Food security: The challenge of feeding 9 billion people. Science (80). 327, 812–818.

Gu, C., Margenot, A.J., 2020. Navigating limitations and opportunities of soil phosphorus fractionation. Plant Soil.

Heanes, D.L.L., 1984. Determination of total organic-C in soils by an improved chromic acid digestion and spectrophotometric procedure. Commun. Soil Sci. Plant Anal. 15, 1191–1213.

Hedley, M.J.J., Stewart, J.W.B., Chauhan, B.S.S., J.W.B., S., Chauhan, B.S.S., 1982. (1982) Changes in inorganic and organic soil phosphorus fractions induced by cultivation practices and by laboratory incubations. Soil Sci. Soc. Am. Proc. 46, 970–976.

Hesterberg, D., Zhou, W., Hutchison, K.J., Beauchemin, S., Sayers, D.E., 1999. XAFS study of adsorbed and mineral forms of phosphate. J. Synchrotron Radiat. 6, 636–638.

Inagaki, T.M., de Moraes Sá, J.C., Caires, E.F., Gonçalves, D.R.P., 2017. Why does carbon increase in highly weathered soil under no-till upon lime and gypsum use? Sci. Total Environ. 599–600, 523–532.

Inagaki, T.M., de Moraes Sá, J.C., Caires, E.F., Gonçalves, D.R.P., 2016. Lime and gypsum application increase biological activity, carbon pools, and agronomic productivity in highly weathered soil. Agric. Ecosyst. Environ. 231, 156–165.

Joris, H.A.W., Caires, E.F., Scharr, D.A., Bini, Â.R., Haliski, A., 2016. Liming in the conversion from degraded pastureland to a no-till cropping system in Southern Brazil. Soil Tillage Res. 162, 68–77.

Kar, G., Hundal, L.S., Schoenau, J.J., Peak, D., 2011. Direct chemical speciation of P in sequential chemical extraction residues using P *K*-Edge X-Ray absorption near-edge structure spectroscopy. Soil Sci. 176, 589-595.

Koch, M., Kruse, J., Eichler-Löbermann, B., Zimmer, D., Willbold, S., Leinweber, P., Siebers, N., 2018. Phosphorus stocks and speciation in soil profiles of a long-term fertilizer experiment: Evidence from sequential fractionation, P K-edge XANES, and ^{31}P NMR spectroscopy. Geoderma 316, 115–126.

Lilienfein, J., Wilcke, W., Ayarza, M.A., Vilela, L., Do Carmo Lima, S., Zech, W., 2000. Chemical fractionation of phosphorus, sulphur, and molybdenum in Brazilian savannah Oxisols under different land use. Geoderma 96, 31–46.

Lins, I.D.G., Cox, F.R., 1989. Effect of extractant and selected soil properties on predicting the optimum phosphorus fertilizer rate for growing soybeans under field conditions. Commun. Soil Sci. Plant Anal. 20, 319–333.

Liu, J., Hu, Y., Yang, J., Abdi, D., Cade-Menun, B.J., 2014. Investigation of soil legacy phosphorus transformation in long-term agricultural fields using sequential fractionation, P *K*-edge XANES and solution P NMR spectroscopy. Environ. Sci. Technol. 49, 168–176.

Liu, J., Yang, J., Cade-Menun, B.J., Liang, X., Hu, Y., Liu, C.W., Zhao, Y., Li, L., Shi, J., 2013. Complementary phosphorus speciation in agricultural soils by sequential fractionation, solution ^{31}P nuclear magnetic resonance, and phosphorus *K*-edge X-ray absorption near-edge structure spectroscopy. J. Environ. Qual. 42, 1763–1770.

Loeppert, R.H., Inskeep, W.P., 1996. Iron, in: Sparks, D.L., Page, A.L., Helmke, P.A., Loeppert, R.H., Soltanpour, P.N., Tabatabai, M.A., Johnston, C.T., Sumner, M.E. (Eds.), Methods of Soil Analysis. Part 3. Chemical Methods. Soil Science Society of America, Madison, p. 26.

Luo, L., Ma, Y., Sanders, R.L., Xu, C., Li, J., Myneni, S.C.B.B., 2017. Phosphorus speciation and transformation in long-term fertilized soil: evidence from chemical fractionation and P *K*-edge XANES spectroscopy. Nutr. Cycl. Agroecosystems 107, 215–226.

Mackay, A.D., Kladivko, E.J., Barber, S.A., Griffith, D.R., 1987. Phosphorus and potassium uptake by corn in conservation tillage systems. Soil Sci. Soc. Am. J. 51, 970–974.

Manceau, A., Nagy, K.L., 2012. Quantitative analysis of sulfur functional groups in natural organic matter by XANES spectroscopy. Geochim. Cosmochim. Acta 99, 206–223.

McKenzie, R.H., Stewart, J.W.B., Dormaar, J.F., Schaalje, G.B., 1992. Long-term crop rotation and fertilizer effects on phosphorus transformations: I. In a Chernozemic soil. Can. J. Soil Sci. 72, 569–579.

Mehlich, A., 1984. Mehlich 3 soil test extractant: A modification of Mehlich 2 extractant. Commun. Soil Sci. Plant Anal. 15, 1409–1416.

Mehlich, A., 1953. Determination of P, Ca, Mg, K, Na and NH_4 by North Carolina soil testing laboratoris. Raleigh Univ. North Carolina 8.

Mehra, O.P., Jackson, M.L., 1960. Iron oxide removal from soils and clays by a dithionite–citrate system buffered with sodium bicarbonate, in: Clays and Clay Minerals: Proceedings of the Seventh National Conference. pp. 317–327.

Menezes-Blackburn, D., Giles, C., Darch, T., George, T.S., Blackwell, M., Stutter, M., Shand, C., Lumsdon, D., Cooper, P., Wendler, R., Brown, L., Almeida, D.S., Wearing, C., Zhang, H., Haygarth, P.M., 2018. Opportunities for mobilizing recalcitrant phosphorus from agricultural soils: a review. Plant Soil 427, 5–16.

Motavalli, P.P., Palm, C.A., Parton, W.J., Elliott, E.T., Frey, S.D., 1995. Soil pH and organic C dynamics in tropical forest soils: Evidence from laboratory and simulation studies. Soil Biol. Biochem. 27, 1589–1599.

Muljadi, D., Posner, A.M., Quirk, J.P., 1966. The mechanism of phosphate adsorption by kaolinite, Gibbsite, and pseudoboehmite: Part II: The location of the adsorption sites. J. Soil Sci. 17, 230–237.

Murphy, J., Riley, J.P., 1962. A modified single solution method for the determination of phosphate in natural waters. Anal. Chim. Acta 27, 31–36.

Nwoke, O.C., Diels, J., Abaidoo, R., Nziguheba, G., Merckx, R., 2008. Organic acids in the rhizosphere and root characteristics of soybean (*Glycine max* L.) and cowpea (*Vigna unguiculata* L.) in relation to phosphorus uptake in poor savanna soils. African J. Biotechnol. 7, 3617–3624.

Ogle, S.M., Swan, A., Paustian, K., 2012. No-till management impacts on crop productivity, carbon input and soil carbon sequestration. Agric. Ecosyst. Environ. 149, 37–49.

Oliveira, F.H.T., Novais, R.F., Smyth, T.J., Neves, J.C.L., 2000. Comparisons of phosphorus availability between anion exchange resin and Mehlich-1 extractions among oxisols with different capacity factors. Commun. Soil Sci. Plant Anal. 31, 615–630.

Pavinato, P.S., Merlin, A., Rosolem, C.A., 2009. Phosphorus fractions in Brazilian Cerrado soils as affected by tillage. Soil Tillage Res. 105, 149–155.

Prietzel, J., Klysubun, W., 2018. Phosphorus K-edge XANES spectroscopy has probably often underestimated iron oxyhydroxide-bound P in soils. J. Synchrotron Radiat. 25, 1736–1744.

Ravel, B., Newville, M., 2005. ATHENA, ARTEMIS, HEPHAESTUS: data analysis for X-ray absorption spectroscopy using IFEFFIT. J. Synchrotron Radiat. 12, 537–541.

Rehm, G.W., Scobbie, A.J., Randall, G.W., Vetsch, J.A., 1995. Impact of fertilizer placement and tillage system on phosphorus distribution in soil. Soil Sci. Soc. Am. J. 59, 1661–1665.

Rivard, C., Lanson, B., Cotte, M., 2016. Phosphorus speciation and micro-scale spatial distribution in North-American temperate agricultural soils from micro X-ray fluorescence and X-ray absorption near-edge spectroscopy. Plant Soil 401, 7–22.

Rodrigues, M., Pavinato, P.S., Withers, P.J.A., Teles, A.P.B., Herrera, W.F.B., 2016. Legacy phosphorus and no tillage agriculture in tropical oxisols of the Brazilian savanna. Sci. Total Environ. 542, 1050–1061.

Schaefer, C., Fabris, J.D., Ker, J.C., 2008. Minerals in the clay fraction of Brazilian Latosols (Oxisols): a review. Clay Miner. 43, 137–154.

Schmieder, F., Bergström, L., Riddle, M., Gustafsson, J.P., Klysubun, W., Zehetner, F., Condron, L., Kirchmann, H., 2018. Phosphorus speciation in a long-term manure-amended soil profile – Evidence from wet chemical extraction, ^{31}P-NMR and P *K*-edge XANES spectroscopy. Geoderma 322, 19–27.

Schmieder, F., Gustafsson, J.P., Klysubun, W., Zehetner, F., Riddle, M., Kirchmann, H., Bergström, L., 2020. Phosphorus speciation in cultivated organic soils revealed by P *K*-edge XANES spectroscopy. J. Plant Nutr. Soil Sci. 183, 367–381.

Selles, F., Kochhann, R.A., Denardin, J.E., Zentner, R.P., Faganello, A., 1997. Distribution of phosphorus fractions in a Brazilian Oxisol under different tillage systems. Soil Tillage Res. 44, 23–34.

Shoemaker, H.E., McLean, E.O., Pratt, P.F., 1961. Buffer methods for determining lime requirement of soils with appreciable amounts of extractable aluminum. Soil Sci. Soc. Am. J. 25, 274–277.

Soil Survey Staff, 2014. Keys to Soil Taxonomy, 12th ed. USDA - Natural Resources Conservation Service, Washington, DC.

Tiecher, T., Veloso, M., Gabriel, V., Batista, M., Bayer, C., Ambrosini, V.G., Amorim, M.B., Tiecher, T., Gomes, M.V., 2017. Assessing linkage between soil phosphorus forms in contrasting tillage systems by path analysis. Soil Tillage Res. 175, 276–280.

Tran, T.S., Simard, R.R., 1993. Mehlich-3 extractable elements, in: Carter, M.R. (Ed.), Soil Sampling and Methods of Analysis. Canadian Society of Soil Science, Ottawa, pp. 43–49.

USPEA, 1993. Methods for the determination of inorganic substances in environmental samples. United States Environmental Protection Agency, Cincinnati.

van Raij, B., Andrade, J.C., Cantarella, H., Quaggio, J.A., 2001. Chemical analysis for fertility evaluation of tropical soils (*in Portuguese*). Campinas.

van Raij, B., Cantarella, H., Quaggio, J.A., Furlani, A.M.C., 1996. Fertilization and liming recommendations for São Paulo Sate, Brazil (*in portuguese*). Campinas.

van Raij, B., Quaggio, J.A., da Silva, N.M., 1986. Extraction of phosphorus, potassium, calcium, and magnesium from soils by an ion-exchange resin procedure. Commun. Soil Sci. Plant Anal. 17, 547–566.

Wei, K., Chen, Z., Zhang, X., Chen, L., 2018. Phosphorus forms and their distribution under long-term no tillage systems. Plant, Soil Environ. 65, 35–40.

Zoca, S.M., Penn, C., 2017. An important tool with no instruction manual: A review of gypsum use in agriculture, 1st ed, Advances in Agronomy. Elsevier Inc.

Supplementary information

Corn yields and nutrient concentrations in leaves: Corn index leaves at the ear base (only the central third parts) were collected randomly from 30 corn plants in each plot avoiding an external perimeter of 0.5 m (Cantarella et al., 1998). The corn plants were flowering, in the R1 stage, period with high P absorption rates. The index leaves parts were dried at 45ºC until constant mass, grounded and sieved through a 0.5 mm sieve to be digested (25 g) in 6 ml of concentrated HNO_3 and 2 ml of 30% (v/v) H_2O_2.

The elements' concentrations in the extracts were determined by Inductively Coupled Plasma Atomic Emission Spectrometry. After maturation, a mechanized harvest was carried out in 3 m long from each of the four central lines, totaling 12 m in each plot. The corn grain yields were calculated based on the sample mass and the harvested area and adjusted to 130 g kg^{-1} water concentration.

The concentrations of N, K and Cu in corn index leaves were not affected (p > 0.05) by treatments (Table S1). Manganese and Fe contents were higher in the control and PG treatments, whereas the opposite trend was observed for Mg, whose concentrations were higher in L and LPG treatments. Calcium concentrations in index leaves were higher in the PG treatment compared with the control. For S, treatments with phosphogypsum (PG and LPG) exhibited the highest concentrations, while the control had the lowest. For P, there was a difference only between LPG treatment and control (Table S1).

Table S1. Nutrient contents in corn index leaves in 2019 crop.

Treatment	N	P	K	Ca	Mg	S	Cu	Zn	Mn	Fe
2016/17	..... g kg^{-1}						..... mg kg^{-1}			
control	33 a	2 b	20 a	2 b	2 b	1 c	12 a	30 a	76 a	266 a
PG	32 a	2 ab	20 a	4 a	2 b	2 ab	11 a	23 b	72 a	228 a
L	35 a	2 ab	18 a	3 ab	3 a	2 b	11 a	20 b	39 b	171 b
LPG	38 a	2 a	19 a	3 ab	4 a	2 a	10 a	19 b	40 b	172 b

Means followed by the same letter in each column are not different (*Tukey,* $p \leq 0.05$, n=4). Lime (L); phosphogypsum (PG); lime + phosphogypsum (LPG); native vegetation (NV).

The corn yield was affected by treatments ($p \leq 0.05$), decreasing in the following order LPG > L > PG > control (Fig. S1). The coefficient of variation (CV) was 3%, and the minimum significant difference was 282 kg ha^{-1} in the analysis of variance.

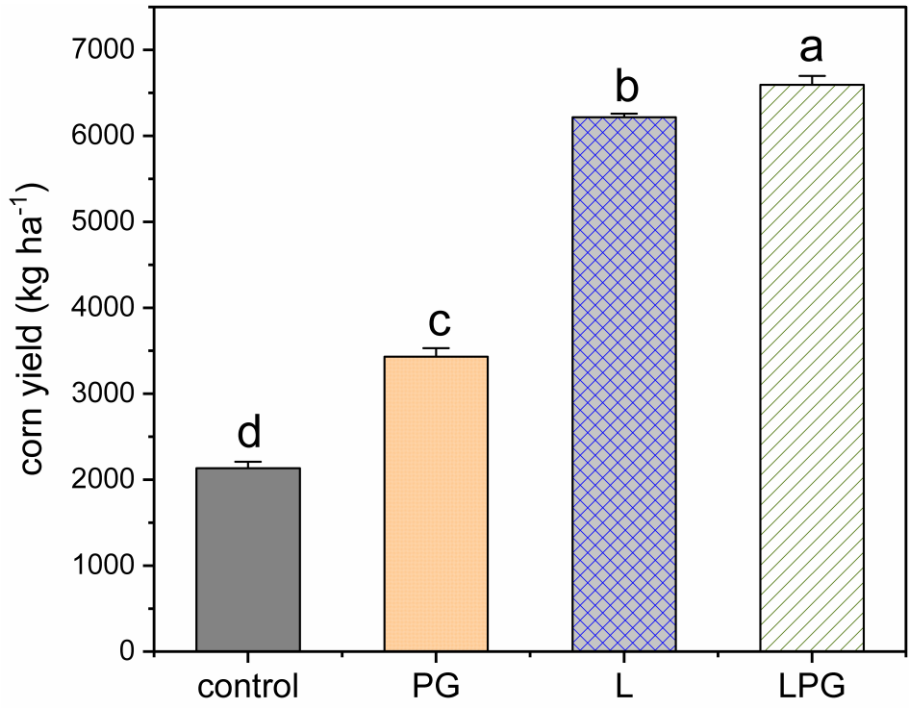

Figure S1. Corn yield in the 2019 crop as a function of long-term amendments broadcast applications (PG – phosphogypsum; L – lime; LPG – lime + phosphogypsum). Different letters indicate difference (Tukey, $p \leq 0.01$, n=4).

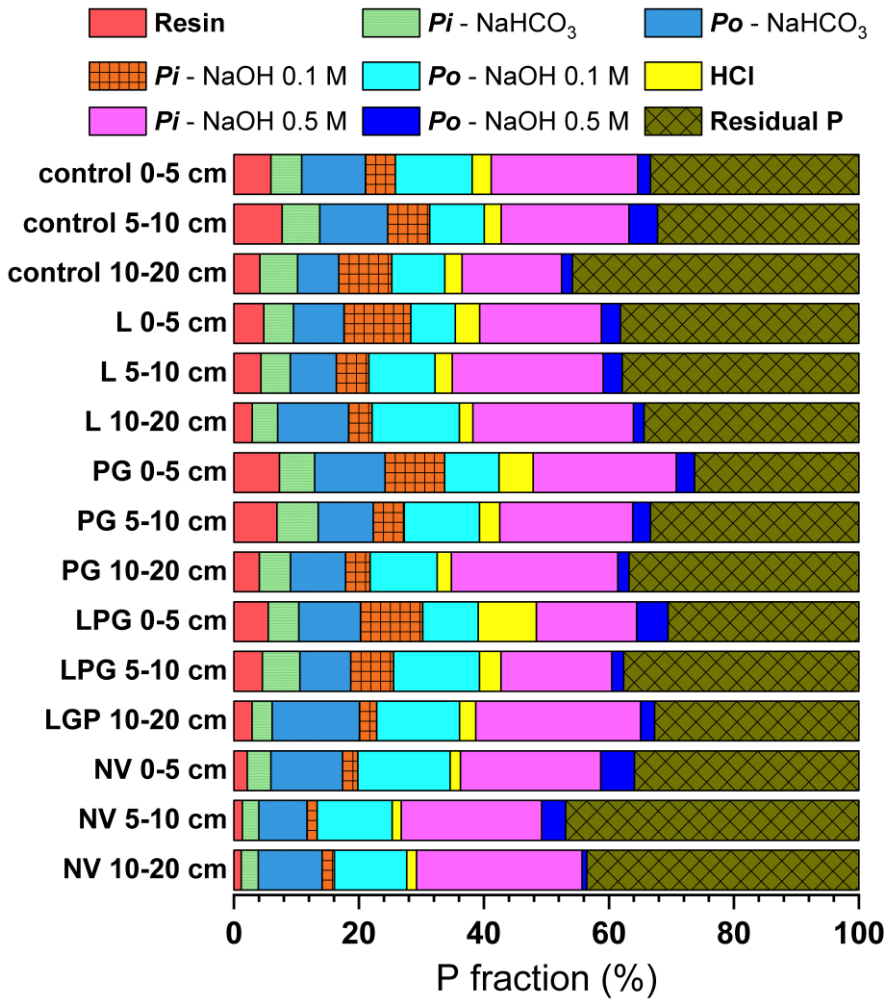

Figure S2. Proportions (relative to 100%) among P-species in the linear combination fitting of soil samples spectra for the treatments: control, lime (L), phosphogypsum (PG), lime+phosphogypsum (LPG) and native vegetation (NV).

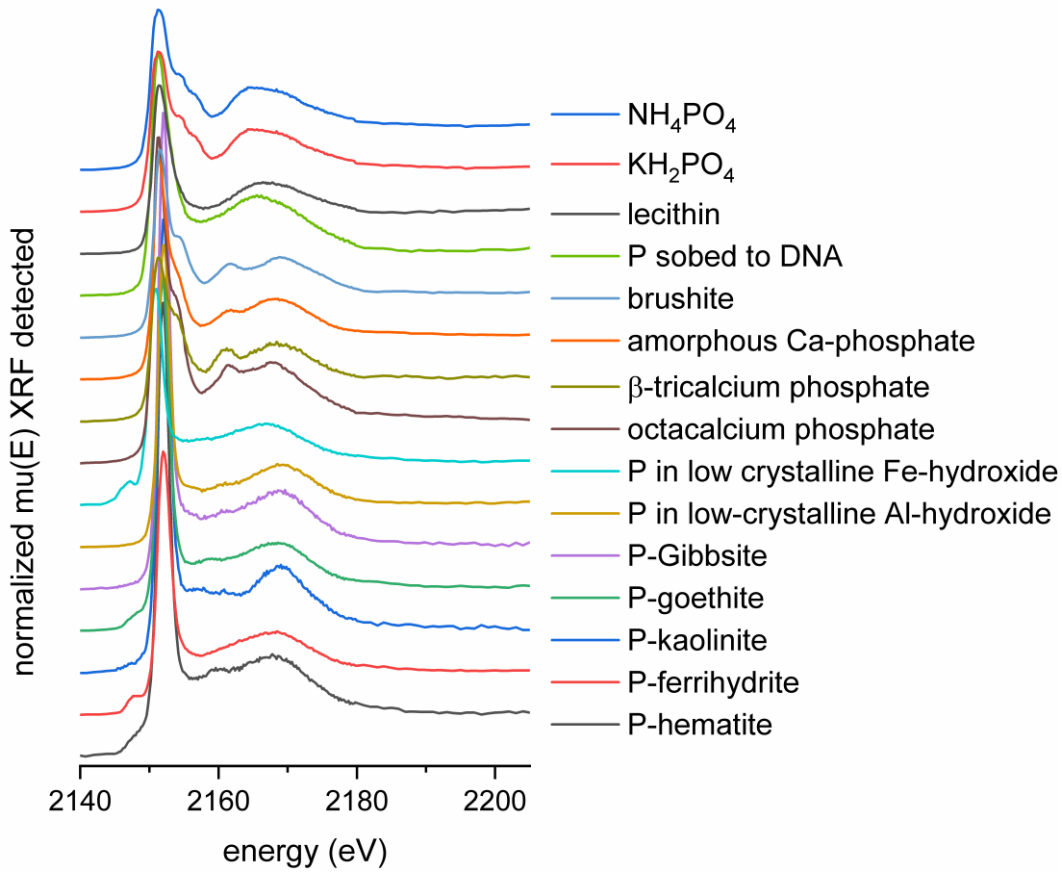

Figure S3. Phosphorus *K*-edge spectra of reference materials and P-sorbed minerals used as standards for the linear combination fitting procedure.

5. LONG-TERM LIME AND PHOSPHOGYPSUM BROADCAST AFFECTS PHOSPHORUS CYCLING IN A TROPICAL OXISOL CULTIVATED WITH SOYBEAN UNDER NO-TILL

ABSTRACT

The broadcast application of lime or phosphogypsum to suppress aluminum (Al) in soils can influence the chemistry and fate of phosphorus (P) in natural environments. However, the long-term effects of these amendments in organic P (P_o) forms and in some soil biochemical properties remain unclear. The objective in this study was to evaluate the effect of lime and phosphogypsum management in P_o contents, soil biochemical properties and soybean (*Glycine max* L.) nutrition and yield. The long-term field experiment was carried out in a highly weathered soil under no-till in southeastern Brazil. Soil chemical attributes commonly used in soil fertility assessments were severely influenced by Al-suppressors broadcast over time. The changes in soil chemical attributes affected nutrient concentrations in soybean index leaves and grain yield, which was higher when lime was associated with phosphogypsum. The activity of enzymes linked to the P and carbon cycles were also influenced by the presence of Al-suppressors in the soil, mainly in the 0-0.2 m layer. The pH was one of the attributes that most influenced the activity of the phosphatases, especially in the limed soil. *Myo*-inositol hexa*kis*phosphate (IHP_6) was the second most abundant P form in the soil after orthophosphates, indicating that the P_o cycle is mainly governed by crops' litter P-inputs. The soil management over time influenced the diversity and abundance of P_o forms measured by ^{31}P nuclear magnetic resonance spectroscopy, when compared to a native vegetation soil.

Keywords: Inositol phosphates; Phosphatases; Soil acidity; ^{31}P NMR Spectroscopy; Tropical soil

5.1. Introduction

Soil acidity is a common problem in the inter-tropics and other regions of the world and drives several effects on physical, chemical and biological soil properties, restraining crop production (Fageria and Baligar 2008). Soils become acidic due to the characteristics of parent material and/or due to inadequate soil management (Narro et al. 2001; Fageria and Baligar 2007; Tiecher et al. 2017). Intensive agriculture and the use of some nitrogen (N) fertilizers combined with non-conservationist practices intensify the process of acidification in soils (Bolan et al. 2004).

Several problems caused by soil acidity in tropical soils have been reported such as the low availability of phosphorus (P) (Edwards 1991; Mcdowell et al. 2002; Rorison 1980; Smeck 1985). The P management can be challenging in humid tropical and subtropical environments because of the high nutrient adsorption by clay silicate minerals and the low natural contents of P (Giaveno et al. 2008; Campos et al. 2016; Roy et al. 2016). These factors reinforce the need to assess the indirect effects of management and agricultural amendments on soil P chemistry.

Aluminum (Al^{3+}) toxicity is a common problem in acidic soils and reduces P absorption, translocation and utilization by plants. The use of lime (L) is an effective practice to reduce soil acidity and Al^{3+} toxicity, also providing calcium (Ca) and magnesium (Mg). After liming, the soil pH_{H_2O} usually increases until ~6.5, and it increases the availability of some nutrients as P, Ca, Mg, N, sulfur (S), boron (B), potassium (K), molybdenum (Mo) and chloride (Cl). This improvement in soil fertility usually results in better plant nutritional status and high yields. On the other hand, phosphogypsum (PG), a byproduct of the phosphate fertilizer industry, is a soil conditioner that reduces reducing Al^{3+} toxicity and supplies Ca to the soil but has practically no effects on soil pH (Fageria et al. 2013).

With the expansion of the no-till system (NTS) in tropical and subtropical agricultural areas, that advocates the minimum tillage and crop residues maintenance on soil surface, lime started to broadcasted on the soil (Caires et al. 2006; Zambrosi et al. 2008; Joris et al. 2016; Fuentes-Llanillo et al. 2018), and it generated some uncertainties about its efficiency because of its low solubility (~14 mg l^{-1} in H_2O), that restricts its action in deeper soil layers. In this context, the use of phosphogypsum became attractive due to its greater solubility compared with lime and the presence of SO_4^{2-} which binds to Al^{3+} and reduces its toxic forms without affecting soil pH. In these conditions, it is important to enlight how P is affected by amendments in different layers of soil profile.

Many researchers have reported the efficiency of lime to reduce P loss from soils to water (Murphy and Stevens 2010; Andersson et al. 2016) and to increase certain

enzyme activities and microbial biomass (Haynes and Swift 1988; Simard et al. 1994; von Tucher et al. 2018). However, most studies have focused mostly on inorganic P forms (Qayyum et al. 2015; Costa and Crusciol 2016; Antonangelo et al. 2017; von Tucher et al. 2018). Therefore, as far as we know, there is a gap about the effects of lime and phosphogypsum on organic P (P_o) forms, in particular regarding soil biochemical attributes and the performance of crops in humid tropical environments.

The objectives in this study were to evaluate the effect of long-term broadcast application of lime and/or phosphogypsum on: (**i**) the stratification of soil chemical properties and enzymes that mineralize P or C; (**ii**) the differences in Po forms by ^{31}P nuclear magnetic resonance (NMR) spectroscopy; and (**iii**) chemical and biochemical soil properties associated with yield and nutrient contents in index leaves of soybean (*Glycine max* L.) cultivated in an Oxisol. We hypothesized that the amendments influence P_o forms and soil properties in the soil, and that there is a stratification of nutrients and enzyme activities in soils under NTS, impacting soybean yields and its nutritional status.

5.2. Material and methods

5.2.1. Experimental site and treatments

A long-term field experiment has been carried out in a Typic Haplorthox (Soil Survey Staff 2014) in Botucatu, state of São Paulo, southeastern Brazil (48º 23' W, 22º 51' S, 765 m a.s.l) under NTS since 2002. The region has a humid subtropical climate with a dry winter and a hot wet summer. The monthly rainfall averages are between 38 mm (minimum) and 224 mm (maximum) with ~1,360 mm annually. The maximum annual average temperature is 26.1ºC, while the minimum is 15.3ºC.

Before establishing the experiment, the 0-0.2 m soil layer had the following chemical properties quantified according to the methodology proposed by van Raij et al. (2001): 4.2 of pH (CaCl2); 21 g kg^{-1} of soil organic matter (SOM); 9.2 mg kg^{-1} of P (extracted by resin); 14 $mmol_c$ kg^{-1} exchangeable calcium ($_{ex}Ca$), 5 $mmol_c$ kg^{-1} of

exchangeable magnesium ($_{ex}$Mg), 1.2 mmolc kg^{-1} of exchangeable potassium ($_{ex}$K) and 2.3 mmol$_c$ kg^{-1} of exchangeable aluminum ($_{ex}$Al; 37 mmol$_c$ kg^{-1} of potential acidity (H+Al) at pH 7.0; and 58 mmol$_c$ kg^{-1} of cation exchange capacity (CEC) ($_{ex}$Ca + $_{ex}$Mg + $_{ex}$K + H+Al). The soil particle size distribution (inorganic matrix) in the 0-0.2 m layer was 545 g kg^{-1} of sand, 108 g kg^{-1} of silt, and 347 g kg^{-1} of clay (Gee and Or 2002).

The experimental design was in randomized complete blocks (RCB) with four replications and experimental units (plots) with 48.6 m^2 (5.4 m x 9.0 m). The following treatments were evaluated: **i**) control (no lime and no phosphogypsum); **ii**) lime (L); **iii**) phosphogypsum (PG); and **iv**) lime + phosphogypsum (LPG). Lime was a grounded anhydrous carbonate mineral, with 17% Ca and 10% Mg. The PG had 20% Ca, 15% S, <0.1% P and <0.1% F. The lime rate was defined according to the chemical analysis of the topsoil (0-0.2 m) to raise a base saturation to 70% (Cantarella et al. 1998), with 2,700 kg ha^{-1} of lime applied in 2002. The rate of PG was calculated according to van Raij et al. (1996), obtained by multiplying the clay content at the 0.2-0.4 m layer by 6, and 2,100 kg ha^{-1} were applied in 2002.

The reapplications of the amendments were performed when the treatment with only lime reached ≤50% of bases saturation, which was verified annually. When lime reapplication was necessary, the PG rate was also reapplied (2,100 kg ha^{-1}). With this, four amendment applications were performed along the experiment. Beyond 2002, 2,000 kg ha^{-1} of lime and 2,100 kg ha^{-1} of PG were reapplied in 2004 and in 2010.

In October 2016, a new application was necessary, but the calculation of lime rate followed Caires et al. (2015) and Joris et al. (2016), resulting in 6,520 kg ha^{-1}. In 2016 the rate of PG was calculated based on previously proposed recommendations described in Caires and Guimarães (2018), resulting in 10,000 kg ha^{-1}. Caires and Guimarães (2018) intended to increase Ca^{2+} saturation to 60% in relation to the effective cation exchange capacity in the 0.2-0.4 m soil layer. These changes were motivated by a tendency to update the methods for lime and phosphogypsum rates calculation that had been used in Brazil until then.

Rates of P were the same in all plots, varying with the requirements of each species cultivated. The applications were always performed in the sowing row as triple superphosphate (20% P, 10% Ca) or simple superphosphate (8% P, 16% Ca, 9% S). The experiment received more than ten plant species. For further details, see Carmeis Filho et al. (2017) and Costa and Crusciol (2016).

5.2.2. Soil sampling

Soil samples were collected through probes (8-cm diameter) during the full bloom of soybeans, from 0-0.05, 0.05-0.1, 0.1-0.2 and 0.2-0.4 m layers, during the 32nd crop of the experiment (January 2018). This sampling period was chosen due to the presence of high amounts of live roots to absorb P and due to greater biochemical activity in the soil. To form a composite soil sample, ten subsamples were collected from each experimental plot, two in the sowing row, four to 11 cm from the sowing row, and four to 22 cm from the sowing row. Isolation of 0.5 m from the edges to the interior of each plot was maintained at the sampling time.

The sampling procedure was chosen because the soil collected in the sowing row is not the only source of P for the plants, although the concentration of P is greater in this region in relation to the inter-row, which could overestimate the P contents in the plot. In addition, the sowing rows have been in different locations over the years, and the sampling procedure could cover soil in a space close to 0.45 m. This area was coincident with the distance of soybean sowing rows and covered the surface that received lime and/or phosphogypsum broadcasted over time. For comparison purposes, soil samples from native vegetation (NV) located ~100 m from the experimental area were also collected. For this sampling, ten collection points were randomly selected in a square area of 225 m^2 inside the forest.

5.2.3. Soil chemical properties analyses

Soil pH was measured using a glass electrode with 1:2.5 (v/v) of soil:0.01 mol l^{-1} $CaCl_2$ solution ratio. Contents of soil organic carbon (SOC) were extracted by chromic

acid digestion (Heanes, 1984). The potential acidity (H+Al) was estimated according to Shoemaker et al. (1961). The $_{ex}$Al was extracted using 1 mol l^{-1} KCl solution and quantified by the titrimetric method with 0.025 mol l^{-1} NaOH (Bertsch and Bloom 1996). The $_{ex}$Ca, $_{ex}$Mg and $_{ex}$K were extracted by ion exchange resin (van Raij et al. 2001) and determined by Atomic Absorption Spectroscopy (AAS) in a Perkin-Elmer 1100B. Sulfate (SO_4^{2-}) was extracted with 0.01 mol l^{-1} $Ca_3(PO_4)_2$ in a 1:2.5 (v/v) soil:solution ratio, with suspensions shaken for 30 min, filtered (Whatman nº 42) and determined by turbidimetry (Fox et al. 1964). Bioavailable P was extracted by ion exchange resin (van Raij et al., 1996) and quantified according to Murphy and Riley (1962) in a Bel Photonics UV-M51 spectrophotometer.

Before extraction with NaOH+EDTA for ^{31}P-NMR, equal masses of field moist soil samples from 0-0.05 m and 0.05-0.1 m were mixed to form samples from 0-0.1 m that usually correspond to the layer with the highest concentration of soybean roots. Another factor that justifies this choice is that analyzes of only 0-0.05 m would overestimate P_o forms. Instead, if we used deeper layers such as 0.2-0.4 m, the P_o concentration would be very low, making it difficult to interpret the results.

Part of the samples were used to extract total P ($_T$P) by microwave acid digestion with concentrated HCl, HNO_3 and HF following the method EPA-3052 (USPEA 1996). Phosphorus contents were determined by Inductively Coupled Plasma Optical Emission Spectrometry (ICP-OES) in a Thermo Scientific iCAP 6200. Another part of the samples was used to extract bioavailable P by ion exchange resin (van Raij et al., 1996). The contents of P extracted by resin were determined both by colorimetry (Murphy and Riley, 1962) and by ICP-OES. Molybdate unreactive P was calculated based on the difference between ICP-P and colorimetry-P concentrations in the extracts.

5.2.4. Enzymes activities assays

Two phosphatases activities involved in P cycle and a β-glucosidase (β-gl) activity involved in C cycle were quantified in fresh, moist 2-mm sieved soil samples. The acid (Acid-P) and alkaline (Alk-P) phosphomonoesterases (EC 3.1.3.2 and EC 3.1.3.1)

were assayed with an equivalent mass of 1 g soil incubated (1 h at 37ºC) with 0.115 mol l^{-1} *p*-nitro-phenylphosphate as substrate with buffer pH values of 6.5 or 11 (Tabatabai 1994). Soil β-gl (EC 3.2.1.21) was assayed with *p*-nitrophenyl-β-D-glucopyranoside (*p*NPG) as substrate (pH 6.0) by incubation (1 h at 37ºC) according to Eivazi and Tabatabai (1988).

After the incubation, 0.5 mol l^{-1} $CaCl_2$ and 0.1 mol l^{-1} tris–hydroxymethyl (aminomethane) adjusted to pH 12 with 0.5 mol l^{-1} NaOH were added to precipitate humic molecules responsible for brown coloration and to extract *p*-nitrophenol, that was added to the blank samples after the incubation. For all enzymes the *p*-nitrophenol was measured photometrically in filtered solutions (Whatman 42) at 410 nm (phosphomoesterases and β-glucosidase) - (Nova NI 2000 UV-VIS). The analyses were carried out in triplicates with one blank for each sample, and the activities were expressed as mg *p*-nitrophenol kg^{-1} soil (dry weight) h^{-1}.

5.2.5. NaOH-EDTA extraction

Phosphorus was extracted by shaking 2 g of air-dried soil (0-0.1 m) with 20 ml of a solution containing 0.25 mol l^{-1} NaOH + 0.05 mol l^{-1} Na_2EDTA (Cade-Menun and Preston 1996). The mixtures were shaken for 16 h at 25ºC, centrifuged at 1500 ×g for 25 min, and the supernatant was collected in falcon tubes after filtration (filter paper – pore size 2.5 µm). The supernatants were set at -80°C for 2 h and then freeze-dried. Molybdate reactive P contents (inorganic P pool) in the NaOH+EDTA extracts were determined using the molybdenum blue colorimetric method of Murphy and Riley (1962) and called MRP. The total concentrations of P in the extracts were determined by ICP-OES and called $_{N\text{-}ICP}P$.

5.2.6. Liquid state ^{31}P-NMR spectroscopy

Freeze-dried NaOH-EDTA extracts (250 mg) were ground and re-dissolved in 1 ml of D_2O + 0.1 ml 10 mol l^{-1} NaOH (to ensure a pH ≥ 12 for signal lock), centrifuged (1500 ×g) for 5 minutes and placed in 5-mm diameter NMR tubes. Solution 1D ^{31}P

NMR spectra were recorded at 25ºC probe temperature using an Advance III HD Bruker 600MHz spectrometer (Bruker, Karlsruhe, Germany) operating at 242,8 MHz with a 5-mm broadband probe, tuned to ^{31}P (untreated samples).

Spectra were collected using a 30º pulse (12 µs pulse duration), an acquisition time of 0.34 s and a relaxation delay time of 3 s, with 16,384 scans (~16 h) and using 1H decoupling. The free induction decay (FID) signals were processed with 10 Hz line broadening and Fourier transformed with signal integrations performed at TopSpin Software from Bruker. Chemical shifts assignments were based on previous studies (Moedritzer et al. 1962; Condron et al. 1985; Turner et al. 2003; Cade-Menun 2005; Abdi et al. 2015).

5.2.7. Sampling and analysis of soybean yield and nutrient contents in leaves

Contents of nutrients in index leaves and yields´ evaluations were carried out for three summer crops: 2016/17, 2017/18 and 2018/19. For index leaves (20 trifoliolate leaflets – 3rd from the plant apex, without petiole) were randomly collected with 0.5 m of isolation from the edges to the interior of each plot. The sampling occurred when soybean was in full bloom (R2) (~50 days before harvest, depending on the cultivar cycle), the stage at which the nutrients uptake occurs at higher intensity (Bender et al., 2015). The leaves were oven-dried at 45°C until constant mass, milled, and sieved through 0.5-mm sieves. The vegetal tissue obtained (0.25 g) was digested in 6 ml of 65% (v/v) HNO_3 and 2 ml of 30% (v/v) H_2O_2.

The digestion was carried out in a microwave oven under the following conditions: 10 min of heating, maintaining the temperature at 170°C for 15 min under 2 MPa pressure, followed by cooling down for 20 min to room temperature (25ºC). The nutrient contents were determined by ICP-OES. The harvests were carried out manually. Grain yields were calculated based on the relationship between the grain masses obtained in the interior (5.4 m^2) of each plot and their respective water content, which were standardized at 130 g kg^{-1} water content and converted into kg ha^{-1}.

5.2.8. Data analysis

All data were analyzed considering their replication, with tests of homoscedasticity and residues normality previously made by *Hartley* and *Shapiro-Wilk*, respectively. Comparisons among means were evaluated using a one-way ANOVA with *Tukey* test at p = 0.05 or 0.01 levels. The linear relationships between variables were based on simple correlations (*Pearson*). Comparison between $_{ICP}$P and $_{Colr}$P means (n = 4) were done by T-test at $p \leq 0.05$. Analyzes were performed on SPSS 20.0 (Chicago, IL, USA) and GraphPad Prism 8.0 (San Diego, CA, USA).

5.3. Results

5.3.1. Soil chemical properties

The pH varied in all layers of the soil samples, ranging from 3.8 in the NV to 5.8 in the LPG treatment (Table 1). Contents of SOM were higher in the NV area in all layers except 0.2-0.4 m, and samples from the control treatment had the lowest SOM contents in the 0-0.05 m layer, but did not differ from PG. The control and L treatments exhibited the lowest contents of SO_4^{2-} in all layers, while the treatments that received phosphogypsum, in general, had the highest contents. The L and LPG treatment had the highest contents of $_{ex}$Ca, with effects up to 0.4 m.

The effects for $_{ex}$Mg were observed up to 0.1 m, with L treatment showing highest contents. The lowest contents of $_{ex}$K were observed in the LPG treatment between 0 to 0.05 m. In deeper layers (0.1-0.2 m and 0.2-0.4 m), the NV had the lowest $_{ex}$K contents. In the 0.05-0.1 m and 0.1-0.2 m layers, the PG and LPG treatments presented higher P bioavailability. In the 0-0.05 m and 0.2-0.4 m layers, there was no difference among the P contents in all the treatments. The P contents in NV were lower compared to the experimental treatments with exception of the 0.2-0.4 m layer (Table 1).

Table 1. Selected soil properties of each treatment in four soil layers.

Layer	Treat.	pH	SOM	$_{ex}$Ca	$_{ex}$Mg	$_{ex}$K	$_{ex}$Al	H+Al	SO_4^{2-}	P
cm		0.01 mol l^{-1} $CaCl_2$	g kg^{-1}			mmol$_c$ kg^{-1}				mg kg^{-1}
0-5	control	4.0 cA‡	37 cA	7 dA	5 cA	2.3 aA	9 bB	67 bA	7 bA	35 aA
	L	5.7 aA	43 bA	64 bA	56 aA	1.9 abAB	1 cC	20 cC	9 bA	39 aA
	PG	4.5 bA	42 bcA	27 cA	2 cA	1.8 abA	6 bcB	51 bA	14 aB	34 aA
	LPG	5.8 aA	45 bA	80 aA	34 bA	1.6 bA	1 cB	18 cB	14 aA	44 aA
	NV	3.9 cA	63 aA	10 dA	4 cA	2.3 aA	19 aA	130 aA	25 aA	10 bA
5-10	control	4.0 bcA	23 bB	4 cA	2 bA	1.9 abAB	14 bA	66 bA	9 aA	32 aA
	L	4.8 aB	26 bB	18 abB	10 aB	2.2 aA	2 cBC	39 cB	7 aA	23 bB
	PG	4.1 bB	22 bB	10 bcB	2 bA	1.5 bcA	10 bA	60 bA	20 aB	32 aA
	LPG	5.0 aB	24 bB	24 aB	7 abB	1.4 bcA	2 cB	33 cA	17 aA	32 aB
	NV	3.9 cA	35 aB	4 cA	2 bA	1.3 cB	20 aA	96 aB	15 aA	10 cA
10-20	control	4.0 bA	16 bC	10 abA	2 aA	1.6 aB	16 abA	58 bA	11 bA	14 abB
	L	4.5 aC	20 bBC	12 abB	6 aBC	1.4 abB	5 cB	42 bcAB	12 bA	10 bC
	PG	4.1 bB	16 bC	6 bB	1 aA	1.2 abA	13 bA	53 bA	40 abB	19 aB
	LPG	4.6 aC	20 bBC	19 aB	5 aB	1.3 abA	3 cB	35 cA	43 aA	16 aC
	NV	3.8 bA	27 aC	2 bA	1 aA	0.9 bBC	19 aA	80 aC	16 bA	8 cA
20-40	control	4.1 cA	14 aC	2 bA	1 aA	1.5 aB	17 aA	58 aA	31 bA	4 aC
	L	4.3 bC	17 aC	7 abB	4 aC	1.4 aB	10 bcA	54 aA	19 bA	5 aC
	PG	4.0 cB	14 aC	6 abB	1 aA	1.5 aA	12 bA	61 aA	81 aA	6 aC
	LPG	4.6 aC	17 aC	14 aB	4 aB	1.2 aA	8 cA	48 aA	60 aA	4 aD
	NV	4.0 cA	15 aD	2 bA	1 aA	0.6 bC	17 aA	61 aD	23 bA	5 aA

(‡) Different lowercase letters in each soil layer indicate difference ($p \leq 0.05$) between treatments. Different capital letters for each treatment in different layers also indicated difference ($p \leq 0.05$).

The soil pH from control treatment and NV did not vary between soil layers. Conversely, samples from L and LPG had higher pH values compared to other conditions up to 0.2 m. In the PG treatment, the pH values were higher in the 0-0.05 m soil layer. For SOM, as expected, the contents were higher at 0-0.05 m in all conditions, with drastic variations among soil layers, as observed for the native vegetation. For the 0-0.05 m layer, the control presented the lowest SOM contents, followed by the amended treatments (L, PG and LPG), whereas the NV presented the highest contents.

No differences were found in the contents of $_{ex}$Ca and $_{ex}$Mg for the control treatment and native vegetation. For L, PG and LPG treatments, the highest $_{ex}$Ca contents were observed in the 0-0.05 m soil layer. For $_{ex}$Mg contents, the L and LPG treatments presented the highest contents at the uppermost (0-0.05 m) soil layer, with

no difference among the other layers in control, PG and NV. There was also no difference in $_{ex}K$ contents in PG and LPG treatments among soil layers.

Exchangeable Al contents were generally lower between 0-0.05 m except in the native vegetation. In the lime-amended treatments, the contents between 0.05 to 0.1 m were less than ~2 $mmol_c\ kg^{-1}$, which represent values ~ten and five times lower than those found in native vegetation and in the control treatment. The H+Al contents (potential acidity) decreased in the treatments containing lime, with effects observed up to 0.2 m.

There was no difference in control and PG treatments among soil layers; however, in L and LPG treatments, H+Al contents were higher in deeper layers. In the NV, the opposite was observed. The SO_4^{2-} contents was changed by PG treatment along the soil profile, with higher values in 0.2-0.4 m. Phosphorus contents were higher in 0.05-0.1 m and 0.1-0.2 m soil layers with the exception of native vegetation, where the contents did not vary along the soil profile.

5.3.2. Soil enzymes activities

The higher Acid-P activity in the 0-0.05 m layer was observed in the PG treatment, although the P-acid activity at 0.05-0.10 m was not different from that observed in the L and LPG treatments. In the 0.1-0.2 m layer, the P-acid activity was lower than in uppermost soil layers (Fig. 1). The effect of lime in Alk-P activities was notorious in the 0-0.05 and 0.05-0.10 m soil layers. In deeper layers, the highest activity was observed in the native forest (0.1-0.2 m) with a tendency to stabilize (absence of difference) with the increase of depth, as observed in 0.2-0.4 m. The β-glucosidase activity in the control treatment was the lowest in 0-0.05 m (Fig. 1a) and 0.05-0.1 m (Fig. 1b) layers. In all studied layers, the highest β-glucosidase activities were found in NF. However, in the 0.05-0.10 m (Fig. 1b) and 0.1-0.2 m (Fig. 1c) layers the β-glucosidase activities found in the NF were not different from those found in the L and LPG treatments (Fig. 1).

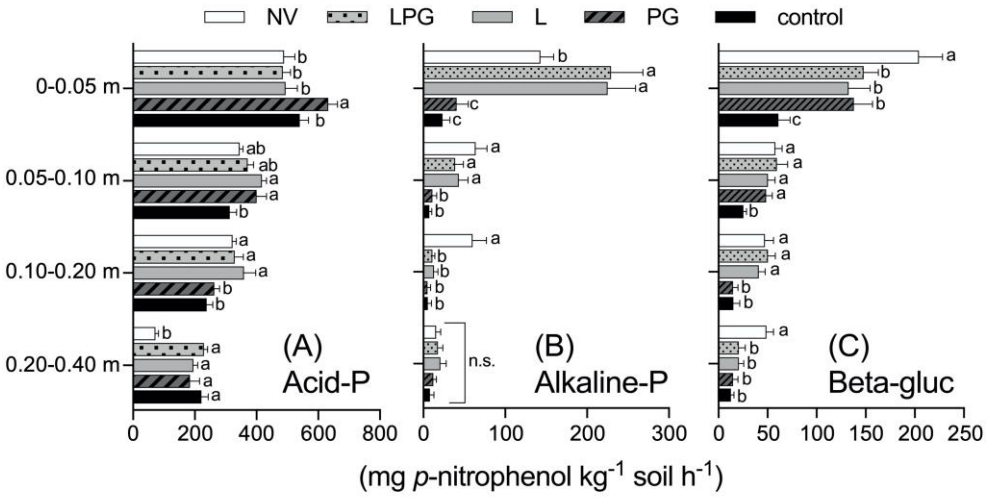

Figure 1. Soil acid phosphomonoesterase (Acid-P) (**A**), alkaline phosphomonoesterase (Alkaline-P) (**B**) and β-1.4-glucosidase (Beta-gluc) (**C**) activities, expressed as mg *p*-nitrophenol kg^{-1} soil h^{-1}. The error bars represent the standard deviations of the means (n = 3). Different letters above the bars indicate difference among treatments in the same soil layer (Tukey, $p \leq 0.05$).

5.3.3. MUP and P forms in NaOH-EDTA extracts by liquid state ^{31}P NMR spectroscopy

The control, L and NV had higher $_{ICP}$P contents in relation to $_{Colr}$P contents (Fig. 2). The highest MUP contents were found in the L treatment (3.6±0.5 mg kg^{-1} P), which represents 10% of the $_{ICP}$P concentrations. The ^{31}P-NMR spectra from the soil solutions are shown in Fig. 3a. The NaOH+EDTA solution extracted 62-72% of the total P in the samples, which exhibited high contents of MRP in the NaOH+EDTA extracts (~80% in the experiment samples and 65% in the native vegetation sample) (Table 2).

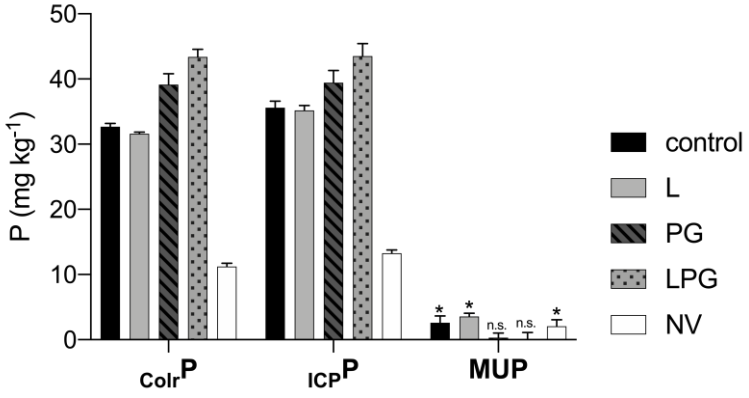

Figure 2. Bioavailable P extracted with ion exchange resin and determined by colorimetry ($_{Colr}$P) and by ICP-OES ($_{ICP}$P). Molybdate Unreachable Phosphorus (MUP) was calculated by the difference between the P contents obtained by ICP determination minus colorimetry determination. (*****) Indicate difference and (n.s.) no difference between the contents of $_{ICP}$P and $_{Colr}$P (T-test comparison, n= 4; $p \leq 0.05$).

Table 2. Phosphorus forms in soil in soil samples determined by ^{31}P-NMR spectroscopy and colorimetry.

treatment					Inorganic P ⁑			Organic P ‡						
								monoesters				diesters		
	$_{T}$P†	$_{N\text{-}ICP}$P†	MRP†	MUP†	Ortho	Pyro	Poly	*myo*-IP	*scyllo*-IP	αβ-glyc	AMP	DNA	OthDi	Phos
	mg kg^{-1}													
control	375	245 (65%)	181	64 (26%)	194§	7.6	1.0	21.6	4.7	3.2	3.7	5.6	2.2	1.5
L	420	304 (72%)	241	62 (20%)	244	6.7	3.2	24.7	5.5	3.3	3.9	4.6	2.1	5.7
PG	427	290 (68%)	234	56 (19%)	233	2.9	3.2	25.2	5.8	3.8	4.1	5.5	2.3	4.9
LPG	458	283 (62%)	238	45 (16%)	224	5.4	0.2	27.1	6.2	4.0	4.2	6.8	2.8	2.5
NV	246	170 (69%)	93	77 (45%)	80	9.5	0.9	35.1	8.5	6.6	3.2	17.5	4.1	4.6

†$_{T}$P, total phosphorus in the soil extracted by microwave acid digestions (method 3052); $_{N\text{-}ICP}$P, phosphorus content in the NaOH+EDTA extract determined by ICP-OES; MRP, orthophosphate obtained by colorimetry (Murphy and Riley 1962) in the NaOH+EDTA extract; MUP, molybdate unreactive phosphorus calculated by the difference between $_{N\text{-}ICP}$P and MRP;

⁑Inorganic P abbreviations: Ortho, orthophosphate obtained by 31P-NMR; Pyro, pyrophosphate; Poly, polyphosphates;

‡Organic P abbreviations: *myo*-IP, myo-inositol hexakisphosphate; *scyllo*-IP, *scyllo*-inositol hexakisphosphate; αβ-glyc, α and β glycerophosphates; AMP, adenosine-5'-monophosphate; DNA, deoxyribonucleic acid; OthDi, orthophosphates diesters except DNA; Phos, phosphonates.

The contents of MUP in the NV soil samples were ~20% higher compared to the experimental area. This occurred even with samples from the experimental area having ~41% more total P than NV. The NMR spectra revealed the dominance of Pi

forms (Table 3; Fig. 3), which was on average 79% in the experiment samples and 53% in the native vegetation. These percentages were in agreement with the proportions of MRP and MUP obtained chemically in the NaOH+EDTA extracts (Table 2).

The inorganic orthophosphate was the most abundant P form in the samples with contents ranging between 80 to 244 mg kg^{-1} P (Table 2), which proportionally represents 47-80% of P extracted by NaOH+EDTA (Table 3). Another Pi form was pyrophosphates that represented 1-6%. The polyphosphates region represented no more than 1% of extracted P in the samples (Table 3).

The dominant P_o compound detected was *myo*-IHP_6, with peaks at 4.48±0.05, 4.14±0.03 and 3.82±0.02 ppm (Fig. 3b). The peak in 3.43±0.04 was assigned to *scyllo*-IHP_6. It was not possible to clearly separate the peaks of α-glycerophosphate (α-gly) and β-glycerophosphate (β-gly); therefore, the peak at 4.68±0.11 ppm was assigned to α-gly+β-gly (αβ-gly) (Fig. 3b). The peak at 4.35±0.04 ppm, referred to as "3" in Fig. 3b, was assigned to mononucleotides based on previous studies (Mcdowell and Stewart 2005; McLaren et al. 2017).

Table 3. Proportions of P forms in soils samples determined by ^{31}P-NMR spectroscopy.

treatment	Inorganic P †			Organic P ‡						
				monoesters				diesters		
	Ortho	Pyro	Poly	*myo*-IP	*scyllo*-IP	αβ-glyc	AMP	DNA	OthDi	Phos
	relative %									
control	79§	3	<1	9	2	1	2	2	1	1
L	80	2	1	9	2	1	1	2	1	1
PG	80	1	1	9	2	1	1	2	1	1
LPG	79	2	<1	10	2	1	2	2	1	1
NV	47	6	1	21	5	4	2	10	2	3

§ Results are averages (n = 3) and the standard deviation are in parentheses; † Inorganic P abbreviations: Ortho, orthophosphate; Pyro, pyrophosphate; Poly, polyphosphates; ‡ Organic P abbreviations: *myo*-IP, *myo*-inositol hexakisphosphate; *scyllo*-IP, *scyllo*-inositol hexakisphosphate; αβ-glyc, α- and β-glycerophosphates; AMP, adenosine-5′-monophosphate; DNA, deoxyribonucleic acid; OthDi, orthophosphates diesters except DNA; Phos, phosphonates.

The native vegetation sample showed better defined peaks, which facilitated the identification of P forms (Fig. 3b). The samples from the experimental area had

peaks with less intensity, but with no variations in P forms. The relative proportions of P forms in the samples from the experimental area were similar. Samples from the cultivated soil, however, had proportions of *myo*- and *scyllo*-IHP_6 less than half of the proportions found in the native vegetation. For DNA, the cultivated soil presented proportions that corresponded to ~20% of those found in the forest soil. On the other hand, the relative proportion of orthophosphate was inferior in native vegetation, highlighting the greater contribution of Po forms (Table 3).

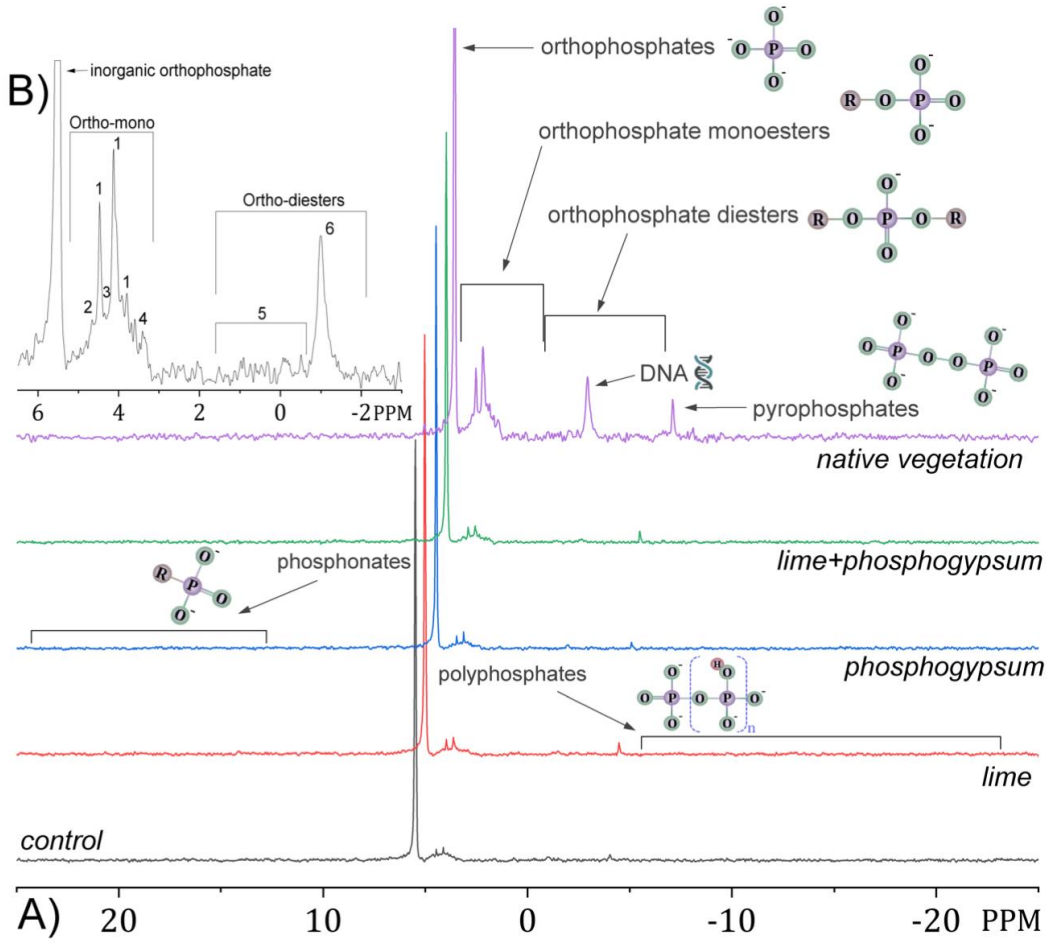

Figure 3. Subfigure (**A**) is the ^{31}P-NMR spectrum of soil solutions from four treatments and one native vegetation. Spectra were processed with 10 Hz line-broadening and are plotted to full height and scaled to the height of the orthophosphate peak. Subfigure (**B**) Spectra (^{31}P-NMR) between 6.5 and -3 ppm of the native vegetation soil sample with emphasis on some spectrum regions that correspond to organic forms of P: (1) myo-inositol hexakisphosphate; (2) αβ-glycerophosphates; (3) monocucleotides; (4) scyllo-inositol phosphate; (5) orthophosphates diesters; (6) deoxyribonucleic acid, DNA.

5.3.4. Soybean nutrition and yield

Phosphorus, K, Cu, Zn and Fe concentrations in index leaves were not affected by treatments in any of the three years evaluated (Table 4). On the other hand, contents of N, Ca, Mg, S and Mn exhibited the same difference patterns in all evaluated years. Nitrogen concentrations were higher in L and LPG treatments, whereas the opposite was observed for Mn (Table 4). Soybean leave tissues from PG and LPG treatments had the highest Ca and S concentrations (r = 0.73 for Ca *vs*. S). However, the highest concentrations of Mg were found in L and control treatments, followed by LPG and then by PG (Table 4). The Mg *vs*. Ca concentration in index leaves presented a high negative correlation of -0.83, just lower than the N *vs*. Mn correlation of -0.87.

Table 4. Nutrient contents in soybeans index leaves (trifoliolate leaflets without petiole) in three consecutive crops.

Treatment	Ca	Mg	K	S	P	N	Cu	Zn	Mn	Fe
2016/17	..... g kg^{-1}						..... mg kg^{-1}			
control	6 c	5 a	23 a	2 c	3 a	53 b	7 a	60 a	184 a	107 a
PG	9 a	2 c	22 a	4 a	4 a	52 b	7 a	65 a	225 a	121 a
L	7 bc	4 a	24 a	3 bc	4 a	60 a	8 a	50 a	67 b	114 a
LPG	8 ab	3 b	22 a	3 ab	4 a	60 a	8 a	48 a	65 b	127 a
2017/18										
control	6 c	5 a	23 a	2 c	3 a	53 b	9 a	38 a	112 a	128 a
PG	9 a	2 c	22 a	3 a	4 a	52 b	11 a	34 a	116 a	125 a
L	7 bc	4 a	23 a	3 bc	4 a	59 a	11 a	35 a	84 b	124 a
LPG	8 ab	3 b	22 a	3 ab	4 a	60 a	11 a	34 a	86 b	112 a
2018/19										
control	6 c	4 a	21 a	2 c	3 a	48 b	7 a	55 a	168 a	97 a
PG	8 a	2 c	20 a	3 a	3 a	48 b	6 a	69 a	206 a	110 a
L	7 bc	4 a	22 a	2 bc	3 a	54 a	7 a	52 a	74 b	113 a
LPG	8 ab	3 b	21 a	3 ab	3 a	55 a	8 a	41 a	78 b	100 a

Means followed by the same letter in the column are not different (*Tukey, p* ≤ 0.05, n=4).

The LPG treatment had the highest yield in 2017/18 but did not differ from L in 2016/17 and 2018/19 (Fig. 4). The control treatment had lower soybean yields in 2017/19 and 2018/19 but did not differ from PG and L treatments in the 2016/17 crop. On average (three years) the control treatment yield was 2,083±149 kg ha^{-1}, 30% less

compared to LPG (3,733±183 kg ha^{-1}). The PG average yield was 2,514±215 kg ha^{-1}, with lower yields compared to LPG in all years. The L treatment did not differ from PG, with an average yield of 3,197±140 kg ha^{-1}.

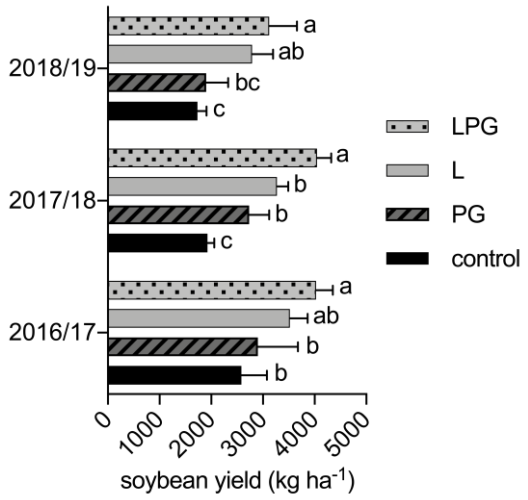

Figure 4. Soybean yield in 2016/17, 2017/18 and 2018/19 summer crops as a function of treatments (L = lime; PG = phosphogypsum; LPG = lime + phosphogypsum). Different letters represent differences between treatments in the same crop year (*Tukey*, $p \leq 0.01$, and n = 4).

5.4. Discussion

5.4.1. Soil chemical properties

Variations in soil pH were expected especially due to lime broadcast in the experimental area. Liming was effective to decrease soil acidity and maintain the pH in values higher than the control and PG treatments (Table 1). The effects of lime on soil pH can last for years in soils under NT in humid tropical regions, *e.g.* 120 months, as reported by Caires et al. (2005), or 156 months, as reported by Blum et al. (2013). Although PG does not change the pH as lime, the excessive displacement of OH^- by SO_4^{2-} can promote partial neutralization of acidity, as reported by Reeve and Summer (1972). The PG was less effective than lime to decrease other acidity components ($_{ex}$Al and H+Al) and maintained similar contents to those observed in the control treatment (Table 1). Changes in soil pH in the control treatments and NV were not expected, as there was no application of soil amendments.

In lime-amended soil (regardless of PG addition), $_{ex}$Ca contents were ~ten times higher than the control in the 0-0.05 m layer. For the PG treatment, the $_{ex}$Ca contents were only lower than those observed in L treatment in the 0-0.05 m layer, which is probably related to the low solubility of the lime in relation to PG and, consequently, the restriction of its action in the most superficial layers. Lime had a direct effect on Mg availability because it is the source of this nutrient. Conversely, PG is not a source of Mg, as evidenced by the absence of difference among PG, control and native vegetation in all soil layers (Table 1). The nutritional unbalance promoted by PG on Mg concentrations in index leaves (Table 4) was a consequence of what happened in the soil (Fig. 4). The abundance of SO_4^{2-} provided by PG can cause Mg deficiency in plants by the formation of the ionic pair ($MgSO_4$), which is a salt not absorbed by plants and is easily leached.

The native vegetation had the highest SOM contents because of the absence of anthropic interference, as well as greater soil coverage with plant residues. However, in the 0-0.05 m layer, SOM contents in the lime-amended treatments were superior to that of control and PG. This was especially related to the higher fertility conditions associated with higher pH that made the plants produce more root and shoot biomass (Carmeis Filho et al. 2017; Inagaki et al. 2017). But it can also be related to an increase in Ca availability in the soil, thus acting as a stabilizer for organo-mineral complexes, as described by Rowley et al. (2018).

The high amounts of Ca added in the LPG treatment changed the proportions among basic cations in the soil exchange complex (Table 1). This effect was notorious only from 0 to 0.05 m due to the greater action of lime in this most superficial layer. The native vegetation had the highest K contents from 0-0.05 m especially because of the abundant presence of plant residues in decomposition on the soil surface and due to the lack of a cationic imbalance induced by the application of high Al-suppressors rates. However, in layers below 0.05 m, the native vegetation had lower contents of K as compared to the experimental treatments especially because of the absence of K-fertilization in the native vegetation.

Soil samples from the PG-amended treatments (PG alone and combined to lime) presented high SO_4^{2-} contents compared to the other treatments, as expected. However, PG-amended treatments did not differ from the native vegetation up to 0.2 m. The distribution pattern of SO_4^{2-} in native vegetation was not similar to that observed in the experimental area as a result of PG inputs, which increased SO_4^{2-} contents with depth and generated a stratification of the nutrient. In native vegetation, a more balanced pattern of SO_4^{2-} distribution was observed along the soil profile, with contents close to 20 mg kg^{-1}. Despite the significant increase in SO_4^{2-}, the P contents were not reduced in these treatments, probably as a consequence of the intimate and specific association between HPO_4^{2-} and $H_2PO_4^-$ ions in colloidal adsorption sites (Geelhoed et al. 1997; Hinkle et al. 2015), besides of the high fixation in Fe and Al hydroxides' surfaces (Campos et al. 2016; Gérard 2016).

The use of phosphatic fertilizers increased the total and the bioavailable contents of P in the most superficial soil layers. However, in the 0.2-0.4 m layer, no difference was found between bioavailable P contents among the samples, evidencing that neither the long-term application of P-fertilizers nor Al-suppressor amendments had effects on soil subsuperficial layers (Table 1). The average P contents in the 0.2-0.4 m soil layer of the experimental area represented 12% of the contents in the 0-0.05 m layer.

The total P buildup by P-fertilization was highlighted by the low contents in the NV (Table 2). According to Yang et al. (2013), in a global soil P assessment, Oxisols are among the classes with the lowest natural P contents, usually not exceeding 300 mg kg^{-1}. This is due to the low contents of P in the parent materials and to the intense weathering and high temperatures of the tropics that do not favor the accumulation of P_o and degrade almost totally apatitic minerals.

In the 0.05-0.1 m and 0.1-0.2 m soil layers, soil samples from the L treatment had lower concentrations of bioavailable P than soil samples amended with PG (Table 1). This result may be related with remnants of phosphate compounds from PG production. However, under acidic conditions, as in the case of the isolated PG use, the

excess of SO_4^{2-} can cause an increase in P-availability by desorption of the phosphate absorbed in a non-specific manner or in positions with higher lability (Geelhoed et al. 1997). The increase in pH reduces P fixation by decreasing the precipitation of low soluble Fe- and Al-phosphates, as well as by increasing negative charges in organic and inorganic colloid surfaces warding off phosphate ions (Fageria and Baligar 2008).

5.4.2. Enzymes

The pattern of β-gluc activity increase with pH was only observed in the 0.1-0.2 m layer, in which the LPG treatment presented higher β-gluc activity in relation to PG and control treatments (Fig. 1). However, other factors than pH had remarkable effects on β-gluc activity, *e.g.* P and N fertilizations as reported by Lupway et al. (2018). For instance, in the 0-0.05 m layer, the samples from the control and native vegetation had pH values that did not differ, but the β-gluc activity in the native vegetation was higher. Acosta-Martinez and Tabatabai (2000) reported positive correlations between β-gluc activity and soil pH.

The β-gluc activities variation in the 0-0.05 m layer (Fig. 1) followed the same SOM variation pattern (Table 1), which highlights the SOM influence on β-gluc activity regulation. This was confirmed by the highest amount of SOM (Table 1). In the other layers, the variation patterns between β-gluc and SOM were not the same, but samples from the native vegetation had greater β-gluc activity, especially in the 0.2-0.4 m layer, which reinforces how agricultural activity can directly impact subsurface biochemical properties linked to the C cycle.

The depletion of P_o forms in the experimental area is in agreement to the findings of Tarafdar and Jungk (1987), who noticed positive correlations between P_o depletion and the activity of phosphatases in the rhizosphere of wheat (*Triticum aestivum*) and clover (*Trifolium alexandrinum*). However, the activities of Acid-P and Alkaline-P in native vegetation were not superior in all studied soil layers, despite the greater abundance of P_o forms detected by ^{31}P-NMR in native vegetation samples compared to the other treatments. This pattern is unusual to that observed in most

studies in which enzyme activities were higher in uncultivated or less-disturbed soils than in cultivated ones (Acosta-Martínez et al. 2007; Omidi et al. 2008; Zhang et al. 2012).

According to Dick et al. (2000), the optimum pH_{H_2O} for Acid-P is 4.0. Our pH results were obtained with a 0.01 mol l^{-1} $CaCl_2$ solution, which is usually 0.5 or 0.6 unit lower than the pH obtained in water (Henderson and Bui 2002). In this sense, the pH values of the native vegetation would correspond to 4.4-4.6 in water, slightly above the optimum for Acid-P activity. Therefore, the abundance of monoesters phosphates may not have an effect as marked as the pH for the activity of the phosphomonoesterases studied. An example of the remarkable effects of pH is the high activities of Alkaline-P in the treatments with lime (Fig. 1) in the 0-0.05 m and 0.05-0.1 m soil layers, which is in agreement with the pH increases observed in the same layers (Table 1).

The high activity of Acid-P in the 0-0.05 m of PG treatment was probably related to the pH of 4.5 in this layer, which is close to the optimum value for Acid-P activity. Zhang et al. (2012) also find no difference between the acid-P activities in woodland (uncultivated) and maize (cultivated) soils and attributed this to the pH values in the cultivated soil. As Alkaline-P originates mostly from the activity of microorganisms, and acid-P can have multiple origins (roots, organic matter, microorganisms, meso and macro soil fauna, *etc*.).

Our results suggest the same in the 0.05-0.1 m and 0.1-0.2 m layers in which native vegetation had high activities of Alkaline-P (Fig. 1). In the 0-0.05 m layer, the Alkaline-P activity did not occur due to the increase in pH close to the optimum for the Alkaline-P activity promoted by liming. However, this hypothesis is reinforced by the higher number of gene counts in native vegetation and by the lower Alkaline-P activities in the control and PG treatments in relation to native vegetation *(supplementary material)*.

Carmeis Filho et al. (2017) also observed that the proportion of easily degradable SOM in the LPG treatment was the highest among all, which reflected a high mineralization of C after soil incubation (0-0.2 m). These results supported our

results with regard to the activity of Alkaline-P, which was superior in the lime-amended treatments up to 0.1 m. The high enzyme activities in the 0-0.05 m layer are related to the higher concentration of organic compounds and microbiological activity. So, as expected, enzyme activities were lower in deeper layers. Anyway, differences were observed in the 0.2-0.4 m layer for Acid-P and β-gluc. Variations in the contents of bioavailable P and SOM in the 0.2-0.4 m layer could help to explain these results; however, they were not observed (Table 1). So, the effects of broadcast Al-suppressors on the studied enzymes were limited to soil layers up to 0.2 m.

5.4.3. Organic phosphorus

The total P contents extracted from the soil was, on average, 33% higher than the P contents in the NaOH-EDTA extracts due to the strength of the acid extractants used in the 3052 method (USPEA 1996) (Table 2). The lowest total P in native vegetation in relation to the experimental plots resulted from the absence of P inputs via fertilizers over time and denote the P retention capacity of the Oxisol. It was possible to identify P_o compounds in the NaOH-EDTA extracts by solution ^{31}P-NMR (Table 2).

The *myo*-IHP_6 was the P_o compound found in highest proportions in all samples. The presence of *myo*-IHP_6 or other orthophosphate monoesters is common in soils with an abundance of Al- and Fe-oxides such as Oxisols and occurs due to the high stability of these P_o compounds when associated with metal oxides (Celi et al. 1999; Giaveno et al. 2010). High concentrations of *myo*-IHP_6 in humid tropical soils are also associated with crops as soybeans which store high amounts of *myo*-IHP_6 in in plant tissues (Turner et al. 2002).

The average *myo*-IHP_6/*scyllo*-IHP_6 ratio in relative percentages was 4.6 (Table 3), which is higher than the ratio of 3.6 found by Liu et al. (2013) in an Ultisol and close to those found by Cade-Menun et al. (2010) (4.3) in the 0-0.05 m layer of a Spodosol under NTS. Although the *myo*-IHP_6 is generally the most abundant form among orthophosphate monoesters, the lack of spiking to confirm the identification of this isomer makes possible an overestimation. However, the possibility of misidentification

was higher in compounds presented in low amounts, such as polyphosphates, AMP, α- and β-glycerophosphates, and other orthophosphates diesters. Nevertheless, the P_o peaks positions in relation to orthophosphate and in relation to each other in the spectra are in agreement with Condron et al. (1990), Turner et al. (2003), Cade-Menun (2005) and Abdi et al. (2015), which makes the results more reliable.

The contents of orthophosphate monoester and diester in the native vegetation soil were higher when compared with cultivated soil (Fig. 3). The well-defined peaks in the native vegetation solution spectra allowed us to identify peaks in samples from the experimental area. However, land use for agriculture proved to be harmful to the diversity of P_o forms. The DNA peak, for instance, was only detected in significant amounts in the native vegetation (Fig. 3), possibly associated with high OC contents and pHs below the isoelectric point of pH 5.0 (Table 1) that enhance DNA adsorption in clay minerals (Khanna et al. 1998). The accumulation of DNA in acid and wet soils was also reported by Makarov et al. (2002) in a Cambisol. The exposure to sunlight during part of the crop period and all inter-crop period may have accelerated the depletion of DNA in the cultivated soil, thus heating the soil to temperatures that accelerate DNA degradation (Sirois and Buckley 2019).

The higher concentrations of *myo*-IHP_6 in the soil under native vegetation (Table 2; Table 3) did not coincide with higher phosphatase activities that mineralize these P_o forms (Fig. 1). As the activities of Acid-P in the extracellular portion of the rhizosphere is critically influenced by the plant species (George et al. 2006), the abundance of soybean roots may favor the presence of Acid-P activities similar to those found in the native vegetation soil.

The soybean roots association with ecto-mycorrhizae may also have enhanced Acid-P activities. However, the number of copies of fungi genes in the native vegetation did not differ only from LPG treatment in the 0-0.05 m layer *(supplementary material)*, and the acid-P activities were not so discrepant between experimental treatments (Fig. 1).

The contents of inorganic orthophosphate estimated by NMR were similar to the contents obtained by colorimetry, which suggests the good accuracy of NMR spectra to estimate the quantity of P forms (Table 4). The determination of inorganic phosphates by colorimetry only measures orthophosphates and excludes complex P_i compounds that do not react with molybdate (Liu et al. 2013; Cade-Menun et al. 2018). Therefore, more complex P_i as pyrophosphates were identified only after the integration of the peaks in the NMR spectra, but they represented a small fraction of the total P_i found.

The reasons why phosphogypsum-amended plots (PG and LPG) did not express MUP contents in the ion exchange resin extraction remain unclear (Fig. 2) because there were no major variations in quantitative or qualitative terms for P_o forms in the samples from the experimental area (Table 2; Table 3). In a highly weathered soil as the Oxisol, high MUP contents were not expected. However, their presence in control, L and native vegetation samples bring the light that ion exchange resin extraction does not access just simple P_i forms, as orthophosphate.

5.4.4. Soybean performance

In the PG treatment, the suppression of Al^{3+} and the increase in Ca and S contents contributed to higher yields in relation to the control. However, they were not sufficient to achieve the same yields as observed in the lime-amended treatments. The pH increases by liming usually increases the availability of most nutrients under variable charge soils. These better general fertility conditions were fundamental for the expression of higher yields in L and LPG (Fig. 4). The isolated application of PG did not provide such benefits and, due to the absence of Mg, the contents in the soil and in the leaves were low in this treatment, which may also influence the yields.

The average concentration of P (3.4 g kg^{-1}) was adequate, while K average concentration (21.8 g kg^{-1}) was high over the three studied crops, based on criteria proposed by Kuhirara et al. (2013). The average concentrations of Cu, Zn and Fe were all between the adequate and high classes, except for Zn in the 2017/18 crop, in which

the concentrations were low. Although the N concentrations increased in index leaves in lime-amended treatments, they were low in control and PG treatments only in the 2018/19 according to Kuhirara et al. (2013). In the other years, N concentrations were adequate. In the case of Mn, the observed effects were inversely related to N and are mainly due to the decrease in available forms of Mn as a result of the increase in soil pH caused by liming (Mehlich 1957).

The concentrations of Ca were only low in control, while they were adequate in the other conditions. This implies that the Ca input by the amendments observed in the soil was effective in increasing the cation concentration in soybean plants, which naturally require high Ca amounts (Lund 1970; Silva et al. 2005). Leaves' samples from the PG treatment had low concentrations of Mg in the three evaluated crops, while samples from the control had the highest concentrations in general, reaching the class considered high. This does not correspond to what was observed for $_{ex}$Mg in the soil of the control treatment, which was below the concentrations observed in the lime-amendment treatments. This is probably related to the high concentration of Ca in the PG treatment, because Ca competes with Mg in the absorption sites in the roots. In addition, Mg was added with the L and LPG treatments because the lime used contained 11% of Mg.

The SO_4^{2-} contents in the PG treatment were high compared to other conditions, which may have hindered the expression of higher yields in this treatment (Fig. 4). Although the same amounts of S were added in the PG and LPG treatments, the LPG did not show such high S concentrations in index leaves mainly due to the joint presence of lime. The increase in pH promoted by lime in LPG probably decreased the amount of positive charges on the colloidal surfaces of the soil, consequently decreasing the retention of SO_4^{2-} (Kamprath et al. 1956). This effect was notable for the stratification of S in the soil (Table 1) and reflected in the anion contents in index leaves.

5.4.5. Environmental remarks

The cultivation and the application of amendments modified some biochemical and chemical properties along the soil profile. The activities of enzymes that mineralize P or C were also influenced by the management with L or PG, with more notable effects associated with pH. However, the abundance of P_o forms can be contrasting even with similar phosphomonoesterases activities. This was observed when comparing soil samples from the native vegetation with soil samples from the experimental area and highlights the importance of the type of dominant root systems and soil microbiological composition.

In general, anthropic interference in the soil through cultivation had a greater degree of importance than the management of Al-suppressors in altering P_o forms. Although they may have been slightly overestimated due to the degradation of diesters to monoesters in the NaOH-EDTA extraction, *myo*-IHP_6 was the major source of P_o for plants in the soil. The presence in low proportions of microbe-associated compounds (*i.e.*, AMP, α- and β-glycerophosphate polyphosphates, pyrophosphates, *etc.*) suggests that P_o cycle is not largely controlled by core microbiological cycling. So, the decomposition of plant litter over the crops is probably the main source of P_o in the investigated soil, especially in the form of $_{myo}$-IHP_6.

One of the concerns arising from the application of high Al-suppressors rates under NTS is the reduction of P availability in the most superficial soil layers due to pH elevation and eventual formation of calcium phosphate. This phenomenon was not observed in this study, which may reduce the concerns about yield drops and possible runoffs with eventual contamination of water bodies.

As final implications, the association of lime and phosphogypsum may be the best way to improve soil fertility conditions, but the tillage system and the rates applied need to be chosen with caution to avoid nutrients stratification. Furthermore, the bioavailable P extractant the determination method (colorimetry or ICP-OES) are factors that should be taken into account for more assertive P recommendations in Oxisols during soil fertility assessments.

5.5. Conclusions

Phosphorus fertilization under no-till limited bioavailable P increased up to 0.2 m. Some chemical properties such as pH, $_{ex}$Al and $_{ex}$Ca, as well as the activity of enzymes linked to the P and C cycles, underwent stratification in the soil profile by long-term Al-suppressors broadcast that generally improved the degree of soil fertility and soybeans yield.

The use of Al-suppressors did not expressively alter the proportions between P_o forms in the soil identified by ^{31}P-NMR, which were mainly composed by IHP_6. However, the changes in soil attributes promoted by Al-suppressors had effects on N, Ca, Mg, S and Mn contents in soybean index leaves and increased the plant's yield.

References

Abdi D, Cade-Menun BJ, Ziadi N, Parent LÉ (2015) Compositional statistical analysis of soil ^{31}P-NMR forms. Geoderma 257–258:40–47.

Acosta-Martínez V, Cruz L, Sotomayor-Ramírez D, Pérez-Alegría L (2007) Enzyme activities as affected by soil properties and land use in a tropical watershed. Appl Soil Ecol 35:35–45.

Andersson H, Bergström L, Djodjic F, et al (2016) Lime placement on subsoil as a strategy to reduce phosphorus leaching from agricultural soils. Soil Use Manag 32:381–389.

Antonangelo JA, Neto JF, Crusciol CAC, Alleoni LRF (2017) Lime and calcium-magnesium silicate in the ionic speciation of an oxisol. Sci Agric 74:317–333.

Bender RR, Haegele JW, Below FE, et al (2015) Nutrient uptake, partitioning, and remobilization in modern soybean varieties. Agron J 107:563–573.

Bertsch PM, Bloom PR (1996) Aluminum. In: Sparks DL (ed) Methods of Soil Analysis Part 3 - Chemical Methods. pp 517–550

Blum SC, Caires EF, Alleoni LRF (2013) Lime and phosphogypsum application and sulfate retention in subtropical soils under no-till system. J Soil Sci Plant Nutr 13:279–300.

Bolan NS, Curtin D, Adriano DC (2004) Acidity. Encycl Soils Environ 4:11–17.

Cade-Menun BJ (2005) Characterizing phosphorus in environmental and agricultural samples by ^{31}P nuclear magnetic resonance spectroscopy. Talanta 66:359–371.

Cade-Menun BJ, Carter MR, James DC, Liu CW (2010) Phosphorus forms and chemistry in the soil profile under long-term conservation tillage: A phosphorus-^{31} nuclear magnetic resonance study. J Environ Qual 39:1647–1656.

Cade-Menun BJ, Elkin KR, Liu CW, et al (2018) Characterizing the phosphorus forms extracted from soil by the Mehlich III soil test. Geochem Trans 19:1–17.

Cade-Menun BJ, Preston CM (1996) A comparison of soil extraction procedures for ^{31}P NMR spectroscopy. Soil Sci. 161:770–785

Caires EF, Barth G, Garbuio FJ (2006) Lime application in the establishment of a no-till system for grain crop production in Southern Brazil. Soil Tillage Res 89:3–12.

Caires EF, Guimarães AM (2018) A novel phosphogypsum application recommendation method under continuous no-till management in Brazil. Agron J 110:1987–1995.

Caires EF, Haliski A, Bini AR, Scharr DA (2015) Surface liming and nitrogen fertilization for crop grain production under no-till management in Brazil. Eur J Agron 66:41–53.

Campos M, Antonangelo JA, Alleoni LRF (2016) Phosphorus sorption index in humid tropical soils. Soil Tillage Res 156:110–118.

Cantarella H, van Raij B, Quaggio JA (1998) Soil and plant analyses for lime and fertilizer recommendations in Brazil. Commun Soil Sci Plant Anal 29:1691–1706.

Carmeis Filho ACA, Penn CJ, Crusciol CAC, Calonego JC (2017) Lime and phosphogypsum impacts on soil organic matter pools in a tropical Oxisol under long-term no-till conditions. Agric Ecosyst Environ 241:11–23.

Celi L, Lamacchia S, Marsan FA, Barberis E (1999) Interaction of inositol hexaphosphate on clays: Adsorption and charging phenomena. Soil Sci 164:574–585.

Condron L, Frossard E, Tiessen H, et al (1990) Chemical nature of organic phosphorus in cultivated and uncultivated soils under different environmental conditions. J Soil Sci 41:41–50

Condron LM, Goh KMK, Newman RH (1985) Nature and distribution of soil phosphorus as revealed by a sequential extraction method followed by ^{31}P nuclear magnetic resonance analysis. J Soil Sci 36:199–207.

Costa CHM, Crusciol CC (2016) Long-term effects of lime and phosphogypsum application on tropical no-till soybean-oat-sorghum rotation and soil chemical properties. Eur J Agron 74:119–132.

Dick WA, Cheng L, Wang P (2000) Soil acid and alkaline phosphatase activity as pH adjustment indicators. Soil Biol Biochem 32:1915–1919.

Edwards AC (1991) Soil acidity and its interactions with phosphorus availability for a range of different crop types. Plant-Soil Interact Low pH 299–305.

Eivazi F, Tabatabai MA (1988) Glucosidases and galactosidases in soils. Soil Biol Biochem 20:601–606.

Fageria NK, Baligar VC (2007) Improving nutrient use efficiency of annual crops in brazilian acid soils for sustainable crop production. Commun Soil Sci Plant Anal 32:1303–1319.

Fageria NK, Baligar VC (2008) Ameliorating soil acidity of tropical Oxisols by liming for sustainable crop production. 99:345–399.

Fageria NK, Moreira A, Castro C, Moraes MF (2013) Optimal acidity indices for soybean production in Brazilian Oxisols. Commun Soil Sci Plant Anal 44:2941–2951.

Fox RL, Olson RA, Rhoades HF (1964) Evaluating the sulfur status of soil by plant and soil test. Soil Sci Soc Am Proc 28:243–246.

Fuentes-Llanillo R, Telles TS, Volsi B, et al (2018) Profitability of no-till grain production systems. Semin Agrar 39:77–86.

Gee GW, Or D (2002) Particle-size analysis. In: Dane JH, Toop GC (eds) Methods of soil analysis: physical methods. Soil Science Society of America, pp 255–293

Geelhoed JS, Hiemstra T, Van Riemsdijk WH (1997) Phosphate and sulfate adsorption on goethite: Single anion and competitive adsorption. Geochim Cosmochim Acta 61:2389–2396.

George TS, Turner BL, Gregory PJ, et al (2006) Depletion of organic phosphorus from Oxisols in relation to phosphatase activities in the rhizosphere. Eur J Soil Sci 57:47–57.

Gérard F (2016) Clay minerals, iron/aluminum oxides, and their contribution to phosphate sorption in soils - A myth revisited. Geoderma 262:213–226.

Giaveno C, Celi L, Richardson AE, et al (2010) Interaction of phytases with minerals and availability of substrate affect the hydrolysis of inositol phosphates. Soil Biol Biochem 42:491–498.

Haynes RJ, Swift RS (1988) Effects of lime and phosphate additions on changes in enzyme activities, microbial biomass and levels of extractable nitrogen, sulphur and phosphorus in an acid soil. Biol Fertil Soils 6:153–158

Henderson BL, Bui EN (2002) An improved calibration curve between soil pH measured in water and $CaCl_2$. Aust J Soil Res 40:1399–1405.

Hinkle MAG, Wang Z, Giammar DE, Catalano JG (2015) Interaction of $Fe_{(II)}$ with phosphate and sulfate on iron oxide surfaces. Geochim Cosmochim Acta 158:130–146.

Inagaki TM, de Moraes Sá JC, Caires EF, Gonçalves DRP (2017) Why does carbon increase in highly weathered soil under no-till upon lime and gypsum use? Sci Total Environ 599–600:523–532.

Joris HAW, Caires EF, Scharr DA, et al (2016) Liming in the conversion from degraded pastureland to a no-till cropping system in Southern Brazil. Soil Tillage Res 162:68–77.

Kamprath EJ, Nelson WL, Fitts JW (1956) The Effect of pH, sulfate and phosphate concentrations on the adsorption of sulfate by soils. Soil Sci Soc Am J 20:463.

Khanna M, Yoder M, Calamai L, Stotzky G (1998) X-ray diffractometry and electron microscopy of DNA from Bacillus subtilis bound on clay minerals. Sci Soils 3:1–10.

Liu J, Yang J, Cade-Menun BJ, et al (2013) Complementary phosphorus speciation in agricultural soils by sequential fractionation, solution ^{31}P nuclear magnetic resonance, and phosphorus *K*-edge X-ray absorption near-edge structure spectroscopy. J Environ Qual 42:1763–1770.

Lund ZF (1970) The effect of calcium and its relation to several cations in soybean root growth. Soil Sci Soc Am J 34:456–459.

Lupwayi NZ, Kanashiro DA, Eastman AH, Hao X (2018) Soil phospholipid fatty acid biomarkers and β-glucosidase activities after long-term manure and fertilizer N applications. Soil Sci Soc Am J 82:343–353.

Makarov MI, Haumaier L, Zech W (2002) Nature of soil organic phosphorus: An assessment of peak assignments in the diester region of ^{31}P NMR spectra. Soil Biol Biochem 34:1467–1477.

Mcdowell RW, Brookes PC, Mahieu N, et al (2002) The effect of soil acidity on potentially mobile phosphorus in a grassland soil. J Agric Sci 139:27–36.

Mcdowell RW, Stewart I (2005) Peak assignments for phosphorus-^{31} nuclear magnetic resonance spectroscopy in pH range 5-13 and their application in environmental samples. Chem Ecol 21:211–226.

McLaren TI, Smernik RJ, Simpson RJ, et al (2017) The chemical nature of organic phosphorus that accumulates in fertilized soils of a temperate pasture as determined by solution ^{31}P NMR spectroscopy. J Plant Nutr Soil Sci 180:27–38.

Mehlich A (1957) Aluminum, iron, and pH in relation to lime induced manganese deficiencies. Soil Sci Soc Am J 21:625–628.

Moedritzer K, Maier L, Groenweghe LCD (1962) Phosphorus-^{31} Nuclear Magnetic Resonance Spectra of Phosphorus Compounds. J Chem Eng Data 7:307–310.

Murphy J, Riley JP (1962) A modified single solution method for the determination of phosphate in natural waters. Anal Chim Acta 27:31–36.

Murphy PNC, Stevens RJ (2010) Lime and gypsum as source measures to decrease phosphorus loss from soils to water. Water Air Soil Pollut 212:101–111.

Narro L, Pandey S, De León C, et al (2001) Implications of soil-acidity tolerant maize cultivars to increase production in developing countries. Plant Nutr Acquis 447–463.

Omidi H, Tahmasebi Z, Torabi H, Miransari M (2008) Soil enzymatic activities and available P and Zn as affected by tillage practices, canola (*Brassica napus* L.) cultivars and planting dates. Eur J Soil Biol 44:443–450.

Qayyum MF, Ashraf I, Abid M, Steffens D (2015) Effect of biochar, lime, and compost application on phosphorus adsorption in a Ferralsol. J Plant Nutr Soil Sci 178:576–581.

Rorison IH (1980) The Effects of Soil Acidity on Nutrient Availability and Plant Response. Eff Acid Precip Terr Ecosyst 283–304.

Rowley MC, Grand S, Verrecchia ÉP (2018) Calcium-mediated stabilisation of soil organic carbon. Biogeochemistry 137:27–49.

Silva IR, Ferrufino A, Sanzonowicz C, et al (2005) Interactions between magnesium, calcium, and aluminum on soybean root elongation. Rev Bras Cienc do Solo 29:747–754.

Simard RR, Angers DA, Lapierre C (1994) Soil organic matter quality as influenced by tillage, lime, and phosphorus. Biol Fertil Soils 18:13–18.

Sirois SH, Buckley DH (2019) Factors governing extracellular DNA degradation dynamics in soil. Environ Microbiol Rep 11:173–184.

Smeck NE (1985) Phosphorus dynamics in soils and landscapes. Geoderma 36:185–199.

Soil Survey Staff (2014) Keys to Soil Taxonomy, 12th ed. USDA - Natural Resources Conservation Service, Washington, DC

Tabatabai MA (1994) Soil enzymes. In: Weaver RW, Angle JS (eds) Methods of soil analysis: Part 2 - Microbiological and biochemical properties. SSSA Book Series, pp 775–833

Tiecher T, Calegari A, Caner L, Rheinheimer D dos S (2017) Soil fertility and nutrient budget after 23-years of different soil tillage systems and winter cover crops in a subtropical Oxisol. Geoderma 308:78–85.

Turner BL, Mahieu N, Condron LM (2003) Phosphorus-31 Nuclear Magnetic Resonance Spectral Assignments of Phosphorus Compounds in Soil NaOH–EDTA Extracts. Soil Sci Soc Am J 67:497–510.

Turner BL, Papházy MJ, Haygarth PM, Mckelvie ID (2002) Inositol phosphates in the environment. Philos Trans R Soc London Ser B Biol Sci 357:449–469.

USPEA (1996) Soil screening guidance: technical background document, 2nd edn. United States Government Publishing Office, Washington, United States of America

van Raij B, Andrade JC, Cantarella H, Quaggio JA (2001) Chemical analysis for fertility evaluation of tropical soils (in Portuguese). Campinas

van Raij B, Cantarella H, Quaggio JA, Furlani AMC (1996) Fertilization and liming recommendations for São Paulo Sate, Brazil (in portuguese). Campinas

von Tucher S, Hörndl D, Schmidhalter U (2018) Interaction of soil pH and phosphorus efficacy: Long-term effects of P fertilizer and lime applications on wheat, barley, and sugar beet. Ambio 47:41–49.

Zambrosi FCB, Alleoni LRF, Caires EF (2008) Liming and ionic speciation of an oxisol under no-till system. Sci Agric (Piracicaba, Braz) 65:190–203.

Zhang A, Chen Z, Zhang G, et al (2012) Soil phosphorus composition determined by 31P NMR spectroscopy and relative phosphatase activities influenced by land use. Eur J Soil Biol 52:73–77.

Zheng M, Huang J, Chen H, et al (2015) Responses of soil acid phosphatase and beta-glucosidase to nitrogen and phosphorus addition in two subtropical forests in southern China. Eur J Soil Biol 68:77–84.

Zobiole LHS, Oliveira Junior. RS, Constantin J, et al (2012) Nutrient accumulation in conventional and glyphosate-resistant soybean under different types of weed control. Planta Daninha 30:75–85.

Supplementary information

Table S1. Crop species, fertilization and amendments application during the 15 years of the field experiment conduction under no till.

Season	Crops		Amendment Application
2002/2003	Summer	*Oriza Sativa* (cv. Caiapó) BF: 300 kg ha^{-1} of NPK 08–28–16 + 4.5% S + 0.5% Zn. TF: 50 N ha of N	Lime: 2,700 kg ha^{-1} (71%ECCE) + Phosphogypsum 2,100 kg ha^{-1}
	Autumn-winter-Spring	*Avena Strigosa* (cv. Comum) BF: 200 kg ha^{-1} of NPK 10–20–10 + 4.5% S	
2003/2004	Summer	*Phaseolus vulgaris* (cv. Pérola) BF: 300 kg ha^{-1} of NPK 08– 28–16 + 4.5%S + 0.5% Zn. TF: 110 kg ha^{-1} of N	
	Autumn-winter-Spring	*Avena Strigosa* (cv. Comum) BF: 200 kg ha^{-1} of NPK 04–20–20 + 7% S	
2004/2005	Summer	*Arachis Hypogaea* (cv. Runner IAC 886) BF: 24 kg kg ha^{-1} N + 84 kg ha^{-1} P_2O_5 + 48 kg ha^{-1} of K_2O + 10% S + 0.5% Zn	Lime: 2,700 kg ha^{-1} (71%ECCE) + Phosphogypsum 2,100 kg ha^{-1}
	Autumn-winter-Spring	*Avena sativa* (cv. IAC 7) BF: 300 kg ha^{-1} of NPK 08–28–16 + 4.5% S + 0.5% Zn. TF: 110 kg ha^{-1} N	
2005/2006	Summer	*Arachis Hypogaea* (cv. Runner IAC 886) BF: 24 kg kg ha^{-1} N + 84 kg ha^{-1} P_2O_5 + 48 kg ha^{-1} of K_2O + 10% S + 0.5% Zn	
	Autumn-winter-Spring	*Avena sativa* (cv. IAC 7) BF: 8 kg ha^{-1} of N + 40 kg ha^{-1} P_2O_5 + 20 kg ha^{-1} of K_2O + 7% S	
2006/2007	Summer	*Zea mays* (cv. 2B570) BF: 24 kg ha^{-1} of N + 84 kg ha^{-1} P_2O_5 + 48 kg ha^{-1} of K_2O + 10% S + 0.5% Zn. TF: 90 kg kg ha^{-1} N	
	Autumn-winter-Spring	*Uruchloa brizantha* (cv. Marandu) The forage seeds were simultaneously sown with corn.	
2007/2008	Summer	*Zea mays* (cv. 2B570) BF: 24 kg ha^{-1} of N + 84 kg ha^{-1} P_2O_5 + 48 kg ha^{-1} of K_2O + 10% S + 0.5% Zn. TF: 90 kg kg ha^{-1} N	
	Autumn-winter-Spring	*Uruchloa brizantha* (cv. Marandu) The forage seeds were simultaneously sown with corn.	
2008/2009	Summer crop	*Glycine max* (cv MGBR-46) BF: 250 kg ha^{-1} of NPK 04–20–20 + 4.5%S + 0.5% Zn.	
	Autumn-winter-Spring crop	*Avena Strigosa* (cv. Comum) No fertilizer was applied	
2009/2010	Summer	*Glycine max* (cv MGBR-46) BF: 250 kg ha^{-1} of NPK 04–20–20 + 4.5%S + 0.5% Zn.	
	Autumn-winter-Spring	*Sorghum Vulgare* (cv. AG1020) No fertilizer was applied	

2010/2011	Summer	*Zea mays* (cv. 2B433) BF: 350 kg ha^{-1} of NPK 08–28–16. TF: 150 kg kg ha^{-1} N	Lime: 2,000 kg ha^{-1} (71%ECCE) + Phosphogypsum 2,100 kg ha^{-1}
	Autumn-winter-Spring	*Crambe abyssinica* (cv. FMS Brilhante) BF: 150 kg ha^{-1} of NPK 08–28–16	
2011/2012	Summer	*Zea mays* (cv. 2B433) BF: 350 kg ha^{-1} of NPK 08–28–16. TF: 150 kg kg ha^{-1} N	
	Autumn-winter-Spring	*Crambe abyssinica* (cv. FMS Brilhante) BF: 150 kg ha^{-1} of NPK 08–28–16	
2012/2013	Summer	*Pennisetum glaucum* (cv. ADR300) No fertilizer was applied	
	Autumn-winter-Spring	*Triticum aestivum* (cv. CD116) BF: 35 kg ha^{-1} N + 70 kg ha^{-1} P2O5 + 40 kg ha^{-1} of K_2O + kg ha^{-1} S + 12 kg kg ha^{-1} Zn	
2013/2014	Summer	*Phaseolus vulgaris* (cv. Pérola) BF: 10 kg ha^{-1} of N + 50 kg ha^{-1} P_2O_5 + 50 kg kg ha^{-1} K_2O + 11 kg ha^{-1} S + 12 kg ha^{-1} Zn. TF: 100 kg ha^{-1} N	
	Autumn-winter-Spring	*Triticum aestivum* (cv. CD116) BF: 35 kg ha^{-1} N + 70 kg ha^{-1} P2O5 + 40 kg ha^{-1} of K_2O + kg ha^{-1} S + 12 kg kg ha^{-1} Zn	
2014/2015	Summer crop	*Phaseolus vulgaris* (cv. Pérola) BF: 10 kg ha^{-1} of N + 50 kg ha^{-1} P_2O_5 + 50 kg kg ha^{-1} K_2O + 11 kg ha^{-1} S + 12 kg ha^{-1} Zn. TF: 100 kg ha^{-1} N	
	Autumn-winter-Spring crop	*Uruchloa brizantha* (cv. Marandu)No fertilizer was applied	
2015/2016	Summer crop	*Uruchloa brizantha* (cv. Marandu)No fertilizer was applied	
	Autumn-winter-Spring crop	*Uruchloa brizantha (cv. Marandu) The forage seeds were simultaneously sown with corn.*	
2016/2017	Summer	*Glycine max* (cv. Soy5917) BF: 300 kg ha^{-1} of NPK 04–20–20 + 18 kg ha^{-1} N+ 3 kg ha^{-1} S + 3 1 kg of ha–1 B + 1 1 kg of ha–1 Cu + , Mn + 1 kg of ha^{-1} Zn + 0,2 kg of ha^{-1} Mo	Lime: 6,300 kg ha-1 (71%ECCE) + Phosphogypsum 10,000 kg ha^{-1}
	Autumn-winter-Spring	*Zea mays* (cv. 2A401PW) BF: 220 kg of ha^{-1} of NPK 08–28–16 + 14 kg kg of ha^{-1} N + 3 kg of ha^{-1} S + 3 kg of ha^{-1} B + 1 kg of ha^{-1} Cu + 1 kg of ha^{-1} + 1 Mn 10 kg of ha^{-1} Zn + 0,2 kg of ha^{-1} Mo	

^{31}P-NMR previous tests: The use of NMR in highly weathered soils is difficult due the low contents of organic P and high contents of Fe and Mn, which interfere in the quality of the results. Preliminary tests were carried out with soil sub-samples from the control treatment to obtain a reliable analytical protocol. In this sense, we developed a robustness test with two levels and seven factors (Table S1). The extraction time (8 or 18 h), the D_2O quantity (0.3 or 0.6 ml), the sample state (air-dried or freeze-dried) and the Na_2S pos-treatment were indifferent to the quality of the spectra.

Table S1. Factors and levels for robustness determination

factor	Level 1	Level 2
Extractant concentration	0.25 mol l^{-1} NaOH + 0.05 mol l^{-1} EDTA (A)	0.25 M NaOH + 0.05 M EDTA (a)
Pre-treatment	with RTA resin (B)	without RTA resin (b)
Pos-treatment	with Na_2S (C)	without Na_2S (c)
Sample state	Air dried (D)	Freeze-dried (d)
Extraction time	16 h (E)	8 h (e)
Soil:solution ratio	1:10 (F)	1:5 (f)
D_2O quantity	0.3 ml (G)	0.6 ml (g)

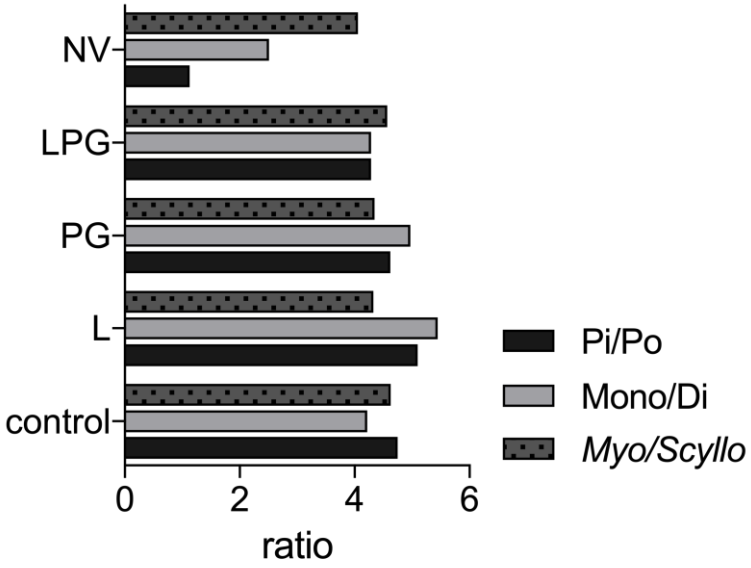

Figure S1. Ratios between inorganic and organic forms of phosphorus (P_i/P_o), monoesters phosphates and diester phosphates (Mono/Di) and *myo*- and *scyllo*-inositol hexa*kis*phosphates (*Myo*/*Scyllo*).

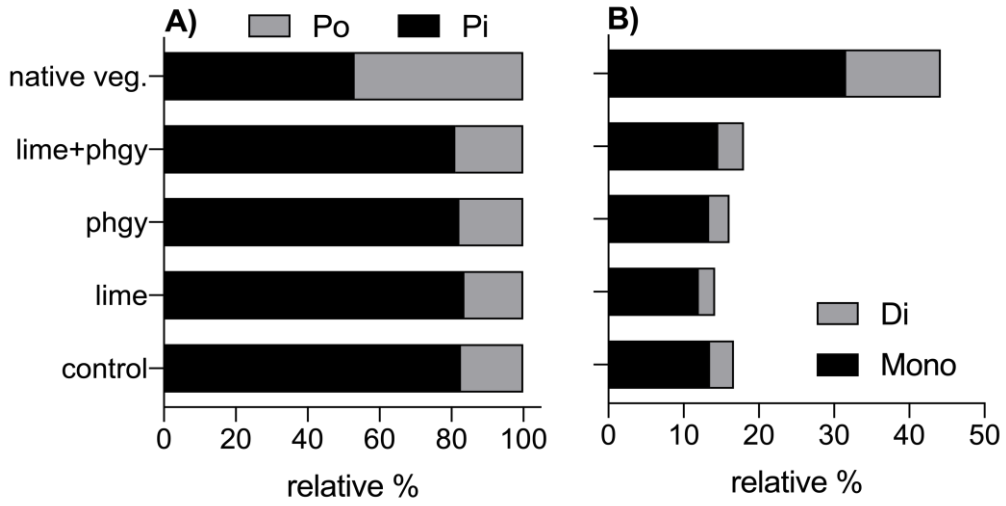

Figure S2. Percentage ratio between the sum of inorganic (P_i) and organic (P_o) forms of phosphorus (subfigure **A**) and between orthophosphates monoesters and diesters (in relation to the total P) (subfigure **B**) obtained by ^{31}P-NMR spectra from five soil samples.

DNA extraction and quantitative PCR (qPCR): Genomic DNA was extracted from 400 mg of soil using the PowerSoil DNA Isolation kit (MoBio Laboratories, Carlsbad, USA). Integrity of samples was assessed through 1.5% agarose gel electrophoresis with 1.5% TAE buffer (400 mmol l^{-1} Tris, 20 mmol l^{-1} acetic acid and 1 mM EDTA) in which 5 µl of the extracted DNA was applied and stained with ethidium bromide solution.

After the DNA extraction from soil samples, the quantification of the number of copies of interest genes was performed using the qPCR methodology. The reactions were performed on the iQ5 (BioRad) equipment with the SYBR GreenI system. All reactions were performed in a volume of 25 µl containing 12.5 µl of the Platinum Quantitative PCR SuperMix-UDG kit (Invitrogen, Brazil), and the primers at a concentration of 100 nM.

For bacteria the primers P1 (5'-CCTACGGGAGGCAGCAG-3') and P2/Eub518R (5'-ATTACCGCGGCTGCTGG-3') were used (Fierer et al. 2005; Rasche et al. 2011), while for fungi the primers ITS1f (5'-TCCGTAGGTGAACCTGCGG-3') and 5.8s (5'-CGCTGCGTTCTTCATCG-3') were used (Fierer et al. 2005).

The amplifications for bacteria were performed with an initial denaturation cycle at 95ºC for 3 min followed by 40 cycles of amplification in two steps; 95ºC for 30 s and 55ºC for 35 s, with a final step at 72ºC for 45 s subsequently (Rasche et al. 2011). For fungi, the amplifications were carried out with an initial denaturation cycle at 95ºC for 15 min, followed by 40 cycles of 95ºC for 1 min, 53ºC of annealing temperature for 30 s and 72ºC for 1 min (Fierer et al. 2005).

For the quantification of the number of copies of the genes of interest, standard curves were obtained, performing amplifications with the number of known copies of the standard DNA added in the reactions. In this way, the amplification data of the DNA extracted from the soil samples were interpolated in the standard curves to determine the number of copies of the gene of interest. Each reaction was duplicated, and we also included positive and negative control samples (free of DNA) to monitor potential contamination.

The efficiency (E) for the 16S rRNA bacteria gene was 92%, while it was 96% for the ITS fungi. The linear coefficients of the standard models were >0.99 in both quantifications. The average number of copies of the 16S rRNA gene was $2.2x10^9$ for the bacteria domain. The control treatment had the lowest numbers of 16S rRNA gene counts for bacteria in the 0-0.05 and 0.1-0.2 m layers. In the 0.05-0.1 m layer, only LPG and NV had numbers of counts higher than the control treatment (Fig. S5).

For the fungus domain, NV showed ~4% higher gene copy numbers as compared to treatments of the cultivated area in the 0-0.05 m and 0.05-0.1 m layers. In the 0.1-0.2 m layer, the LPG treatment did not differ from the NV, which had the highest number of copies.

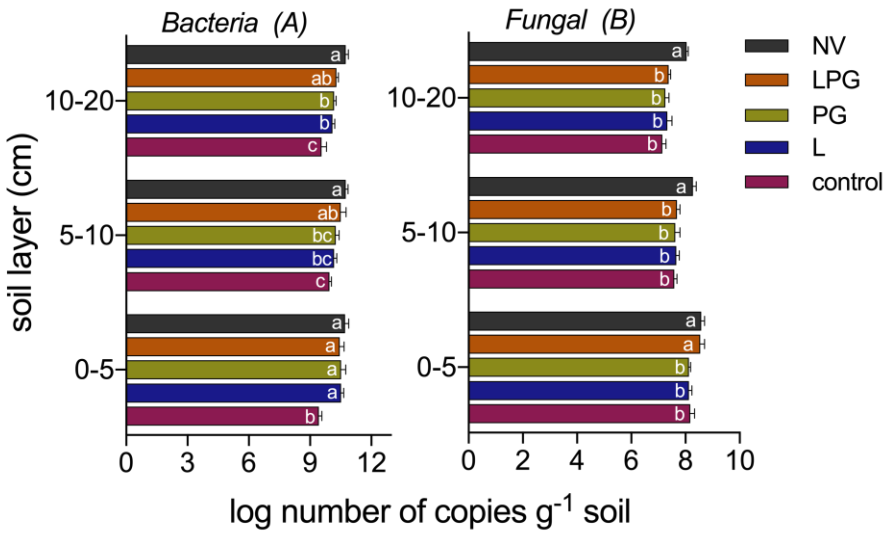

Figure S3. Number of copies of the 16S rRNA gene from bacteria (**A**) and fungi ITS region (**B**) from Oxisol samples in a long-term experiment. The values indicate the logarithm of the number of copies (n = 4). Bars containing the same letter within the same soil layer do not differ by *Tukey* test, at $p \leq 0.05$.

6. FINAL REMARKS

The nature of the P adsorption process in soils, whether in the form of phosphate or IHP_6, is complex and variable as function of several factors. More than one adsorption mechanism was involved in the adsorption of phosphate molecules on the hematite's surface, and the presence of Ca and Mg notably influenced this process. Lime, that contains Ca and Mg, influenced the adsorption of phosphate molecules in the soil, as well as other attributes linked to soil fertility, enzyme activity and soybean yield, specially when associated with phosphogypsum. Phosphorus fractions operationally defined and even P-species in solid state were influenced by lime or/and phosphogypsum. However, species and fractions of Fe tended to have less influence from the long-term use of these amendments, as well as the organic P forms, whose cycles were directly based on forms of inositol phosphate. Phosphorus species adsorbed to Kln may have low lability, and this greater stability added to the abundance of Kln in tropical and subtropical soils make more detailed studies necessary, especially to clarify the type of bonding established and ways to desorb it. Much of the legacy P in soils is in organic forms, therefore, further investigation is needed in this matter, especially to understand how important is the organic P mineralization process in highly weathered soils. In this sense, the evolution of spectroscopic and nuclear magnetic resonance techniques may lead to future research and bring new information to our environment.